# UNIVERSITA' DEGLI STUDI DELLA CALABRIA

---

## DIPARTIMENTI DI CHIMICA E FISICA


**Dottorato di Ricerca in**
**"Scienze e Tecnologie delle Mesofasi e dei Materiali Molecolari"**
**- ($STM^3$) - Dottorato Internazionale XIX° CICLO**

# Ph. D. THESIS

# Polarization holographic recording in polymeric and liquid crystalline materials

**Settore disciplinare: FIS03**


**Supervisore**
**Prof. Gabriella Cipparrone**

**Candidato**
**Dr. Clementina Provenzano**

**Coordinatore**
**Prof. Marcello Longeri**


---


**Anno accademico 2006-2007**

# Acknowledgements

I would like to thank the many people who have helped and supported me during my studies leading to this dissertation.

First of all, I wish to express my highest gratitude to my advisor, Professor Gabriella Cipparrone, without whom this work would have been impossible to accomplish. I greatly appreciate her support and guidance given to me during my doctorate.

I would also like to thank my collaborator and friend, Dr. Pasquale Pagliusi for helping me whenever it was necessary during the three years.

I am grateful to Professor Lev Blinov for providing invaluable suggestions and comments during my studies.

I would like to thank Alfredo Pane and Ornella Pizzino: they were very kind to me and always helpful.

In addition, I wish to thank my family, my father, my mother and my brother for their continual supports and cheering through the years.

Finally, I would like to give my special and everlasting thanks to Francesco for his love, support, understanding, and caring.

# Abstract

Optical studies related to polarization holographic recording in photosensitive materials, as azo compounds, liquid crystals and polymeric mixtures, and dye doped polymers, were carried out. The interest in this type of holographic recording is due to the improved signal to noise ratio and the possibilities for image and signal processing, optical switch, beam steering, optical polarizers and selective erasure. We focused our investigation on the mechanisms that can possibly induce diffraction gratings in these different types of photosensitive materials, on the peculiarities of the achieved diffractive devices and on their possible applications. In particular we investigated the effects of polarization holography on azo-dye Langmuir-Blodgett films, on polymer dispersed liquid crystal (PDLC), and on liquid crystal films confined by dye-doped polymers aligning layers.

In the first system, conventionally used for polarization holographic recording, we investigated the influence of the particular Langmuir-Blodgett deposition technique on the features of the recorded structures in order to obtain pure polarization gratings. The absence of surface reliefs gratings (SRG), the stability of the recorded devices and the high induced birefringence of the selected material, open up the possibility of interesting applications. In particular, we report the design and the implementation of a photopolarimeter for simultaneous measurements of Stokes parameters of light, in which the basic element is the actual polarization grating.

PDLC is a non conventional system for polarization holographic recording, because no azo-compounds are present in the polymeric and liquid crystalline mixtures. Polarization holographic storage produces diffraction gratings that originate mainly from the liquid crystal alignment inside the droplets of the solid polymeric matrix, created during the polymerization and phase separation processes. Polarization properties and electro-optical switching behaviour of the gratings are studied. We also report the unexpected observation of SRG in a system without azo compound, where photoisomerization and chromophore reorientation processes do not occur.

In the last systems, we exploit a new method for spatially varying liquid-crystal alignment using patterned surfaces obtained by means of a polarization holographic exposure on a dye-doped polyimide. This idea is based on the fact that holographic gratings on some photosensitive material provide a periodic alignment of the nematic liquid crystals. In fact, putting in contact a

thin film of liquid crystal with the aligning layers, we obtain a replica-grating in the bulk with the same properties of the gratings recorded on photosensitive layers.

We describe the high flexibility of these replica-gratings, related to the control of the diffraction efficiency by means of an external electric field, and the very singular properties of the polarization states of the beams diffracted from this device.

We also obtain two dimensional (2D) gratings consisting of a 2D array of differently twisted structures of nematic liquid crystal, achieved by a crossed assembling of polarization holograms recorded at the surfaces of the aligning substrates. These devices diffract the incident beam in several diffracted beams with various polarization states at the same time. The energy distribution can be controlled by means of the polarization state of the incident beam. Additionally, the distribution of the intensity on the diffracted beams can be completely controlled by means of a low external applied voltage. These features make the optical devices very interesting for beam steering, beam shaping and other modifications of light intensity or phase.

# List of figures

# List of tables

# Contents

# Introduction

## 0.1 Introduction

This dissertation presents optical studies related to polarization holographic recording in several photosensitive organic materials, as azo compounds, nematic liquid crystals and polymer mixtures, and dye doped polymers. We focused our investigations on the mechanisms that can possibly induce diffraction gratings in these different types of samples, on the peculiarities of the diffractive devices and on their possible applications. In order to study the different photoinduced phenomena, we used polarization holography as analytical technique[1-6]. Since the invention of holography by Gabor[7], many applications of this technique, such as the elaboration of holographic optical elements, scanners, optical disc systems, optical computing, holographic display and integrated optics, have been developed.

## 0.2 Holographic recording

A holographic grating can be considered as an elementary hologram, which is similarly produced by the interference of a reference and an object wave as a hologram in general. Interference produces a spatially periodic light intensity and/or polarization distribution which, in turn, changes the optical properties of a photosensitive material placed into the interference region. The spatial modulation of the optical material parameters acts as a diffraction grating. Permanent gratings have been produced in this way for many years[7-10]. However, in spite of the time spent on research, there are some important aspects regarding the formation of holograms that are still not clear, making the study and development of such materials still important. A good knowledge of the physicochemical properties and the way they affect the holograms generated in these materials is essential in designing and developing new materials.

Molecules may undergo several transformations after irradiation with an electromagnetic field: when a material is placed into the interference region of the pump waves, some light-matter interaction creates a corresponding spatial modulation of some material property, as, for

example, the population of an excited electronic state, the conduction electron density, the space charge and its accompanying field, the molecular orientation and the concentration.

The experimental arrangement for the production of holographically induced optical gratings is sketched in figure 0.1: light from a laser is split into two beams A and B, with wave vectors $\vec{k}_A$ and $\vec{k}_B$, electric field amplitudes $\vec{A}_A$ and $\vec{A}_B$, and intensities $I_A$, $I_B$. The two beams intersect at an angle $\alpha$ at the sample and create an interference pattern[11], the grating vector $\vec{q}$ of which is $\vec{q} = \pm(\vec{k}_A - \vec{k}_B)$

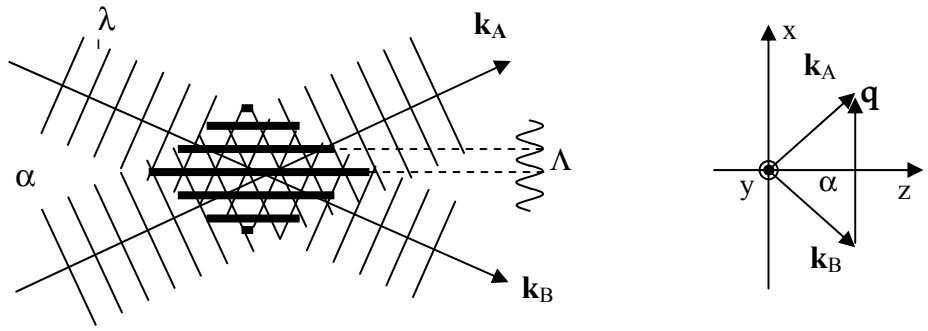


**Fig 0.1** Grating production by interference of two light waves whit intensities $I_A$, $I_B$ and wave vectors $\vec{k}_A$ and $\vec{k}_B$.

The periodicity of the grating is related to $\vec{q}$ by the relation $\Lambda = 2\pi/|\vec{q}|$ and can be expressed in terms of the wavelength of the writing field and $\alpha$ as $\Lambda = \lambda/[2\sin(\alpha/2)]$. By varying the intersection angle, the grating period can be changed.

The interference patterns can be created to have spatially periodic intensity modulations and/or spatially varying polarization state. When two coherent beams of arbitrary polarization interfere, the polarization state and the intensity of the total field change spatially in orientation and magnitude because of the phase difference between the two beams[12]. Afterwards, accordingly to the polarization state of the two interfering beams, it is possible to distinguish two different holographic recordings: scalar or intensity holography, where object and reference beams have the same polarization state, and vector or polarization holography which employs mutually orthogonal polarized beams, that do not create intensity fringes, but rather a spatially variable

polarization of the total field. As a consequence, numerous interfering geometries that produce countless patterns can be obtained simply changing the polarization state of the writing beams. In the following scheme few interference patterns are reported, which are produced by different pair of beams with parallel and orthogonal polarization states.

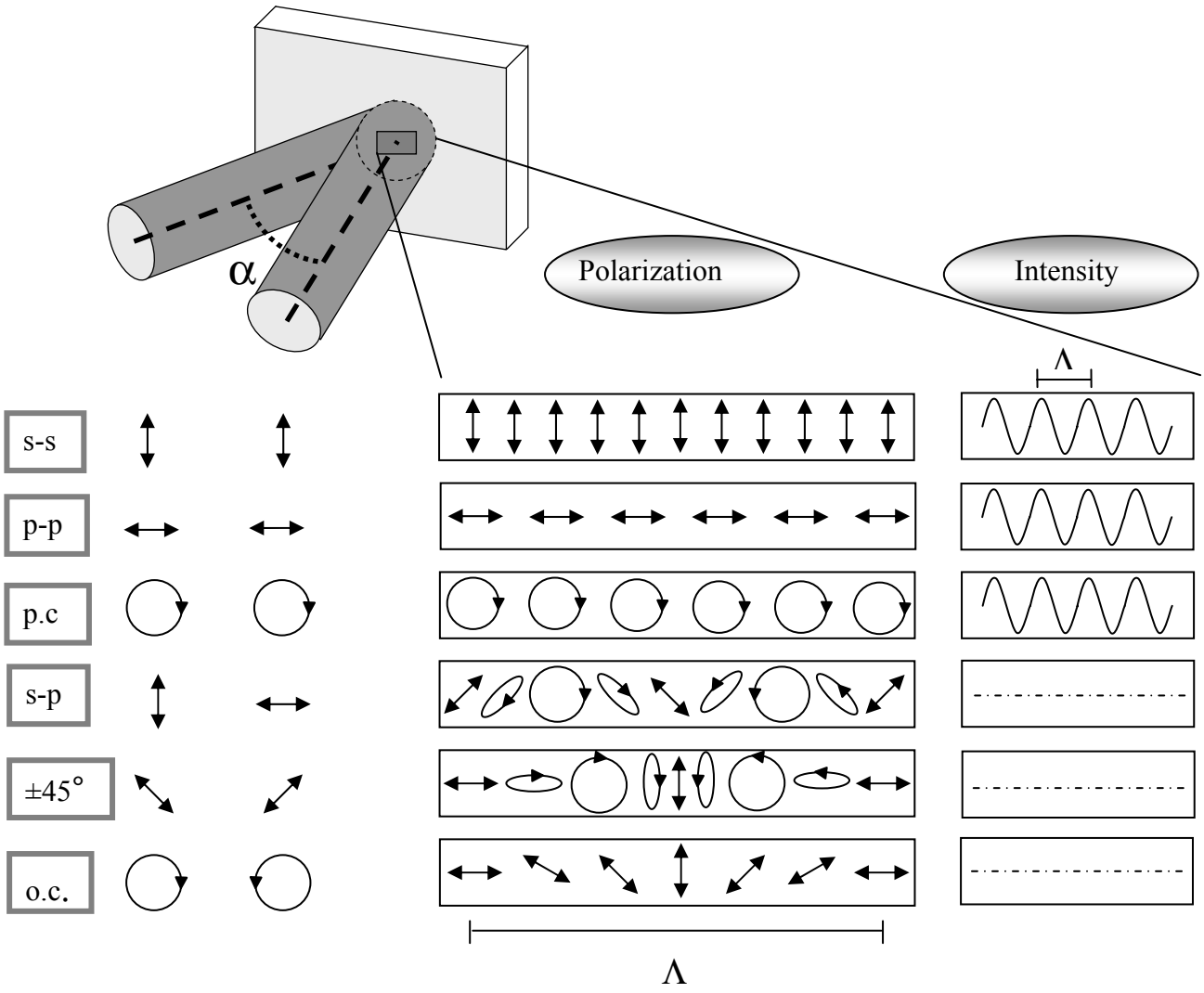


**Fig 0.2** Polarization geometries produced by different pair of beams whit parallel and orthogonal polarization states. s: linear s; p linear p; ±45°linear +45° and -45°; p.c.: parallel circular; o.c.: opposite circular.

The figure 0.2 shows the polarization state of the two interfering plane waves and the resulting total field interference pattern. The first three cases (s-s, p-p, p.c.) describe holographic intensity patterns, in which the two recording beams present the same polarization state. The polarization

state of the total field is everywhere equal to the writing beams and its direction remains unchanged. The phase modulation between the two interfering beams is encoded as a pure intensity modulation.

The last three cases (±45°, s-p, o.c.) illustrate holographic polarization patterns, in which the two recording beams have orthogonal polarization states. Unlike the previous case, the spatial intensity distribution is almost uniform, and the phase variation is encoded in the polarization state modulation of the total field. It is important to underline that even in opposite polarizations configurations, the presence of a small intensity modulation depends on the crossing angle, especially in the opposite circular and ±45° configurations, and small crossing angles yield negligible intensity modulations. It is possible to see that parallel orthogonal polarization states produce an interference pattern where the polarization state of the total field pass through linear, circular and elliptical polarization states, while two opposite circular interfering beams produce a polarization state that is everywhere linear, but rotates along the grating wave vector with a constant angular frequency.

The possibility to have numerous interference patterns depending on the polarization states of the writing waves, represents a great advantage for creation and characterization of diffractive devices for optoelectronics, that makes holography a technique characterized by a very high flexibility. In fact, it is possible to choose the intensity holography or the polarization holography in order to investigate the behaviour of a photosensitive material, provided that the material is sensitive to the intensity or the polarization state of the light, respectively.

## 0.2.1 Photo-anisotropic materials for polarization holography

Polarization holographic storage in azo compound based systems has been an area of interest in the past years because of its high resolution, permanent storage capability and large diffraction efficiency. The interest in this type of holographic recording was due to the improved signal to noise ratio and the possibilities for image and signal processing, optical switch, beam steering, optical polarizers and selective erasure[2]. Moreover, the technique makes it possible to study the behaviour of photosensitive material that have high sensitivity to the polarization states and the intensity of light. In this case, the photo chemical reactions involved could be photoisomerization

as well as photodimerization.

In fact, a class of organic materials undergoing rapid development for holographic applications is the photosensitive anisotropic systems[13]. The idea is to use anisotropic molecules that allow a selective excitation of molecules oriented in a given direction. In this scheme holograms have been recorded either by conventional holography or by polarization holography[2-5,14,15]. At now the research activity has been mainly addressed to photoisomerizable materials: azo compounds, azo dye doped or functionalized polymers have been largely synthesized and investigated for polarization holography. These systems incorporate azo-dye chromophores that are highly optically anisotropic and that undergo optically induced reorientation. Thus, optical irradiation produces a large refractive index change through the birefringence induced by this reorientation process. A recording medium of this type could have a very high dynamic range, and thus the potential for high data storage density, and perhaps be reversible, hence enabling rewritable storage.

## 0.3 Scope of thesis

In this thesis we studied the performance of different photo-recordable materials by means of polarization holography as analytical technique. In particular we investigated the effects of polarization holography on photosensitive azo-dye Langmuir-Blodgett films, on polymer dispersed liquid crystal (PDLC), and on liquid crystal film confined by dye-doped polymeric aligning layers. The first system is conventionally used for polarization holographic recording. It is well know that, upon any holographic grating inscription, at least two distinct processes take place, namely the formation of a linear and/or circular birefringence grating, and a surface relief grating (SRG). In our experiment, we investigate the influence of the particular Langmuir-Blodgett structure on the features of the recorded gratings in order to obtain pure polarization holograms. In our gratings topographic modulations (SRG) are absent: the layered structure, due to the deposition technique, seems to obstruct the topographic reliefs formation. As a consequence, the diffraction properties of the gratings and their long time stability make them good candidates for polarimetric applications.

In the other two systems, polymer dispersed liquid crystals (PDLC) and liquid crystal between

photosensitive aligning layers, the achieved gratings are not mere polarization holograms but are mediated by the interface interactions between the polymeric photosensitive material and the liquid crystal. In PDLC no azo-compounds are used and the gratings originate mainly from the liquid crystal alignment inside the droplets of the solid polymeric matrix, created during the polymerization and phase separation processes. Switching can be obtained applying an external electric field. In the last case, taking advantage of the interactions at the interface between a holographic patterned dye-doped polyimide substrate and a thin film of liquid crystal, we obtained diffractive devices characterized by high diffraction efficiency and low scattering, whose diffracted and transmitted beams can be modulated in intensity by means of a low external voltage[1]. Indeed, the idea of our work is based on the fact that holographic gratings on some photosensitive materials provide a periodic alignment of the nematic liquid crystals.

The results obtained in these different cases have required systematic studies to understand the basic physical principles, and the characterization of the produced device.

It is worth to underline that this work deals not only with basic research on the materials and on the fundamental mechanisms for hologram formation, but also design and implementation of the devices.

## 0.3.1 Organization of the dissertation

This dissertation is organized as follows: the first chapter deals with polarization holography on an azo-compound photoisomerizable system. We describe the properties of the material chosen for the holographic recording, the Langmuir-Blodgett technique to deposit the azo-dye onto a glass substrate, and the peculiarities of the obtained polarization gratings[16,17]. The characterization of this device revels that the singular diffraction features and the long time stability, make it particularly appropriate for polarimetric investigations. We report the project of an instrument based on the polarization grating: a photopolarimeter for real time measurements of Stokes parameters. We illustrate the functioning principle and a run test that demonstrate the capability of the device to measure any polarization state of light[18].

In the second chapter we present results obtained from experimental and theoretical studies of the diffractive properties of diffraction gratings, produced by means of polarization holography

on polymer dispersed liquid crystal. After a comparison between standard recording holographic technique, that uses two interfering parallel polarized beams, and holographic polarization technique, that uses two waves with orthogonal polarization states, we investigate the polymer and liquid crystal mixtures used for the storage, and characterisation of the gratings[19-21].

These investigations reveal that, beside orientational gratings, also SRGs are induced, which have never been observed by polarization holography in non-photoisomerizable systems. A model of the composite gratings has been carried out which considers the topography modulation of the PDLC film in addition to the photoinduced linear birefringence due to the nematic director orientation inside the droplets[22].

In the last section, we exploit a new method of surfaces patterning for liquid-crystal alignment using a polarization pattern exposure on a photoisomerizable polymer[24]. The patterned surfaces induce a similar nematic director configuration in the LC bulk, characterized by low scattering and high efficiency, with the same diffraction properties of the polarization holograms recorded on photosensitive layer. We describe the high flexibility of these replica-gratings, related to the control of the diffraction efficiency by means of an external electric field, and the polarization properties of the device. Several geometries of LC cells with one or both patterned aligning substrates have been investigated.

Incited by the wide interest in optical devices that can perform beam steering, beam shaping and other modifications of light intensity or phase, we also developed two dimensional devices that diffract the incident beam in several diffracted beams with opposite linear and/or circular polarization states at the same time. The energy distribution can be controlled by means of the polarization state of the incident beam. Additionally, exploiting the high sensitivity of the liquid crystal based devices to the external fields, the distribution of the intensity on the diffracted beams can be completely controlled by means of a low applied voltage[25].

# References:


**1** S. Calixto and R. A. Lessard, *Appl. Opt.* **23**, 4313

**2** L. Nikolova and T. Todorov, *Optica Acta* **31**, 579

**3** T. Todorov, L. Nikolova, and N. Tomova, *Appl. Opt.* **23**, 4309

**4** T. Todorov, L. Nikolova, and N. Tomova, *Appl. Opt.* **23**,4588

**5** P.A. Blanche, Ph. C. Lemaire, C. Maertens, P. Dubois, and R. Jérôme, *Opt. Commun.* **139**,92

**6** P.A. Blanche, Ph. C. Lemaire, C. Maertens, P. Dubois, and R. Jérôme, *Opt. Commun.* **185**, 1

**7** D. Gabor, *Nature* **161**,777

**8** O. Wiener, *Ann. Phys.,* **40**, 203

**9** M. Born, E. Wolf, Principle of Optics, *Pergamon Oxford 1975*

**10** E. N. Leith, J. Upatnies, *J. Opt. Soc. Am.* **53**, 1377

**11** H.J. Eichler, P. Gunter, D.W. Phol, Laser Induced Dynamic Gratings, *Springher-Verlag*

**12** T. Huang, K.H. Wagner, *J.Opt. Soc. Am B*, **13**, 282

**13** S. Blaya, L. Carretero, R.F. Madrigal, A.Fimia, Photosensitive materilas for holographic recording, *Handbook of advanced Electronic and Photonic Materials and Devices,* Vol **7**, edited by H.S. Nalwa

**14** L. Nikolova, T. Petrova, M. Ivanov et al, *Appl. Opt.* **35**, 306.

**15** L. Nikolova, T. Petrova, M. Ivanov et al, *J. Mod. Opt.* **39**, 1953

**16** G. Cipparrone, A. Mazzulla, et al, *Appl. Phys. Lett.,* **77**, 2106

**17** G. Cipparrone, A. Mazzulla, L.M. Blinov, *J. Opt. Soc. Am.* B **19**, 1157

**18** C. Provenzano, G. Cipparrone, A. Mazzulla, *Applied Optics*, **45**, No 17, 3929

**19** A. Mazzulla, A. Dastoli, G. Russo, L.Lucchetti, G. Cipparrone, *Liq. Cryst.*, **30**, 87

**20** G. Cipparrone, A. Mazzulla, G. Russo, *J. Opt. Soc. Am. B*, **18**, 1821

**21** G. Cipparrone, A. Mazzulla, G. Russo, *Appl. Phys. Lett.,* **78**, 1186

**22** A. Mazzulla, P. Pagliusi, C. Provenzano, et al, *Appl. Phys. Lett.,* **85**, 2505

**23** L.M. Blinov, G. Cipparrone, A. Mazzulla, C. Provenzano, et al, *Appl. Phys. Lett.* **87,** 061105

**24** C. Provenzano, P. Pagluisi, G. Cipparrone, *Appl. Phys. Lett.* **89,** 121105

**25** C. Provenzano, P. Pagluisi, G. Cipparrone, Electrically switchable 2D gratings of twisted nematic liquid crystal induced by polarization holograms, in preparation for *Opt. Expr.*

# Chapter 1

## 1.1 Introduction

This chapter deals with the achievement of a pure phase polarization grating, recorded in a Langmuir-Blodgett film of an azo compound, by means of a polarization holographic writing technique. Polarization gratings are particular devices in which the anisotropy parameters change across the input face, in spite of the ordinary anisotropic elements, as linear polarizers and wave plates, that have uniform properties across their input and output faces. Polarization gratings are of potential interest in the analysis of polarized light as well as in interferometry and in optical processing of information.

Since Torodov[1-3] and co-workers reported optically induced birefringence of azobenzene groups in a variety of polymer matrices, numerous researchers have concentrated on exploration of materials with high diffraction efficiency, resolution and sensitivity. In this context, systems containing azobenzene chromophores seem to be very promising for holographic storage applications. In fact, previous works have shown the possibility to record holographic gratings in these systems[1-7], and a special attention were paid to the polarization holography. In fact, pure polarization holographic gratings can be used for numerous applications[4]. A particular feature that makes them suitable for image processing and spectral photopolarimeters is the polarization selectivity of their diffraction properties[8].

The basic mechanism responsible of the storage effect in azo compounds is the anisotropic reorientation of the trans-azobenzene chromophores, which gives the material birefringence and dichroism properties[9]. In such systems, in fact, anisotropic gratings due to the photoinduced linear and circular birefringence are recorded. But generally the anisotropic phase grating is simultaneously recorded at a surface relief grating (SRG) [1-4,10]. The presence of SRG is a disadvantage for some applications of the polarization gratings, because the relief changes the polarization properties of gratings.[6,7,10,11]. In addition to the simultaneous writing of the birefringence and topographic gratings, there are some other drawbacks for these materials, as for example, lifetime of the photoinduced birefringence. Unfortunately, despite the fact that experimental investigations of pure phase gratings have been reported, the lifetime of the

gratings was shown to be very short, which ranges from few seconds to several hours after special thermal treatment[4]. In other systems, long time memory has been demonstrated, however, it is strongly influenced by temperature and material parameters such as the glass transition point of the specific polymer.

In this chapter, we report on a study of thin permanent phase gratings recorded in Langmuir-Blodgett films composed of amphiphilic azo dye molecules using a polarization holographic technique. The proposed devices are free of the drawbacks described above. In fact, the polarization gratings written in our material are pure polarization gratings: AFM measurements do not show topographical reliefs formations. Moreover the phenomenon of photoinduced reorientation exhibits very long time stability, more than three years, because the films tend to become crystalline. Finally, the gratings are also temperature independent in a wide range[12]. The obtained polarization gratings, because of their extraordinary features, have been selected as basic element for a photopolarimeter which is able to measure simultaneously and in real time the Stokes parameters of an electromagnetic wave.

## 1.2 Polarization holograms

Pure phase gratings in thin film of azo compound material can be achieved using a polarization pattern obtained by a superposition of two waves with opposite circular polarization.

When two orthogonally circularly polarized beams with equal intensity overlay at a small angle $\alpha$, the resulting modulation pattern can be evaluated in the following way[9,12]: if $\vec{E}_L$ is the field of the left circularly polarized wave and $\vec{E}_R$ is the field of the right circularly polarized wave, the resulting field is linearly polarized but rotates along the grating wave vector with a constant angular frequency, and can be written as:

$$\vec{E}_{TOT} = \vec{E}_L + \vec{E}_R = \begin{bmatrix} E\exp(-i\theta(x)/2) \\ E\exp[i(\pi/2-\theta(x)/2)] \end{bmatrix} + \begin{bmatrix} E\exp(i\theta(x)/2) \\ E\exp[i(-\pi/2+\theta(x)/2)] \end{bmatrix} = 2E\begin{bmatrix} \cos\theta(x)/2 \\ \sin\theta(x)/2 \end{bmatrix}$$

where $\theta(x) = 2\sin(\alpha/2)\frac{2\pi}{\lambda}x = k\,x\sin(\alpha/2) = \frac{2\pi\,x}{\Lambda}$ is the phase difference at the location $x$ of the writing wave. The transmission matrix of the recorded polarization grating $T_P$ can be obtained as:

$T_P = R^{-1}TR$, where

$$R = \begin{bmatrix} \cos(\theta/2) & sen(\theta/2) \\ -sen\,(\theta/2) & \cos\,(\theta/2) \end{bmatrix}$$

describes a rotation through an angle $\theta/2$, and

$$T = \begin{bmatrix} \exp(i\Delta\phi) & 0 \\ 0 & \exp(-i\Delta\phi) \end{bmatrix}$$

is the transmission matrix that describes the linear birefringence, with $\Delta\phi = \frac{\pi\,\Delta n\,d}{\lambda}$, in which $\Delta n$ is the photo induced birefringence, $d$ is the thickness of the film and $\lambda$ is the wavelength of the writing waves. Finally, we obtain for the transmission matrix of the polarization grating $T_P$ the following form:

$$T_P = \begin{bmatrix} \cos(\Delta\phi) + isen(\Delta\phi)\cos\theta & isen(\Delta\phi)sen\theta \\ isen(\Delta\phi)sen\theta & \cos(\Delta\phi) - isen(\Delta\phi)\cos\theta \end{bmatrix}$$

If a monochromatic plane wave $\vec{E}_{IN} = \begin{pmatrix} \widetilde{E}_x \\ \widetilde{E}_y e^{i\delta} \end{pmatrix}$ arbitrarily polarized, in which $\widetilde{E}_x$ and $\widetilde{E}_y$ are the components of the field along the $x$ and $y$ axes, and $\delta$ is the phase difference between the two

components, impinges at normal incidence on the grating, using the above transmission matrix $T_P$ we obtain the expression of the light field just after the grating:

$$\vec{E}_{OUT} = T_P \vec{E}_{IN} = \begin{bmatrix} \cos(\Delta\phi) + isen(\Delta\phi)\cos\theta & isen(\Delta\phi)sen\theta \\ isen(\Delta\phi)sen\theta & \cos(\Delta\phi) - isen(\Delta\phi)\cos\theta \end{bmatrix} \begin{pmatrix} \widetilde{E}_x \\ \widetilde{E}_y e^{i\delta} \end{pmatrix} =$$

$$= \cos(\Delta\phi) \begin{pmatrix} \widetilde{E}_x \\ \widetilde{E}_y e^{i\delta} \end{pmatrix} + i\frac{sen(\Delta\phi)}{2} \begin{bmatrix} \exp(i\theta) + \exp(-i\theta) & i(\exp(-i\theta) - \exp(i\theta)) \\ i(\exp(-i\theta) - \exp(i\theta)) & -(\exp(i\theta) + \exp(-i\theta)) \end{bmatrix} \begin{pmatrix} \widetilde{E}_x \\ \widetilde{E}_y e^{i\delta} \end{pmatrix}$$

The terms containing $\exp(i\theta)$ and $\exp(-i\theta)$ represent the waves diffracted into the +1 and -1 orders, the term with $\cos(\Delta\phi)$ represents the zero order[12-14]. Using the Jones formalism, the three waves $\vec{E}_0$, $\vec{E}_{+1}$ and $\vec{E}_{-1}$ can be written as:

$$\vec{E}_0 = \cos(\Delta\phi) \begin{pmatrix} \widetilde{E}_x \\ \widetilde{E}_y e^{i\delta} \end{pmatrix} \tag{1.1}$$

$$\vec{E}_{+1} = i\frac{sen(\Delta\phi)}{2} \left(\widetilde{E}_x - i\widetilde{E}_y e^{i\delta}\right) \begin{pmatrix} 1 \\ -i \end{pmatrix} \tag{1.2}$$

$$\vec{E}_{-1} = i\frac{sen(\Delta\phi)}{2} \left(\widetilde{E}_x + i\widetilde{E}_y e^{i\delta}\right) \begin{pmatrix} 1 \\ i \end{pmatrix} \tag{1.3}$$

It is possible to see that the zero order wave is the same as the incident wave except for the amplitude factor $\cos(\Delta\phi)$; moreover the +1 order is a left circularly polarized wave, but it is proportional to the right component of the incident wave; the -1 order is a right circularly polarized wave, but it is proportional to the left component of the incident wave. For linearly polarized probe beam, the intensities of the first orders are equal

$$I_{+1} = I_{-1} = I_0 \frac{(\sin\Delta\phi)^2}{2}$$

and the corresponding diffraction efficiencies, defined as the ratio of the first diffracted beam intensity to the total incident intensity, are

$$\eta_{+1} = \eta_{-1} = \frac{I_{+1}}{I_0} = \frac{I_{-1}}{I_0} = \frac{(sen\,\Delta\phi)^2}{2}.$$

If the probe beam is left (or right) circularly polarized, the intensity and the diffraction efficiency of the +1 (-1) order is 0, whereas for the -1 (+1) order the diffracted beam is right (left) circularly polarized with intensity $I_{-1} = I_{+1} = I_0\,(sen\Delta\phi)^2$ and diffraction efficiency $\eta_{-1,+1} = (sen\Delta\phi)^2$. For an elliptical polarization state of the probe beam we observe a different intensity of the two diffracted beams, but their sum $\eta_{+1} + \eta_{-1}$ remaining constant. Due to the above described behaviour of the grating we can conclude that this kind of device is able to recognize the polarization state of a light beam that impinges on it. The transmitted waves obtained in the polarization grating are multiplied for the amplitude factors, $\cos(\Delta\phi)$ in the zero order wave and $sen(\Delta\phi)/2$ in the $\pm 1$ orders waves: they describe the characteristic of the material used and the variations induced by the writing electric field.

## 1.3 Material and experimental results

### 1.3.1 Material

The material selected for the polarization grating is an azo compound (dye), characterized by high photoinduced optical anisotropy and long time stability of the chromophores reorientations[12,14]. The basic mechanism responsible for the storage in organic materials as side-chain azobenzene and azo-dye guest-host polymer systems is a statistical polarized light-induced reorientation of the azobenzene chromophores, promoted by the trans-cis-trans isomerization cycles[15]. The chemical formula of a generic azo-compound with the trans and cis isomers is shown in figure 1.1:

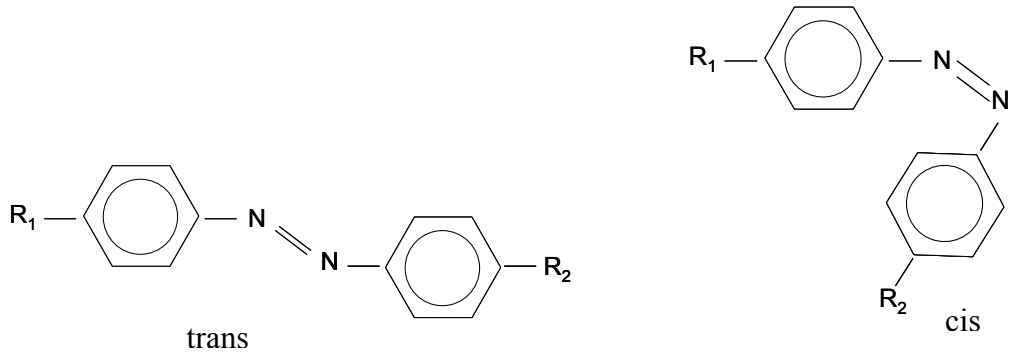


**Fig 1.1** Chemical formula of a generic azo-compound in the trans and cis state.

The molecule consist of an azo-benzene core and terminal constituents $R_1$ and $R_2$. The role of the azobenzene core is crucial: under illumination, it manifests reversible trans-cis-trans isomerization. Photoisomerization is the reversible chemical transformation of a material due to photon absorption, in two different states, trans and cis. After photoisomerization the dye molecule has optical properties distinct from those in its original ground state: for example, the trans and cis states present different absorption spectra. This photochemical reaction changes only the spatial configuration of the molecule, as demonstrated in figure 1.1. The exact mechanism behind the trans-cis isomerization is not completely understood: both a rotation around the excited N=N bond and an inversion mechanism may be activate in the azobenzene photoisomerization. Whereas the direct reaction trans-cis is induced by light, the inverse reaction cis-trans can take place both photo-chemically or thermically or verifies spontaneously.

Isotropic dye molecules absorb a photon with equal probability for arbitrary spatial orientation of the linear input polarization. When all the dye molecules at a given location have been isomerised, then no further optically induced transformation can occur. This phenomenon is called saturation, and for isotropic molecules, the saturation is polarization and orientation independent; it depends only on intensity of the light[9]. For a highly anisotropic dye molecule, the absorption cross section depends on the molecule orientation relative to the polarization direction of the light, in addition to its saturating dependence on light intensity. In particular, for anisotropic molecules, the transition probability from the fundamental state to the excited state is proportional to $\left|\vec{\mu}_{trans} \cdot \vec{E}\right|^2$, where $\vec{\mu}_{trans}$ is the transition dipole moment of molecule, and $\vec{E}$ is the electric field. Then, when the principal absorption oscillator axis of dye molecule is parallel

to the incident polarization direction, the probability for the molecule of absorbing a photon is the highest; the probability is lowest when the oscillator axis is perpendicular to the polarization direction. As a result of this anisotropic transition probability, for uniform orientational distribution, more dye molecules whose absorption axes are parallel to the polarization direction are isomerized than molecules that have other absorption axis orientation. Qualitatively, the explanation of the photoinduced optical orientation can be as follows: because the cis state is thermally unstable at room temperature, the molecules spontaneously go back in the trans state, with the molecular axis oriented casually[18,19]. For prolonged expositions, therefore, the molecules undergo numerous cycles trans-cis-trans. This situation continues until the molecules reorient with the axis orthogonal to the polarization direction: in this case, the molecule have lower probability to be excited. The final result is that the molecules are preferentially oriented with their axis perpendicular to the polarization direction. In conclusion, photoisomerization is the basic mechanism for the photo induced reorientation of chromophores under action of polarized light and appearance of the corresponding photoinduced optical anisotropy[9,15,16].

The role of the constituents $R_1$ and $R_2$ in the azo dye molecule is also very important: if $R_1$ possesses donor electron properties and $R_2$ is an electron acceptor, the absorption spectrum of the compound is shifted to the longer waves with respect to the azobenzene, and the compound is referred to as a dye. On the other hand, if at least one of constituents is a hydrophobic tail, a molecules becomes amphiphilic and capable to form dense monolayers on the water surfaces which can be transferred onto a solid substrate by the Langmuir-Blodgett or Langmuir-Schaefer technique.

The material selected for the grating storage is an azo-dye, MEL63, with very high photoinduced birefringence, $\Delta n = 0.4$, and very long time stability of the chromophores reorientation phenomenon[16,19]. The chemical formula of the azo compound is shown in the figure 1.2:

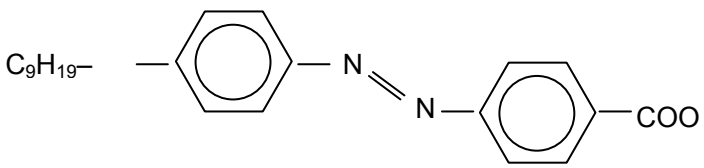


**Fig 1.2** Chemical formula of MEL63.

This molecule absorbs light strongly in the spectral region $400-520nm$. The molecule contains an azobenzene core, a polar tail $(-COOH)$ with electron acceptor properties and a hydrophobic tail $(-NHC_9H_{19})$ with electron donor properties. Because the dye molecules spontaneously form crystallized films on a water surfaces, we use the Langmuir-Schaefer method to prepare multilayer films. In fact, the films are prepared by using successive transfer of monomolecular layers from the water surface onto glass substrate[16]. A procedure that gives good homogenous films is obtained using a limited spreading area on water, about $400cm^2$, and using the compound in 0.01% solution of chloroform. The dye molecules show high reflectivity in the visible region of the spectrum, so during spreading one can easily observe the crystallization process. This crystallized film increasingly occupies the free area when more material is added. The spreading procedure is stopped when the film covers almost all the available surface. Microscope analyses and *X*-ray measurements are performed in order to characterize the obtained film: microscope observation between crossed polarizers show domain structures of about $0.5\mu m$ in size and with optical axes randomly distributed in the plane of the film. *X*-ray measurements show layered structure of period $18.5A$, parallel to the substrate[9]. It is evident that it is possible to obtain a particular film thickness, transferring onto the glass substrate an opportune number of layers. In our experiment, we used a film consisting of 50 monolayers, with a thickness of $110nm$.

## 1.3.2 Experiment

Pure phase gratings in thin film of azo compound material can be achieved using a polarization holographic technique, exposing the photosensitive films to the interference pattern obtained by a superposition of two waves with opposite circular polarization. In this experimental geometry, the pattern corresponds to a uniform rotation of the electric vector along the grating wave vector, while the intensity distribution is quite uniform. Figure 1.3 shows the pattern produced by the two interfering beams and the experimental set-up used for the storage:

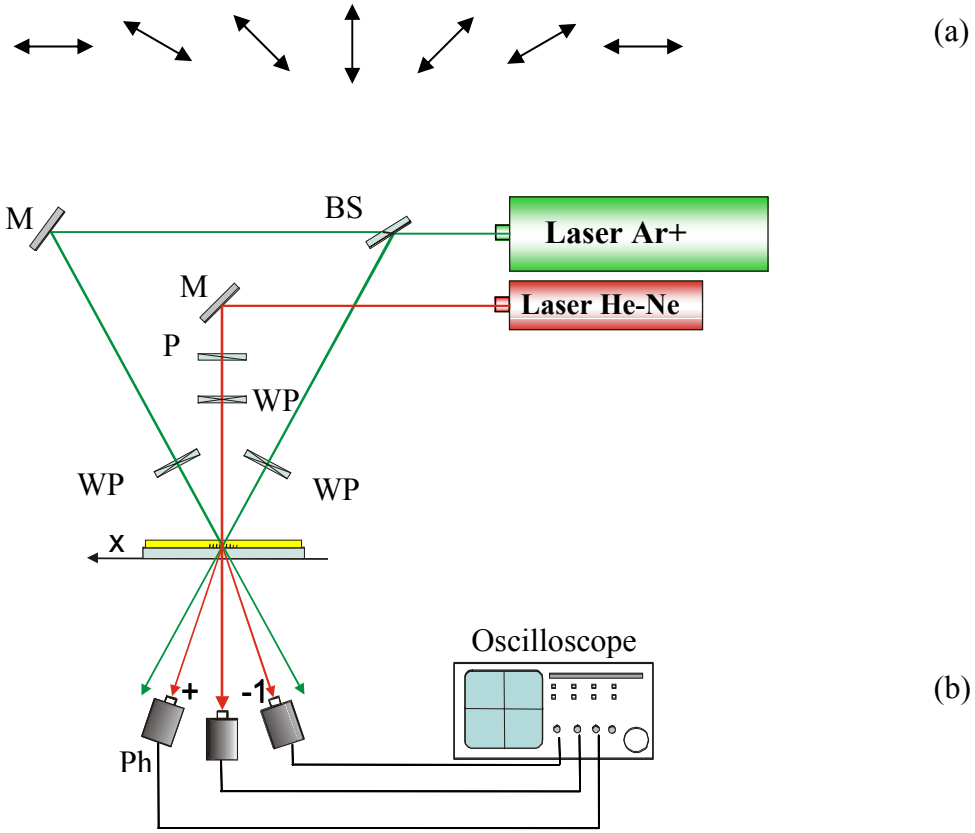


**Fig 1.3** Pattern produced by two opposite circular interfering beams (a). Experimental set-up used for the holographic writing (b). BS beam splitter; M mirror; WP wave plate; P polarizer; Ph photodiode.

Two circularly polarized left and right laser beams with wavelength $\lambda = 514\,nm$ with equal intensities and crossing at an angle $\alpha \approx 7.4^{\circ}$ impinge on the film in the superposition region. The periodicity of the gratings is $\Lambda \approx 4\mu m$. The permanent polarization holographic gratings are recorded at $200-300\,mW/cm^2$ light power density and $30\,s$ exposure time. Under these conditions no topographical reliefs are formed as shown by AFM measurements. A He-Ne laser beam with linear, circular and elliptical polarization was used as a probe beam in order to investigate the light fields diffracted by the grating. The probe beam does not influence the recorded gratings because it is not absorbed by the azo dye.

## 1.3.3 Results

In order to verify that the photoinduced polarization gratings are pure phase one, the analysis of the polarization states of the beams diffracted by the recorded structure has been done for different polarization states of the impinging probe beam. The polar plots displayed in figure 1.4 represent the polarization analysis of the diffracted beams when the probe is linearly polarized: the +1 and -1 orders have equal intensity, as shown in the graph, and both polarizations are circular, left and right respectively. The diffraction efficiency is $\eta_{+1} = \eta_{-1} = 0.02$.

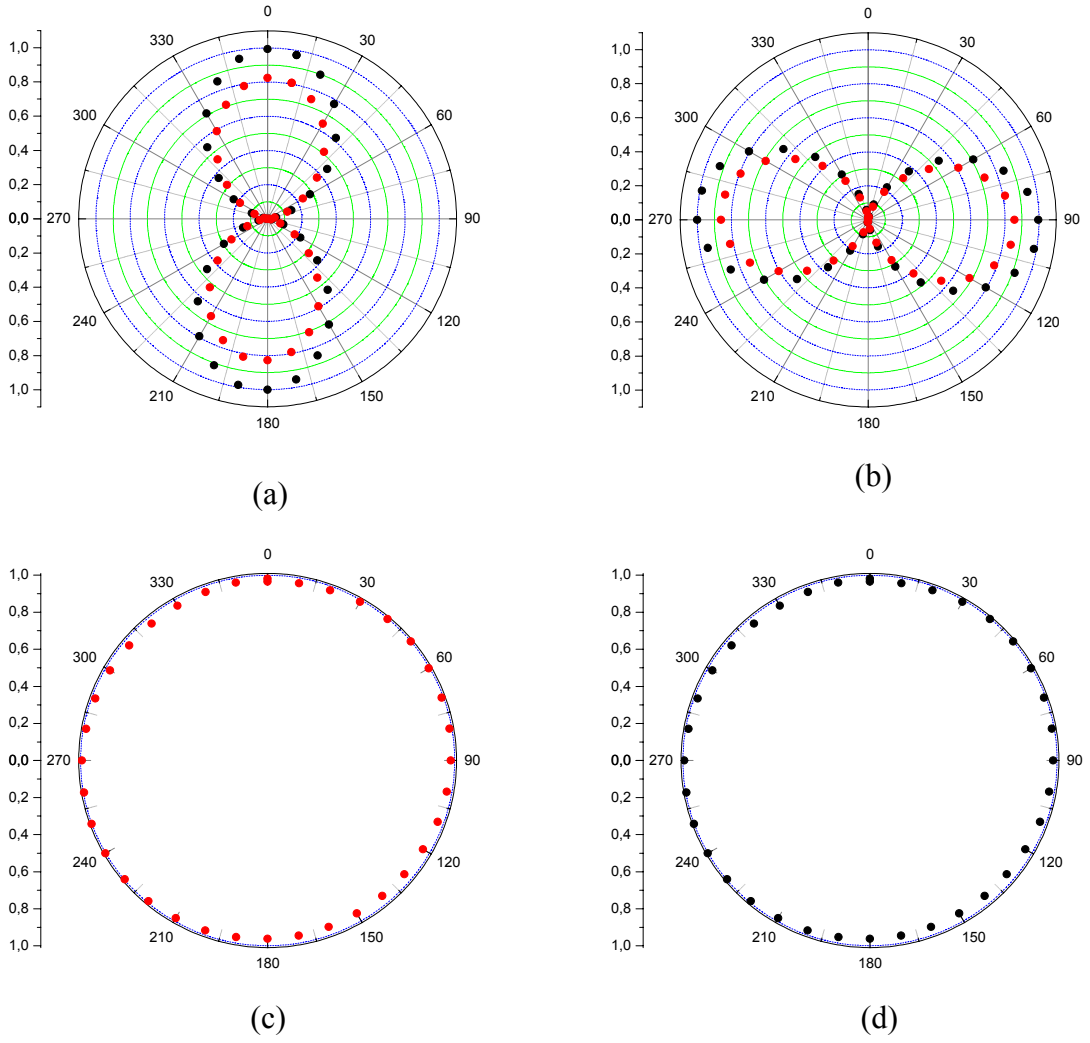


**Fig 1.4** Polarization analysis of the normalized intensities of the linear s and p incident beams (black circles) (a) and transmitted zero order beam (red circles) (b); in figure (c) and (d) are reported the diffracted +1 (black circles) and -1 (red circles) orders.

For the left circularly polarized probe beam, only the right circularly polarized -1 order appears with efficiency $\eta_{-1} = 0.04$. Correspondingly, for the right circularly polarized probe beam, only the left circularly polarized +1 order is visible with the same diffraction efficiency $\eta_{+1} = 0.04$. Complete information on the polarization state of diffracted beams has been obtained using a Four Detectors Polarimeter.

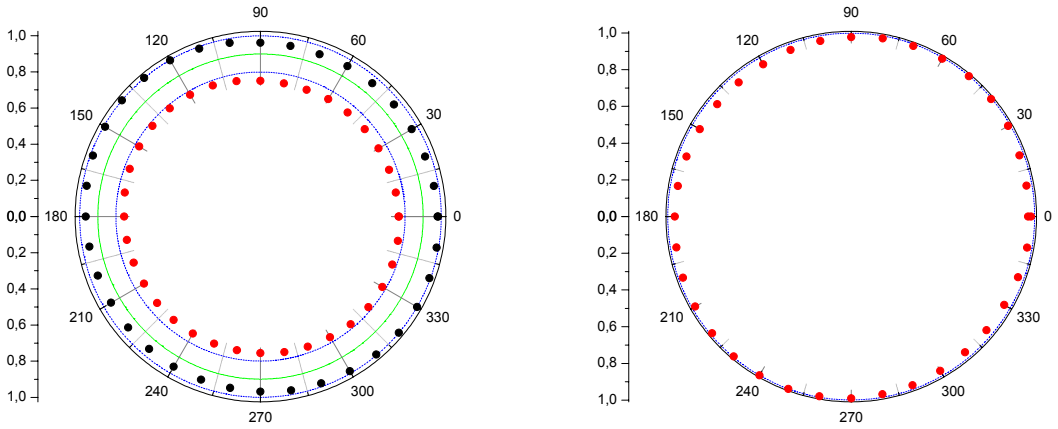


**Fig 1.5** Polarization analysis of the normalized intensities of the left circular incident beam (black circles) and transmitted zero order beam (red circles) (a); in figure (b) is reported the diffracted -1 (red circles) orders.

The results show that for different polarization states of the incident beam energy exchange between the two diffracted orders are observed, with constant $\eta_{+1} + \eta_{-1}$. The layered structure, obtained by means of Langmuir-Blodgett deposition technique, seems to obstruct the topographic reliefs formation, under the experimented writing conditions. In this way, we can obtain pure polarization gratings, with the peculiarities in the diffraction properties that we have described.

The gratings written on MEL63 do not change over time, at least three years there was no traces of degradation. In fact, after a certain time, the film becomes crystalline: this fact is a drawback for the rewriting, because the azo compound systems can be easily erased and successively restored, but, for our purposes, crystallization represents a very important feature. In fact, the stability of the recorded gratings and the high induced birefringence of the material, open up the

possibility of interesting applications of the gratings to different optical devices: in the next section, we will describe a photopolarimeter achieved using the polarization grating as basic element[8].

## 1.4 Application: photopolarimeter

This section deals with the design and realization of a new photopolarimeter able to measure simultaneously and in real time the Stokes parameters of an electromagnetic wave, in order to evaluate its polarization state. Photopolarimeter is based on the acquisition of four signals, obtained with appropriate separation of the investigated beam. Stokes parameter $S_i$ are calculated from the measured values $I_j$ of these four intensities, according to the relation $S_i = A_{ij} I_j$, where $A_{ij}$ is the matrix describing the device.

Several instruments are developed that allow to perform measurements of the Stokes parameters[20-25].

Basic elements of the proposed photopolarimeter are two diffraction gratings, through which it is possible to separate the investigated beam in the required four beams. For this reason we called our device Two Gratings Photopolarimeter (TGP). In particular, one of the two gratings, is the polarization grating described above, obtained by means of a polarization holographic recording, on a photosensitive azo-compound, while, the other is an ordinary transmission grating obtained by means of an intensity holographic technique, based on the interference of two waves with parallel polarization states, on a thin layer of acrylate monomeric mixture.

Compared with other devices employed in polarimetric measurements, TGP present several advantages, as for example: the compactness of the structure, that do not require any modulating optics or moving parts; a very short measurement time, related only to the speed of the detectors and electronics; a great facility to align the device; absence of complex calibration procedures. In addition, because the instrument is based on diffraction gratings, it allows operation with white-light source to provide spectral information. Optical alignment of the photopolarimeter is fast and very easy, and the calibration procedure is performed with a single measurement of a linearly polarized beam, of known intensity and wavelength. The easiness of the calibration procedure is related to the fact that, the polarization grating is able to recognize the polarization

state of the investigated light. Finally, a LabView code that manages acquisition, elaboration and memorization processes has been developed, which makes the photopolarimeter very fast and user friendly.

However we need to mention that several devices [23,24] that allow to perform real-time measurements of the Stokes parameters have been developed in the last years. Nevertheless, the devices proposed have some limitations and drawbacks. Some of them are difficult to align and often need a complex calibration procedure[20-21]. Other one based on diffraction gratings with the same scheme of the instrument proposed in this work, present some intrinsic stability limits.

Our device introduces relevant improvements and makes the instrument free of the drawbacks mentioned above.

## 1.4.1 The polarization of the electromagnetic waves

In the electromagnetic theory of light, beams of light are represented by electromagnetic waves propagating in the space. The polarization state of the wave describes the temporal behaviour of the vector associated to the wave, when the vector is observed from at a fixed point in space. The polarization state of the light is in general elliptical. A complete description of an elliptical polarization includes the orientation of the ellipse in its plane, its shape and the sense in which it is described. The parameters that describe the ellipse in its plane are:

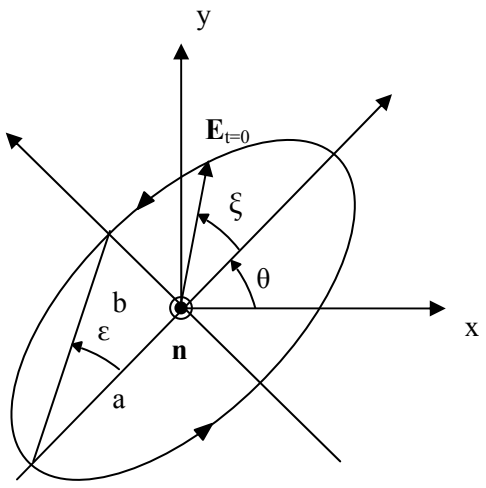


**Fig 1.6** The four parameter that define the ellipse of polarization: the azimuth $\theta$, the ellipticity $e = \pm b/a = \pm \tan \varepsilon$ , the size , and the phase absolute $\xi$ .

the azimuth $\theta$, the angle between the major axis of the ellipse and the positive direction of the $x$ axis; the ellipticity $e = \pm b/a$, where $a$ and $b$ are the half lengths of the principal axes of the ellipse; the size of the ellipse can be defined in terms of the lengths $a$ and $b$ of the principal axes as $A^2 = \left(a^2 + b^2\right)$ ; the handedness that determines the sense of revolution in which the ellipse is described. In particular, the polarization is right-handed (left-handed) if the endpoint of the electric vector will revolve in a clockwise (counter-clockwise) direction. It is mathematically convenient to incorporate the handedness in the definition of ellipticity, by allowing the ellipticity to assume positive and negative values, to correspond to right-handed and left-handed polarization respectively. Using this notation, it is easily seen that all physical ellipticity values can be obtained by limiting $e$ to the range $-1 \le e \le 1$. We will find convenient to introduce an ellipticity angle $\varepsilon$ such that $e = \tan\varepsilon$.

We have seen that the elliptical polarization is most general state of polarization of any optical field; circular and linear states of polarization are special cases of the more general state of elliptical polarization. In particular, a beam is said to be linearly polarized if the electric field vector vibrates in a constant direction in the $xy$ plane and a beam is said to be circularly polarized if the electric field vector undergoes uniform rotation in the $xy$ plane. According to our convention, the circular and linear states of polarization are generated when the ellipticity $e$ takes the special values of $\pm 1$ and 0, respectively, that is, the value $e = +1$ corresponds to the right-handed circularly polarized state; the value $e = -1$ corresponds to the left-handed circularly polarized state; when $e = 0$ the light wave is linearly polarized[25,26].

Now we discuss an important polarization space in the form of a spherical surface whose points are in one-to-one correspondence with the different states of polarization of light. This spherical polarization space is referred to as Poincaré sphere. The properties of the Poincaré sphere can be summarized in a single statement: a polarization state of light characterized by an azimuthal angle $\theta$ and an ellipticity angle $\varepsilon$ is represented on the surface of the Poincaré sphere by a point whose longitude is equal to $2\theta$ and whose latitude is equal to $2\varepsilon$ (see figure 1.7).

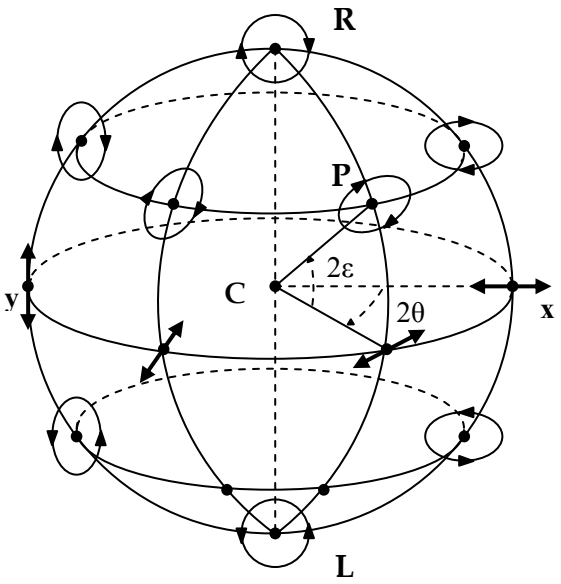


**Fig 1.7** Poincaré's representation of the state of polarization of a monochromatic wave.

Consider a Cartesian coordinate system $S_1S_2S_3$ at the centre $C$ of the sphere, with the $S_3$ axis direct from the south pole to the north pole and orthogonal to the plane formed by $S_1$ and axes $S_2$.

If $S_0$ is the radius of the sphere, the polar coordinates of a point P on the spherical surface are given by:

$$S_1 = S_0 \cos 2\varepsilon \cos 2\theta \tag{1.4}$$

$$S_2 = S_0 \cos 2\varepsilon \, sen 2\theta \tag{1.5}$$

$$S_3 = S_0 sen 2\varepsilon \tag{1.6}$$

$S_0, S_1, S_2, S_3$ are the Stokes parameters, a set of four real quantities, each of which has the dimensions of intensity, by means it is possible to describe all the possible polarization states of a transverse electric monochromatic wave of light. In terms of the Cartesian components of the transverse electric field, the four Stokes parameters are defined as follows[25,26]:

$$S_0 = \widetilde{E}_x^2 + \widetilde{E}_y^2 \tag{1.7}$$

$$S_1 = \widetilde{E}_x^2 - \widetilde{E}_y^2 \tag{1.8}$$

$$S_2 = 2\widetilde{E}_x \widetilde{E}_y \cos\delta \tag{1.9}$$

$$S_3 = 2\widetilde{E}_x \, \widetilde{E}_y \, sen\,\delta \tag{1.10}$$

The right-handed polarization is represented by points on the sphere which lie above the equatorial plane and left-handed polarization by points on the sphere which lie below this plane. Linear polarization is represented by points in the equatorial plane. Right-handed circular polarization is represented by the north pole, and left-handed circular polarization by the south pole. From equation (1.7) it is evident that the parameter $S_0$ gives the total intensity of the light wave, and therefore it is always positive. $S_1$ as defined in the equation (1.8) gives the difference between the intensities of the $x$ and $y$ components and can be either positive, negative or zero, depending on whether the wave has stronger preference to the $x$ linear polarization, to the $y$ polarization, or to neither one of these two states, respectively. The Stokes parameter $S_2$, as defined in the equation (1.9), represents the preference of the wave to have either the $+\pi/4$ or the $-\pi/4$ linearly polarized component. If $S_2$ is positive the wave has stronger preference to the $+\pi/4$ linear polarization; if $S_2$ is negative the wave has stronger preference to the $-\pi/4$ linear polarization; if $S_2$ is zero the wave has no preference to either one of these two polarization. The Stokes parameter $S_3$, as defined in the equation (1.10), represents the preference of the wave to have either the right-handed or the left-handed circularly polarized component. $S_3$ is positive, negative or zero, dependent on the wave possessing stronger preference to the right-circular state, the left-circular sate or to neither one of these two states[25].
The above discussion on the significance of the Stokes parameters suggests a simple experiment by which they may be measured for a given wave. In particular, if $I_0$ is the total intensity of the wave, and $I_x, I_y, I_{+\pi/4}, I_{-\pi/4}, I_r$ and $I_l$ represent the intensities transmitted by an ideal variable polarized placed in the path of the wave and adjusted to transmit the $x$, $y$, $+\pi/4$ and $-\pi/4$ linear polarization and left and right circular polarization, respectively, in terms of these intensities, the Stokes parameters are given by:

$$S_0 = I_0 = \left(I_x + I_y\right) = \left(I_{+1/4\pi} + I_{-1/4\pi}\right) = \left(I_l + I_r\right)$$

$$S_1 = \left(I_x - I_y\right)$$

$$S_2 = \left(I_{+\pi/4} - I_{-\pi/4}\right)$$

$$S_3 = \left(I_l - I_r\right)$$

The azimuth $\theta$ and the ellipticity angle $\varepsilon$ of the ellipse of polarization can be written in terms of Stokes parameters as[25]:

$$\theta = \frac{1}{2}\arctan\frac{S_2}{S_1} \qquad \varepsilon = \frac{1}{2}arcsen\left[\frac{S_3}{\left(S_1^2 + S_2^2 + S_3^2\right)^{1/2}}\right].$$

## 1.4.2 Two Gratings Photopolarimeter

In the last section we have seen that the polarization state of the light can be suitably described by means of the Stokes parameters: for this reason, most polarimeters are destined to their measurement. Now we describe the operation principles of our photopolarimeter TGP, which are strictly related to the theoretical properties of two diffraction gratings.

Starting from the polarization grating that we have described in the previous sections, we show that the separation performed by this device can be used for evaluation of the Stokes parameters of a light beam. Recalling that the Stokes parameters can be written in terms of the Cartesian components of the transverse electric field as in (1.7)-(1.10)

$$S_0 = \widetilde{E}_x^2 + \widetilde{E}_y^2$$

$$S_1 = \widetilde{E}_x^2 - \widetilde{E}_y^2$$

$$S_2 = 2\widetilde{E}_x \widetilde{E}_y \cos\delta$$

$$S_3 = 2\widetilde{E}_x \widetilde{E}_y \, sen\,\delta$$

we suppose that the beam that is to be analyzed is sent through the polarization grating, and that the intensities of 0, +1 and -1 orders are measured. The intensities of the +1 and -1 orders are equal to (see equations (1.2) and (1.3)):

$$I'_{+1} = \frac{1}{16}\left(\widetilde{E}_x^2 + \widetilde{E}_y^2 + 2\widetilde{E}_x\widetilde{E}_y \sin\delta\right) \tag{1.11}$$

$$I'_{-1} = \frac{1}{16}\left(\widetilde{E}_x^2 + \widetilde{E}_y^2 - 2\widetilde{E}_x\widetilde{E}_y \sin\delta\right) \tag{1.12}$$

We suppose that the transmitted beam passes trough an ordinary polarizer set at an angle $\beta$ respect to the $x$ axis: the field transmitted by the polarizer is equal to

$$E'(\beta) = E_x \cos\beta + E_y sen\beta$$

In our case we have (see equation (1.1))

$$E'_0(\beta) = \frac{\widetilde{E}_x}{2}\cos\beta + \frac{\widetilde{E}_y\, e^{i\delta}}{2} sen\beta$$

whose intensity is equal to

$$I'_0(\beta) = \frac{1}{4}\left(\widetilde{E}_x^2 \cos^2\beta + \widetilde{E}_y^2 \sin^2\beta + \widetilde{E}_x\widetilde{E}_y \sin 2\beta \cos\delta\right)$$

From the last expression it is easy calculate the intensity for $\beta = 0$ and $\beta = \pi/4$:

$$I'_0(0) = \frac{1}{4}\widetilde{E}_x^2 \tag{1.13}$$

$$I'_0(\pi/4) = \frac{1}{8}\left[\widetilde{E}_x^2 + \widetilde{E}_y^2 + 2\,\widetilde{E}_x\widetilde{E}_y \cos\delta\right] \tag{1.14}$$

Using (1.11), (1.12), (1.13), (1.14), we can rewrite the Stokes parameters in terms of the measured intensities as

$$S_0 = 8(I'_{+1} + I'_{-1}) \tag{1.15}$$

$$S_1 = 8[I'_0(0) - I'_{+1} - I'_{-1}] \tag{1.16}$$

$$S_2 = 4[I'_0(\pi/4) - I'_{+1} - I'_{-1}] \tag{1.17}$$

$$S_3 = 4(I'_{+1} - I'_{-1}) \tag{1.18}$$

By setting the polarizer at the two values $\beta = 0$ and $\beta = \pi/4$, and measuring the corresponding intensities of the undiffracted beam together with the intensities of the first order beams, we can obtain the Stokes parameters and consequently to know the polarization state of the investigated beam. The device works equally well at any wavelength. In fact, the only effect of the wavelength change is the different direction of the first order diffracted beams.

## 1.4.3 Ordinary transmission grating

In order to make a real time measurement of the Stokes parameters, avoiding the sequential determinations of the transmitted beam intensities after its passage through the linear polarizer at the angles $\beta = 0$ and $\beta = \pi/4$, we need a diffraction grating whose diffracted beams must reproduce exactly the polarization state of the incident light, as in the case of reference 23, 24. This grating have to behave as a medium whose optical properties, as for example the refractive index $n$, change periodically along $x$. The Jones matrix describing this device is

$$T = \begin{bmatrix} \exp(i\Delta\varphi\cos(2\pi x/\Lambda)) & 0 \\ 0 & \exp(i\Delta\varphi\cos(2\pi x/\Lambda)) \end{bmatrix}$$

where the term $\cos(2\pi x/\Lambda)$ describes the spatial periodicity of the grating, and $\Delta\varphi = \frac{\pi \Delta n d}{\lambda}$ contains the information related to the refractive index, $d$ is the thickness of the grating[25]. If an incident wave $\begin{bmatrix} \widetilde{E}_x \\ \widetilde{E}_y e^{i\delta} \end{bmatrix}$ impinges on the grating, the diffracted beams can be calculated as:

$$\vec{E}_{out} = T\vec{E}_{in} = \begin{bmatrix} \exp(i\Delta\varphi\cos(2\pi x/\Lambda)) & 0 \\ 0 & \exp(i\Delta\varphi\cos(2\pi x/\Lambda)) \end{bmatrix} \begin{bmatrix} \widetilde{E}_x \\ \widetilde{E}_y e^{i\delta} \end{bmatrix} =$$

$$= \begin{bmatrix} \widetilde{E}_x \exp(i\Delta\varphi\cos(2\pi x/\Lambda)) \\ \widetilde{E}_y e^{i\delta} \exp(i\Delta\varphi\cos(2\pi x/\Lambda)) \end{bmatrix}$$

The amplitudes of the transmitted beams are equal to

$$E_m = A_i (i)^m J_m(\Delta\varphi)$$

where $A_i$ are the amplitude of the field components and $J_m(\Delta\varphi)$ is the $m$-th Bessel function of the first kind.

For $m = 0$ $\quad E_0 = A_i J_0(\Delta\varphi)$, (1.19)

$m = +1$ $\quad E_{+1} = i\, A_i J_{+1}(\Delta\varphi)$, (1.20)

$m = -1$ $\quad E_{-1} = -i\, A_i J_{-1}(\Delta\varphi)$. (1.21)

It is possible to demonstrate that, for small values of $\Delta\varphi$, the Bessel functions of first kind can be approximated to

$$J_m(\Delta\varphi) \approx \frac{1}{m!}\left(\frac{\Delta\varphi}{2}\right)^m$$

Taking into account the last expression and considering that for integer values of $m$ is valid the relation

$$J_{-m}(\Delta\varphi) = (-1)^m J_m(\Delta\varphi)$$

the equations (1.19), (1.20), and (1.21) become:

$$\vec{E}_0 \approx \begin{pmatrix} \widetilde{E}_x \\ \widetilde{E}_y e^{i\delta} \end{pmatrix}$$

$$\vec{E}_{+1} \approx i\begin{pmatrix} \widetilde{E}_x \\ \widetilde{E}_y e^{i\delta} \end{pmatrix}\left(\frac{\Delta\varphi}{2}\right)$$

$$\vec{E}_{-1} \approx i\begin{pmatrix} \widetilde{E}_x \\ \widetilde{E}_y e^{i\delta} \end{pmatrix}\left(\frac{\Delta\varphi}{2}\right)$$

From the previous equations it is evident that the polarization states of the transmitted and the diffracted beams are equal to the incident beams.

In our device, the second grating used has been recorded in a thin film of a photocrosslinkable monomeric mixture by means of an intensity holographic technique. UV curing is typically used to transform a multifunctional monomer mixture into a crosslinked polymer by a chain reaction initiated by reactive species, as free radicals or ions, which are generated by UV irradiation[27]. Most monomers do not produce initiating species with sufficiently high yields when they are exposed to UV light, so that a photoinitiator must be added to the mixture. Once initiated, the chain reaction will develop very much, following a process that can be represented schematically in the figure:

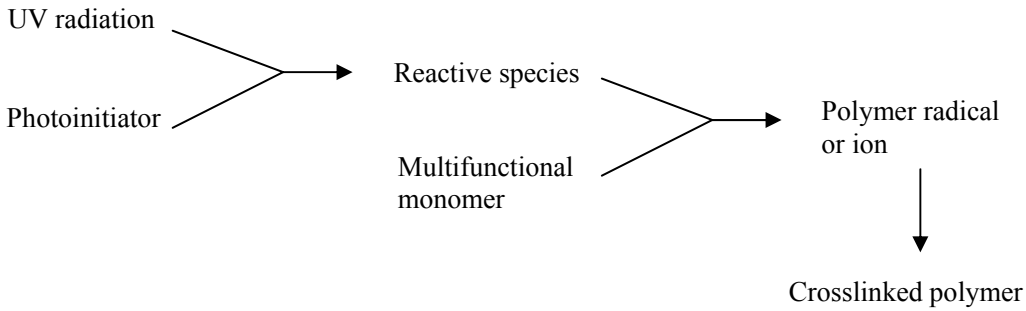


**Fig 1.8** Schematic representation of photopolymerization reaction.

The material selected for the grating storage consists of a prepolymer mixture composed by the monomer Dipentaerytrol Hydroxy Penta Acrylate (DPHPA), N-Vinylpyrrolidone (NVP) with 10wt.%, *N*-phenylglycine $10^{-3} M$ , and the photoinitiator 2,2-dimethoxy-2-phenylacetophenone $10^{-4} M$ [28,29]. For a correct functioning of the photopolarimeter, the ordinary transmission grating must preserve the polarization state of the incident beam in the diffraction. This is possible only if an isotropic structure is induced by the light exposure. The isotropy of the structure is strictly related to the intensity pattern used for the storage: the holographic technique is based on the interference of two waves having parallel circular polarization states, which gives rise to a periodic intensity modulation, in which light and dark regions alternate. Since the photopolymerization is activated only in the regions where the electromagnetic field is present, the periodic structure is due to a spatial modulation in the degree of polymerization. In order to obtain an isotropic grating, it is important that no anisotropy in the photoinduced polymerization occurs. This condition has been guaranteed since total field in the interference pattern presents everywhere a circular polarization state, which avoids any photoinduced alignment. Another important requirement is the long time stability. In fact, since the photopolymerization reaction is activated only in the illuminated regions, in the dark regions, the mixture of monomers reacts much more slowly and, hence, is more sensitive to temperature variations as well as by ambient light. For this reason we used a mixture with photoinitiator in the UV range, which is not sensitive to the visible light. Furthermore, for the materials that we have selected, the thermal activation of the polymerization is negligible in a wide range. The experimental set-up used for the storage is the same reported in figure 1.3b, but in this case, the polarization states of the

writing waves are parallel. The cell was assembled putting $8\mu m$ thick Mylar spacers between two glass substrates and gluing them with epoxy resin from the outside. The cell was filled with the above described mixture. Film polymerization was induced by means of exposure to the interference pattern of two left circularly polarized laser beams at $\lambda = 352\,nm$, with equal intensities and crossing angle of $7.2°$. In this configuration the polarization state is everywhere circular, and a deep modulation of the light intensity distribution occurs. As discussed above, this writing configuration has been chosen to avoid any photoalignment effect and to allow an isotropic growth of the polymer chains. The grating is permanently recorded by exposing the film for 300 s. A test of the transmitted beams has been performed to verify the correct behaviour of the grating, i.e., the requirement that transmitted and diffracted beams preserve the polarization state of the incoming beam, and that their intensities are independent of the polarization state of the incident beams. The polar plots displayed in Fig. 1.9 represent the polarization analysis of the transmitted and diffracted beams when the probe is circularly polarized:

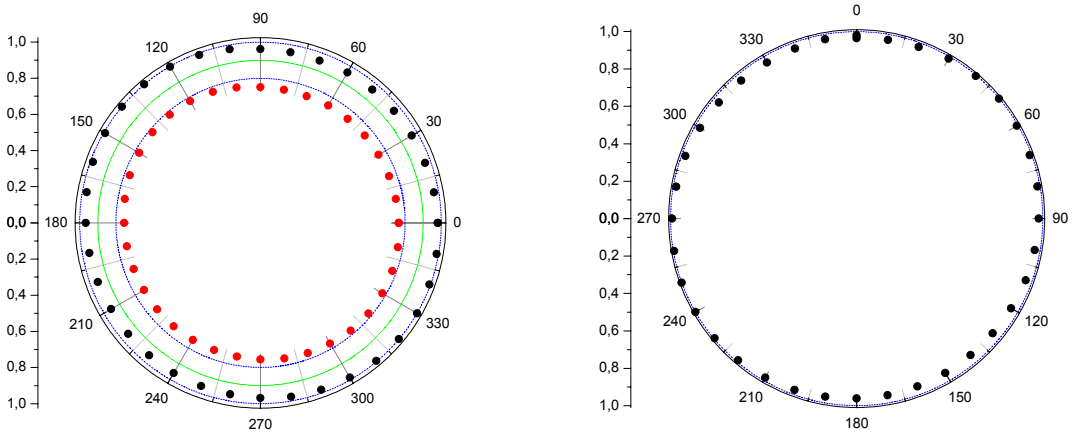


(a) (b)

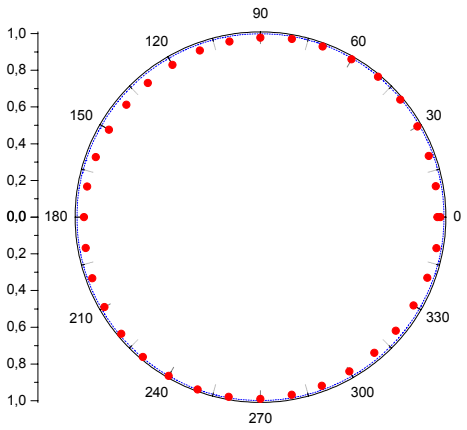


(c)

**Fig 1.9** Polarization analysis of the normalized intensities of the left circular incident beam (black circles) and transmitted zero order beam (red circles) (a); in figure (b) is reported the diffracted -1 (black circles) order; in figure (c) is reported the diffracted +1 (red circles) order.

As demonstrated by the polar graphs, we can see that the ordinary transmission grating does not change the polarization states of the incident wave. Moreover, the diffraction efficiency of the horizontal polarized (p) probe beam is equal to the efficiency of the vertically (s) polarized one. Furthermore, the gratings written do not change over time.

## 1.4.4 Functioning principle of the TGP

Starting from the peculiarities of these two different gratings, it is possible to obtain a photopolarimeter for real time measurements of the four elements of the Stokes vector. We have demonstrated that it is possible to calculate the Stokes parameters of a light beam using only the polarization grating, measuring first the intensities of the firsts orders diffracted beams $I_{+1}$ and $I_{-1}$ and successively the intensities $I_0(0)$ and $I_0(\pi/4)$ of the transmitted beams after the passage though the linear polarizer. Evidently this is a sequential measurement; in order to overtake this limitation, we put the ordinary transmission grating in succession to the polarization grating. In this way, the 0 order diffracted beam of the polarization grating is diffracted by the ordinary

transmission grating, and the first orders diffracted beams present the same polarization state of the impinging beam.

A scheme of the two-gratings photopolarimeter is shown in figure 1.10

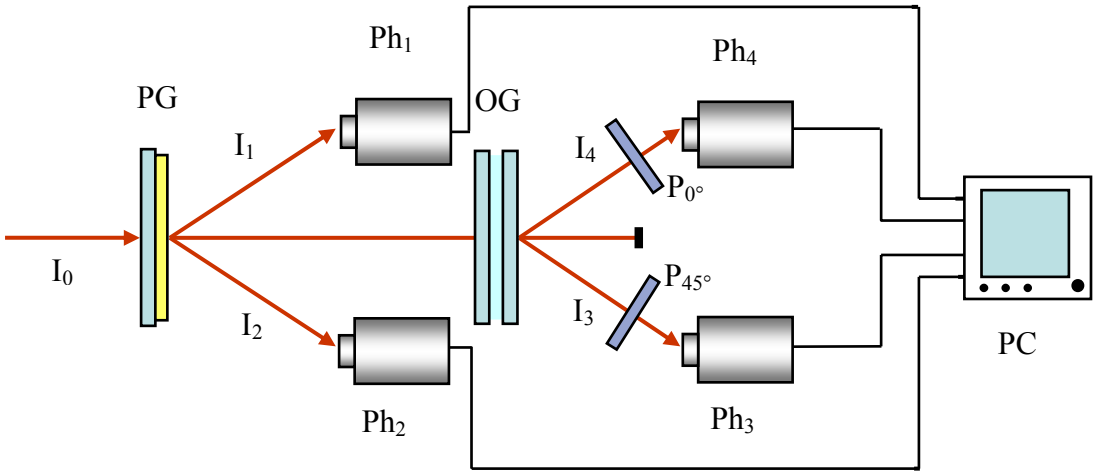


**Fig 1.10** Scheme of two gratings photopolarimeter. $I_0$ incident beam, $I_1$-$I_4$ diffracted beams, PG polarization grating, OG ordinary transmission grating, $P_{0°}$ and $P_{45°}$ polarizers, $Ph_1$-$Ph_4$ photodiodes, PC computer and acquisition system.

The light beam to be measured $(I_0)$ impinges onto the polarization grating PG, and the first diffracted orders $I_{-1}$ $(I_1)$ and $I_{+1}$ $(I_2)$ are detected by the photodiodes $Ph_1$ and $Ph_2$, respectively. The transmitted beam (zero order) is diffracted by the ordinary transmission grating OG in which the first orders $(I_3)$ and $(I_4)$ are collected, after passing through polarizers $P_{45°}$ and $P_{0°}$, by the photodiodes $Ph_3$ and $Ph_4$. The four output signals are sent to an analog-to-digital circuit board of a computer that controls the experiment.

It is possible to establish a relation between the Stokes parameters and the four signal registered by photodiodes; in particular $S_0, S_1, S_2,$ and $S_3$ are expressed in terms of some coefficients $K_1$, $K_2$, $K_3$ and $K_4$ that depend on the diffraction grating efficiency, the polarizer absorption, and the photodiode sensitivities[8]. For a particular wavelength, the relationships between the four signals and the Stokes parameters are established as follows. The Jones vector of the incident wave is

$$\vec{E}_{IN} = \begin{pmatrix} \widetilde{E}_x \\ \\ \widetilde{E}_y e^{i\delta} \end{pmatrix}$$

where $\widetilde{E}_x$ and $\widetilde{E}_y$ are the field components along the *x* and *y* axes and $\delta$ is the phase difference between these components. The measured signal by first photodiode is proportional to the $\vec{E}_R$ wave, the signal registered by the second photodiode is proportional to the $\vec{E}_L$, the third signal is proportional to the wave passing trough the 45° polarizer and the last signal it is proportional to the wave passing trough the 0° polarizer. Then we can write

$$I_1 = I_{-1} = \frac{E_R^2}{K_1} = \frac{\widetilde{E}_x^2 + \widetilde{E}_y^2 - 2\widetilde{E}_x\widetilde{E}_y \sin\delta}{2K_1} = \frac{S_0 - S_3}{2K_1}$$

$$I_2 = I_{+1} = \frac{E_L^2}{K_2} = \frac{\widetilde{E}_x^2 + \widetilde{E}_y^2 + 2\widetilde{E}_x\widetilde{E}_y \sin\delta}{2K_2} = \frac{S_0 + S_3}{2K_2}$$

$$I_3 = I(\pi/4) = \frac{\widetilde{E}_x^2 + \widetilde{E}_y^2 + 2\widetilde{E}_x\widetilde{E}_y \cos\delta}{2K_3} = \frac{S_0 + S_2}{2K_3}$$

$$I_4 = I(0) = \frac{\widetilde{E}_x^2}{K_4} = \frac{S_0 + S_1}{2K_4}$$

Inverting the previous equations, the Stokes parameters can be expressed in terms of the measured signal values as:

$$S_0 = K_1 I_1 + K_2 I_2$$

$$S_1 = -K_1 I_1 - K_2 I_2 + 2K_4 I_4$$

$$S_2 = -K_1 I_1 - K_2 I_2 + 2K_3 I_3$$

$$S_3 = -K_1 I_1 + K_2 I_2$$

To calibrate the TGP, $K_i$ coefficients are found for each wavelength by a preliminary measurement of the signals $I_i$ for a *p*-polarized incident light beam of known intensity. The $K_i$ coefficients are thus given by

$$K_1 = \frac{I_0}{2I_1}; \qquad K_2 = \frac{I_0}{2I_2}; \qquad K_3 = \frac{I_0}{2I_3}; \qquad K_4 = \frac{I_0}{I_4}.$$

For a He–Ne incident beam, $\lambda = 632.8\,nm$, the $K_i$ coefficient values are found to be $K_1 = 42.57$, $K_2 = 42.57$, $K_3 = 30.20$, and $K_4 = 32.60$, within an accuracy of 0.01. As a consequence, by using the TGP, the ellipticity of an incident light beam can be evaluated from the simple relation $K_1 = K_2$

$$e = \tan\left[\frac{1}{2}\arcsin\left(\frac{I_1 - I_0}{I_1 + I_0}\right)\right]$$

Then, acquiring the four signals $I_i$, the set of Stokes parameters of the light beam is calculated. It is noteworthy that the TGP does not require any wave plates or polarizer prisms, which are used in other methods to determine the parameters, and as a consequence it operates at any wavelength in the same original configuration.

## 1.4.5 Run test

In order to demonstrate that the photopolarimeter can measure any polarization state of the light, a simple test has been performed. A He–Ne laser beam has been used, followed by a polarizer at a 0° angle from the incidence plane and a quarter-wave plate. The latter is completely rotated from 0° to 360° in steps of 5°; this rotation generates different polarization states: linear, elliptical, and circular. The normalized Stokes parameters and the ellipticity in this case are written as follows:

$$S_0 = 1 \tag{1.22}$$

$$S_1 = \frac{1}{2} + \frac{1}{2}\cos 4\omega \tag{1.23}$$

$$S_2 = \frac{1}{2}\sin 4\omega \tag{1.24}$$

$$S_3 = \sin 2\omega \tag{1.25}$$

$$e = \tan\left[\frac{1}{2}\arcsin(\sin(2\omega))\right] \tag{1.26}$$

where $\omega$ is the rotation angle of the wave plate. Figure 1.11 shows the plots of these quantities as continuous curves, and the Stokes parameters measured by the photopolarimeter are represented by red circles.

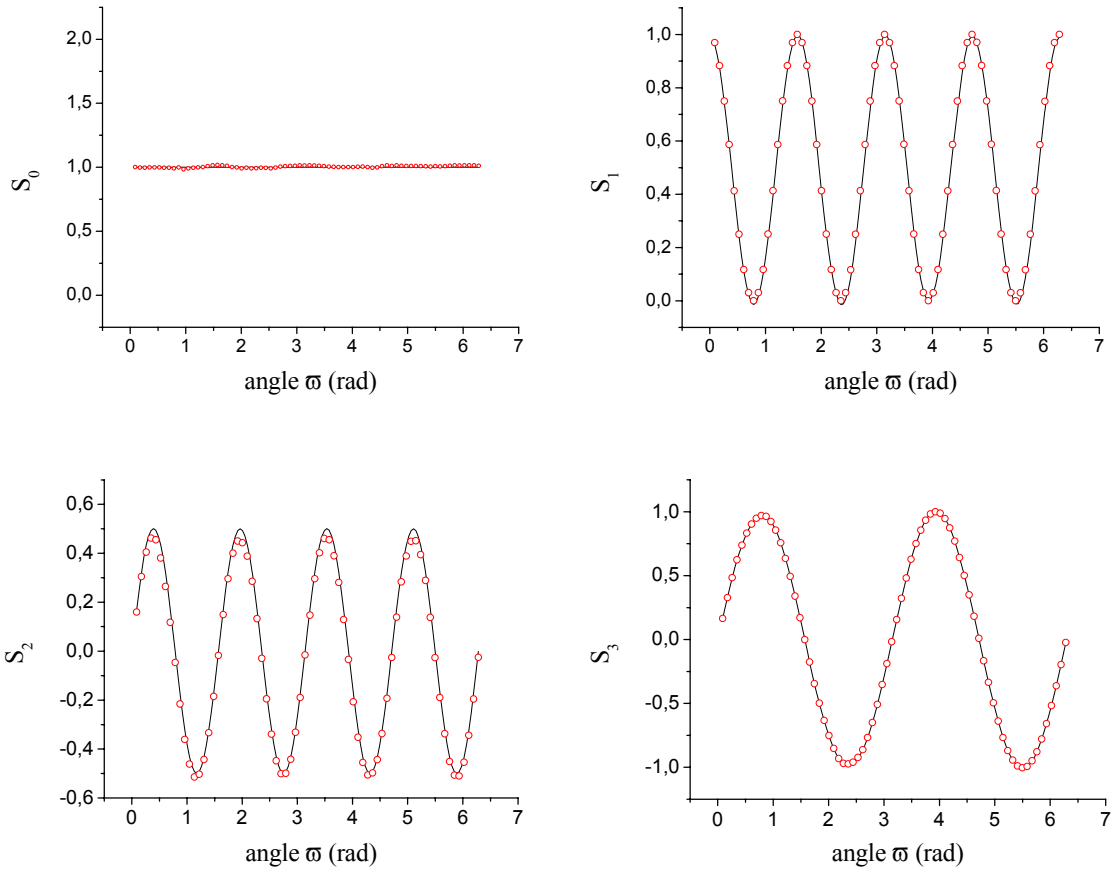


**Fig 1.11** Comparison between theoretical (solid curve) and experimental (red circles) Stokes parameters.

As can be seen from the graphs, even assuming ideal polarizing optics, the agreement between theory and experiment is good. The maximum error, 2%, occurs in the $S_1$ measurement, whereas the average error for all parameters is much less; it is estimated as below 1%. The slight deviations between theory and experiment seem to be systematic errors due to optical component imperfections; photopolarimeter appears to be a powerful tool to characterize such imperfections. To verify measurement repeatability, the time stability of the device has been tested. A single polarization state, linear p, was monitored over a period of more than seven hours. A variation within 1% of the mean values is found, indicating the successful operation of the photopolarimeter. The precision achieved is satisfactory; however, it can be improved by low-noise electronics[8]. Figure 1.12 represents a run test of the ellipticity $e$ of the light beam transmitted by the quarter-wave plate as a function of the rotation angle $\omega$ of its optical axis.

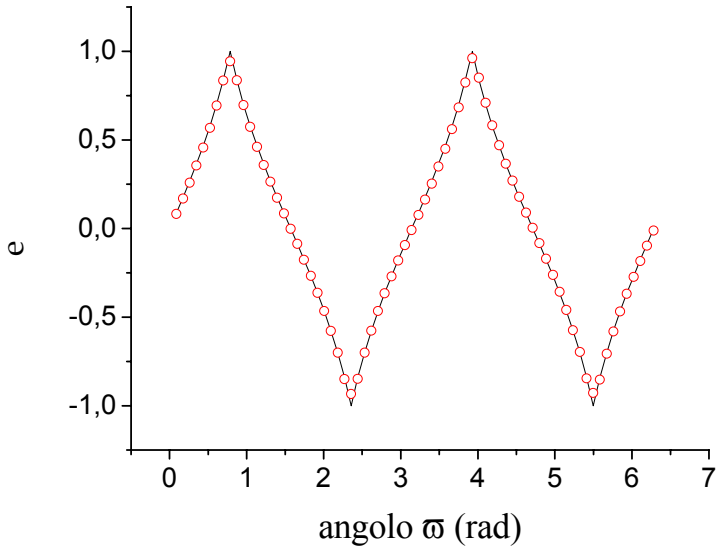


**Fig 1.12** Comparison between theoretical (solid curve) and experimental (red circles) ellipticity.

Our device is able to perform this measurement in a straightforward way; in fact, only the diffracted beam signals from the polarization grating are involved, $I_1$ and $I_2$, as from equation (1.26). The data (circles) are compared with the theory: The ellipticity measurements fit well with the theory, confirming the high reliability of the polarization grating[8].

In the figure 1.13 and 1.14 are reported two photos that illustrate the TGP assembled on the optical work bench in our laboratory, where it is possible to see the compactness and the size of the device:

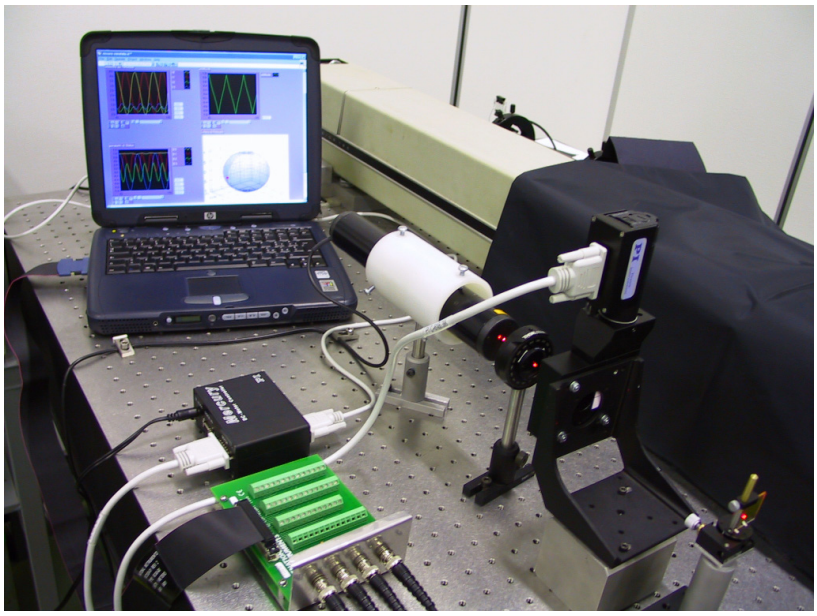

**Fig 1.13** Photo of TGP.

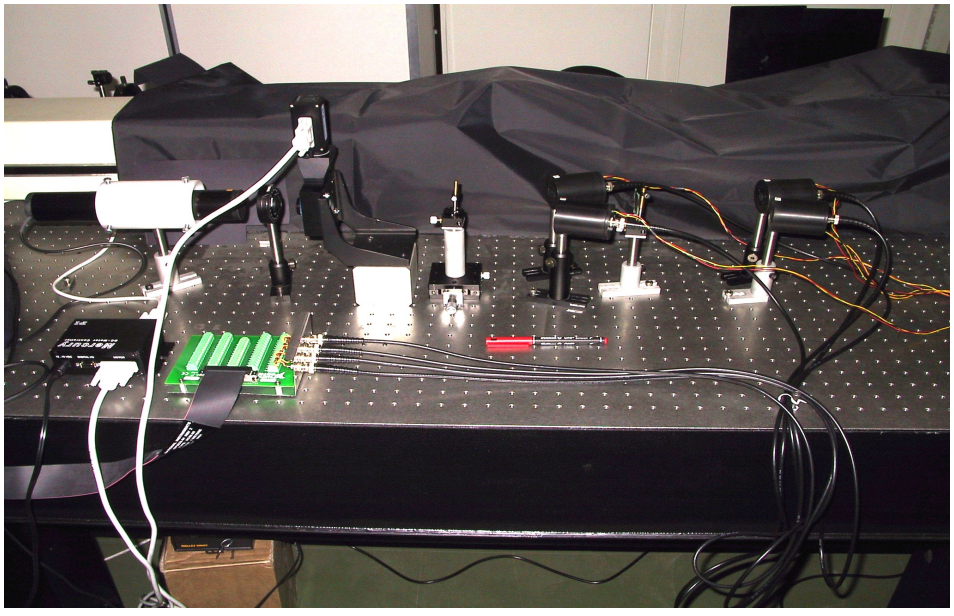

**Fig 1.14** Photo of TGP.

A LabView code for acquisition and data processing has been realized. The figure 1.15 shows the LabView page of the program, where are reported the intensities of the four diffracted beams measured by the photodiodes, the Stokes parameters and the ellipticity of a run test. The position of the point on the Poincaré sphere makes immediately possible to know the polarization state of the investigated beam.

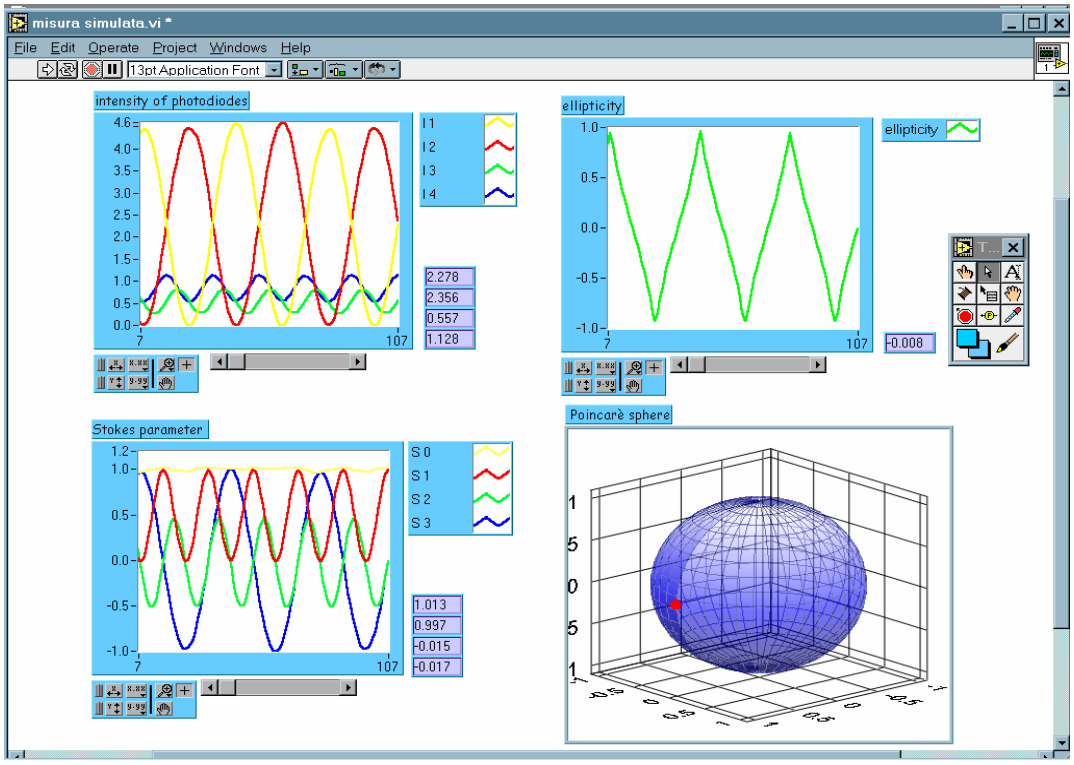


**Fig 1.15** LabView page of the acquisition and data processing program.

## 1.5 Conclusion

In conclusion, we have carried out an investigation of the polarization properties of light diffracted by a thin permanent phase polarization grating recorded in Langmuir-Blodgett films composed of amphiphilic azo-dye molecules, using two orthogonal circularly polarized laser beams. The diffractive element is characterized by pure polarization grating diffraction properties, very long time stability, small thickness and high efficiency. All these features make it a very interesting device for various applications. In fact, the polarization grating has been

selected as the basic element for a photopolarimeter able to measure simultaneously and in real time the Stokes parameters of an electromagnetic wave, in order to determine its polarization state.

Furthermore, we have reported the design and implementation of a photopolarimeter based on two diffraction gratings recorded by means holographic techniques on thin films of organic materials. The proper holographic recording geometries, the material composition, and film preparation allowed us to obtain diffraction properties of the gratings suitable to be combined for a spectropolarimeter extension. The photopolarimeter proposed in this work has an extreme simplicity of tuning, is free of modulating or moving parts, and is easy to calibrate. It has been satisfactorily tested for a single wavelength, but it can operate over the whole visible spectral range. The only requirement is the estimation of the $K_i$ coefficients for each wavelength. Four CCD linear arrays can replace the four photodiodes to allow for the spectral acquisition of a dispersed polychromatic beam. Proper research of materials is required to enlarge the working spectral range of the device, mainly in the UV range where the device could have the most interesting applications. Only detector speed and electronics acquisition processes limit the rate at which data can be manipulated by the instrument; hence it can be useful in real-time measurements.

# References:

**1** T.Torodov, L.Nikolova, and T.Tomova, *Appl. Opt.*, **23**, 4309

**2** T.Torodov, L.Nikolova, and T.Tomova, *Appl. Opt.*, **23**, 4588

**3** T.Torodov, L.Nikolova, K. Stoyanova, and T. Tomova, *Appl. Opt.*, **24**, 785

**4** L.Nikolova and T. Torodov, *Opt Acta,* **31**, 579

**5** T. Huang, K.H. Wagner, *J. Opt. Soc. Am. A*.,**10**, 306

**6** F. Lagugnè Labarthet, P. Rochon , et al *Appl. Phys. Lett.*, **75**, 1377

**7** M. L.Blinov, G. Cipparrone, and S. P. Palto, *J. Nonlinear Opt. Phys. Mater*., **7,** 369

**8** C. Provenzano, G. Cipparrone, A. Mazzulla, *Applied Optics*, **45**, No 17, 3929

**9** T.Huang, K.H. Wagner, *J. Opt. Soc. Am. B*.,**13**, 282

**10** N. C. R.Holme, L. Nikolova, P. S. Ramanujam, et al, *Appl. Phys. Lett.*, **70**, 1518

**11** L. Nikolova, T. Torodov, M. Ivanov, F. Andruzzi, *Appl. Opt.*, **35**, 3835

**12** G. Cipparrone, A. Mazzulla, S. P. Palto, S. G.Yudin, L. M. Blinov, *Appl. Phys. Lett.*, **77**, 2106

**13** F. Gori, *Optics Letters*, **24**, No 9, 584

**14** G. Cipparrone, A. Mazzulla, M.L. Blinov, *J. Opt. Soc. Am. B*.,**19**, 1157

**15** H. J. Eichler, P. Gunter, D.W. Pohl. *Laser-induced dynamic gratings.* Springer-Verlag

**16** S. P. Palto, S. G. Yudin, C. Germain, G. Durand, *J. Phys. II France,* **5**, 133

**17** J. Ronayette, R. Arnaud, and J. Lemaire. *II. Can.J.Chem*. **52**, 1858

**18** K. Anderle, R. Birenheide, M. Eich, and J:H: Wendorff. *Makromol. Chem. Rapid Commun*.,**10**, 477

**19** S.P. Palto and G. Durand. *J. Phis. II France* **5**, 963

**20** R. M. A. Azzam, E. Masetti, I. M. Elminyawi and F. G. Grosz. *Rev Sci. Instrum* **59**, 84

**21** R. M. A. Azzam, A. M. El-Saba, M.A.G. Abushagur. *Thin Solid Films* **313**, 314

**22** E. Masetti and A. Krasilnikova, *Thin Solid Films* **455,** 138

**23** T. Todorov and L. Nikolova, *Opt. Lett.* **17,** 358

**24** L. Nikolova, M. Ivanov, T. Todorov, and S. Stoyanov, *Bulg. J. Phys.* **20,** 46

**25** R. M. A. Azzam and N. M. Bashara. Ellipsometry and polarized light. *Elsevier*

**26** M. Born and E. Wolf. Principles of optics. *Pergamon Press*

**27** C. Decker, *Prog. Polym. Sci.*, **21**, 593

**28** R. L. Sutherland, L. V. Natarajan, V. P. Tondiglia and T. J. Bunning. *Chem. Mater*. **5**, 1533

**29** T. J. Bunning, L. V. Natarajan, V. Tondiglia , R. L. Suterland,et al *Polymer*, **14**, 2699

# Chapter 2

## 2.1 Introduction

In this section we report an experimental and theoretical study of holographic gratings recorded exposing a homogeneous mixture of prepolymer and liquid crystals to a polarization light pattern. Diffraction gratings with a large anisotropy were obtained, indicating a particular alignment of the liquid crystal inside the droplets of the polymeric matrix.

PDLC is the acronyms of Polymer Dispersed Liquid Crystal, a liquid-crystalline polymeric material, in which liquid crystal droplets are dispersed in a solid polymeric matrix.

In the last years, a particular attention is turned towards this kind of materials, because of numerous possible applications, that range from the displays to smart windows, thermic sensors and optical storage devices[1-7].

It is possible to obtain PDLC samples starting from homogenous mixtures obtained dissolving the liquid crystal in a suitable pre-polymer. When polymerization reaction is initiated it induces phase separation process, during which the liquid crystal solubility in the mixture decreases and hence, during the solid polymer matrix creation, the liquid crystal separates from the polymer. The complete phase separations causes the formations of liquid crystal droplets embedded in a polymeric environment.

There are three different techniques to obtain a PDLC sample, according to the monomer used in the mixture. The first method, the Solvent-Induced Phase Separation (SIPS), is employed when the polymer and the liquid crystal are dissolved in a common solvent to form a homogenous mixture. The solution is placed on a substrate, the solvent is removed by evaporation with consequent polymer solidification and phase separation. The second method, Thermally-Induced Phase Separation (TIPS), is particularly used in thermoplastic polymers, that melt at a certain temperature. The homogeneous mixture is obtained heating the components above the polymer melting point. Phase separation occurs during the cooling process. The third method, Polymerization-Induced Phase Separation (PIPS), is used when it is possible to dissolve the liquid crystal in a mixture of monomers; the polymerization process, that can be initiated in several ways, produces the phase separation and, thus, the PDLC film[8].

The most widely used technique, in particular for holographic applications, is the PIPS method, in which the polymerization and phase separation processes are induce by light exposure.

The PDLC mechanism formation, the shape and the dimensions of the droplets, strongly depend on the composition of the material and on the properties of the components, as polymer viscosity and liquid crystal solubility. In the case of photo-activated polymerization, for example, it is possible to control the droplets dimension, properly tuning the light intensity and the exposure time.

The most evident optical property of PDLC is the light scattering, and the great interest for this kind of materials derives from the possibility to control this property by means of an external electric field, that makes transparent a PDLC opaque film.

The PDLC scattering depend on several factors related to the film realization, as for example dimension, shape and density of the liquid crystal droplets dispersed in the polymeric matrix, but also from the refractive index of monomer and liquid crystal. Nevertheless, the most important factor is the liquid crystal orientation inside the droplets. In fact, in a PDLC film the liquid crystal droplets are casually oriented, and the refractive index varies between the droplets depending from their orientation: in this case the light is strongly scattered. When an external electric field is applied to the PDLC sample, the symmetry axis of every droplet is aligned with the field. Then, if the liquid crystal refractive index is near to the polymer refractive index, the PDLC film becomes transparent[8].

PDLC films are largely used in optical storage processes: it is possible to store on these materials the field produced from the interference of two electromagnetic waves. Switchable holograms can be created exposing a homogenous monomer-liquid crystalline mixture containing an appropriate photoinitator, to a holographic intensity pattern. As well know, intensity holographic technique is obtained by the interference of two waves with parallel polarization states. This geometry produces a spatially modulated intensity distribution, in which illuminated and dark regions alternate; as a consequence, during the system curing, liquid crystal separates as a distinct phase in the dark fringes of the optical interference pattern. Therefore, the polymerization kinetics is spatially modulated according to the intensity pattern, and the grating originates from the modulation of the internal morphology of the materials. As a result, a volume grating is created that consists of periodic polymer dispersed liquid crystal layers separated by solid polymer stripes. The structure is called a holographic polymer dispersed liquid crystal, H-PDLC. If the grating is subjected to an external electric field, liquid crystal molecules will orient

with the field, changing the optical properties of the holograms[9,10]. H-PDLC optical elements have been under development for several years. Both reflection and transmission holographic gratings have been exploited in various applications, as for example for wide field of view wearable display[11,12], electronic addressable filter stack for portable video projectors[13,14], optical switching component for telecommunications applications[15-17], and so on.

In the present work, we describe the holographic grating formation in PDLC sample exposing the homogeneous mixture of prepolymer and liquid crystal to a polarization pattern. In this case, we obtain a Polarization Holographic-PDLC (PH-PDLC). Polarization patterns are obtained by a spatial superposition of two waves having orthogonal polarization. In these geometries, the intensity modulation is absent or negligible, because of small crossing angles. The variation of the phase difference between the two writing beams leads only to a change of the polarization state along the wave vector of the grating. The idea of using the polarization holographic technique comes from few considerations. The first one is the occurrence of the photoinduced alignment effect in the components of the PDLC, that is, in the polymer and in the liquid crystal[18-20]. The second one is the possibility to achieve the liquid crystal alignment control inside the droplets, during the photo-induced polymerization phase separation, instead of the usual polymerization control[1-3]. The third motivation is the possibility to obtain more stable structures, because photopolymerization and phase separation take place under a uniform illumination, possibly preventing monomer diffusive processes that can favour structure degradation. Finally, because the photochemical reaction occurs uniformly, any spatial modulation of the relative densities of the chemical components is avoided: this fact should yield a better electrical switching efficiency of the grating.

These considerations suggested to use the alternative procedure of polarization holographic to record diffraction gratings.

After the polarization light pattern exposure, a diffraction grating composed of liquid crystal droplet having a particular internal alignment is observed, with diffraction efficiency values ranging from 1% to 30 %. A large anisotropy of the diffraction efficiency characterizes the recorded gratings. This means that the efficiency of the horizontally polarized (p) probe beam is higher than the efficiency of the vertically polarized (s) one. Results from optical characterization of the diffracted and transmitted beams suggest that, besides the linear birefringence due to the orientation of the liquid crystal director, also surface reliefs on the film topography should be considered. This particular topography is unexpected for polarization

holographic recording in materials that do not contain azo benzene compounds, and to our knowledge it has been never observed before. Topography measurements, performed on the H-PDLC film by Atomic Force Microscopy, proof the presence of regular reliefs with depth ranging from 50 to 220$nm$ depending on the total recording intensity. This observation adds several questions to the open topic related to the mechanisms of the surface reliefs formation. In fact, the theoretical models proposed in order to explain the surface reliefs formation reported in literature, are strictly related to mechanisms present in azo-compound systems. Our results indicate that a more general explanation for surface reliefs formation needs to be considered[45].

## 2.2 Material and experimental results

### 2.2.1 Material

In our experiments, the used preparation technique for the PDLC achievement is the polymerization induced phase separation, triggered by light exposure.

As well known, photopolymerizable materials work by means of radical polymerization reactions of the monomers initiated by the absorption of photons[21]. A photopolymerizable system is composed of a number of elements: one is the photoinitiator that absorbs in the zone of the laser emission and produces radicals that initiate the polymerization reaction. The most important component is the monomer or system of monomers that forms the mixture. Once initiated, the polymerization chain reaction will develop very much, following a process that has been described in figure 1.10.

We have tested several commercial materials for the PH-PDLC realization, but the best results are obtained with a homogeneous pre-polymer mixture of a monomer having refractive index $n = 1.48$ (PWL01 B-component, 52.9% wt) a nematic liquid crystal with refractive indices $n_o = 1.52$ and $n_e = 1.72$ (PWL01 C-component of TL-mixture series, 47 %wt), both by Merk, and a small amount (0.1% wt) of photo-initiator dye Bengal Rose (Fluka).

## 2.2.2 Experiment

In figure 2.1 is reported the experimental set-up used to write the polarization holograms: interference patterns are produced by an argon-ion laser beams, $\lambda = 514nm$

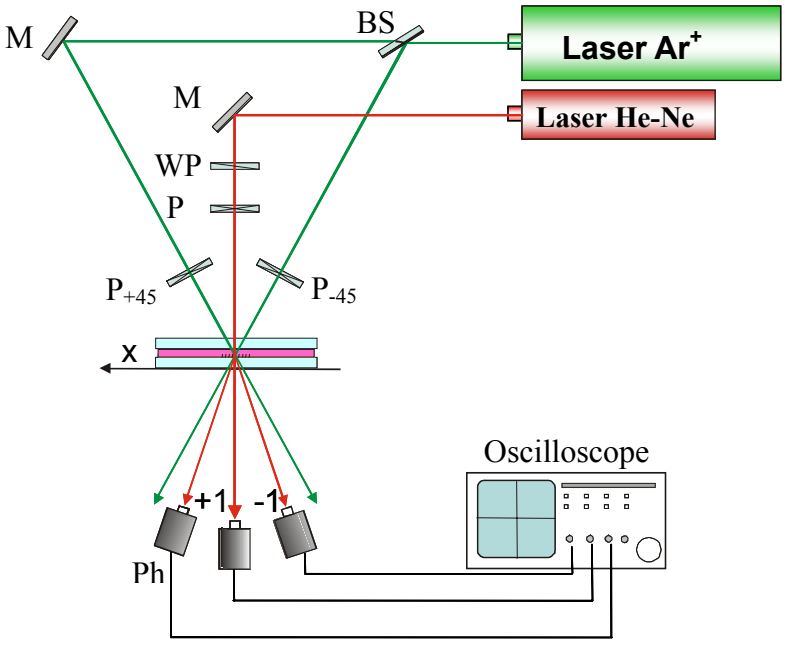


**Fig 2.1** Experimental set-up used for the holographic writing: BS beam splitter; M mirror; WP wave plate; P polarizer; Ph photodiode

The beam from the laser is split into two waves having equal intensity and with orthogonal polarizations states. Several experimental geometries have been investigated: an opposite circular polarized waves configuration, two orthogonal linear configurations (p and s, $+45°$ and $-45°$ with respect to the plane of incidence). Here we only report the results related to the last polarization pattern ($\pm 45°$), for which we have obtained the best results. The two waves crossed in the sample at an angle $\theta = 3.2°$ corresponding to a spatial periodicity of $7\mu m$. When two orthogonal linear polarized beams are superimposed at a small angle $\theta$, the total field in the superposition region can be written in terms of Jones vector in the following way: if $\vec{E}_{+45}$ is the

field of the linear polarized wave at $+45°$ and $\vec{E}_{-45}$ is the field of the linear polarized wave at $-45°$, the total field $\vec{E} = \vec{E}_{+45} + \vec{E}_{-45}$ keeps a polarization distribution that can be written as:

$$\vec{E} = \frac{2}{\sqrt{2}} \begin{bmatrix} \cos(\theta/2)\cos(\delta/2) \\ i\sin(\delta/2) \end{bmatrix}$$

where $\delta = 2\sin(\theta/2)(2\pi/\lambda)x$ is the phase difference at location $x$ of the writing waves and $\lambda$ is the laser wavelength. In this configuration the intensity distribution is almost uniform, since the crossing angle is small, while the polarization state of the total field changes along the grating vector, as represented in figure 2.2:

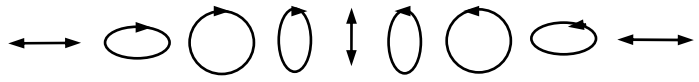

**Fig 2.2** Polarization modulation of the interference light field recording the grating in the orthogonal linear $\pm 45°$ configuration

Two Glan-Tompson polarizers, with extinction ratio less than $10^{-5}$ were used to achieve good linear polarization. Holographic gratings have been obtained from light intensity values ranging from $50 - 400 mW/cm^2$ and exposure time from 10-5 minutes, respectively.
The cells assembled by ITO coated glasses were $8\mu m$ thick. A linearly polarized He-Ne laser with $\lambda = 632.8nm$ was used as a probe beam in order to investigate the diffracted light field.

## 2.2.3 Results

Since both polymerization and phase separation processes occur under illumination having a spatially modulated polarization state, but uniform intensity, the obtained PH-PDLC has different features from the one produced by standard intensity technique.

In fact, unlike in the conventional method, where the gratings originate from the modulation of the internal morphology, as demonstrates figure 2.3,

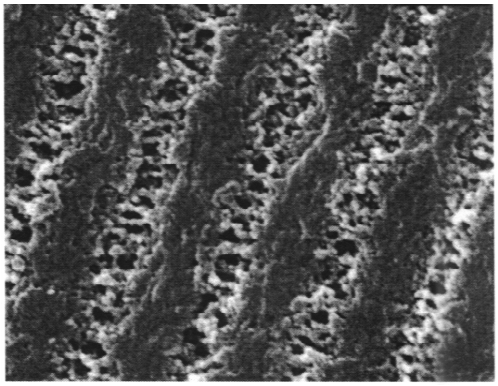

**Fig 2.3** Internal morphology of H-PDLC

in the case of polarization pattern exposition, the internal morphology of the PH-PDLC is fairly uniform, as supported by the SEM images reported in figure 2.4[22]:

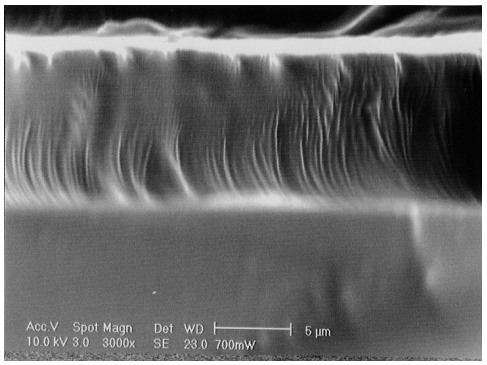


(a)

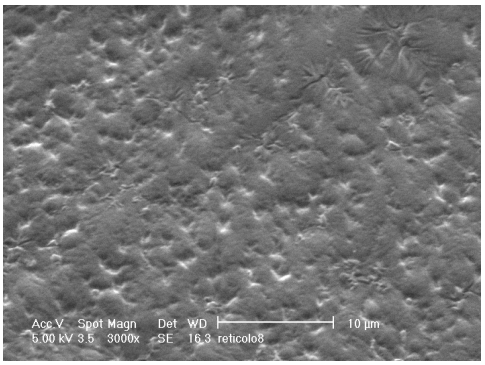


(b)

**Fig 2.4** SEM images of the grating: (a) internal morphology; (b) surface topography.

The analysis of the topography suggests the presence of a corrugation on the surface of the sample.

In figure 2.5 is reported the evolution of the first order diffraction efficiency $\eta_{+1}$ during the first minutes of the writing process, for horizontal p (0°) and vertical s (90°) probe beam polarization. The 0° position corresponds to the polarization state along the grating wave vector.

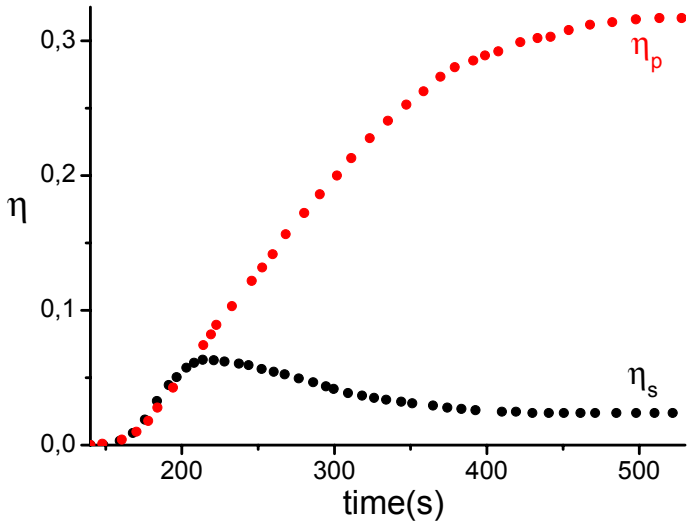


**Fig 2.5** Temporal evolution of the first order diffraction efficiency for p and s polarization state of the probe beam. Recording intensity: 270 mW/cm$^2$

The diffraction efficiency $\eta_{\pm 1} = I_{\pm 1} / I_0$ is defined as the ratio of the first diffracted beam intensity to the total incident intensity. The Ar-ion laser is turned on at the time $t = 0\,s$, the probe diffracted beams arise after 1min, at the same time, due to the phase separation, scattered light appears. This formation time depends on the recording intensity: for low intensity, even 10 minutes pass before the grating builds up. As is possible to see from the figure, $\eta_p$ increases monotonically, reaching its maximum after tens of seconds, then stabilized to this value; the dynamics of $\eta_s$ is different: it reaches its maximum in a few seconds after the appearance of the first-order diffracted beams, then it decreases slowly. When the final steady value is reached, the efficiency for *s* and *p* probe beam polarization was measured: anisotropy of the recording structure is evident. $\eta_p$ value is always higher than $\eta_s$ value and this difference grows increasing the writing intensity value[23].

In figure 2.6 optical polarizing microscope images observed with crossed polarizers are reported.

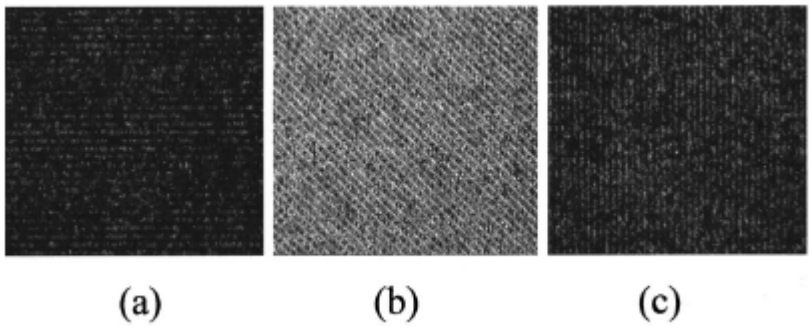


**Fig 2.6** Images observed to the optical polarizing microscope with crossed polarizers when the grating wave vector has an angle of 0 ° with respect to the incident light vector (a), an angle of 45° (b), and an angle of 90° (c).

Figure 2.6a is the image observed when the grating wave vector make an angle of 0° with respect to the incident light vector, in figure 2.6b the angle is 45° and in figure 2.6c it is 90°. The images indicate that the liquid crystal inside the droplets, within the stripes that become bright at 45°, see figure 2.6b, should be well aligned along the grating wave vector, as measured by optical compensation technique. The recorded gratings have the same spatial periodicity as the interference pattern. A very efficient grating optical switching can be observed applying a suitable voltage to the PDLC. We can see in the figure 2.7 the optical microscope images, between crossed polarizers, having the same geometry of figure 2.6b, without applied voltage and applying an ac voltage of $40V$ at $f = 1kHz$. For this voltage, a complete electrical erasure of the optical modulation is obtained [24].

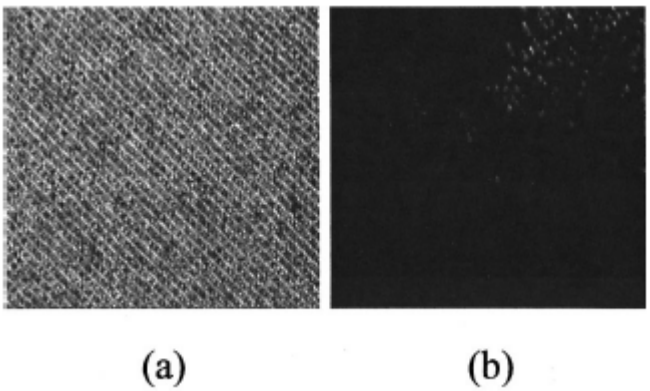


**Fig 2.7** Images observed to the optical polarizing microscope with crossed polarizers when the grating wave vector makes an angle of 45° with respect to the incident light vector. Without applied voltage (a) and applying 40 V at 1 kHz frequency (b).

In figure 2.8 is reported the response time of the first order diffracted beam for the transition from the maximum to the minimum transmission states, applying an electric field of frequency $f = 100Hz$ and amplitude $60V_{rms}$:

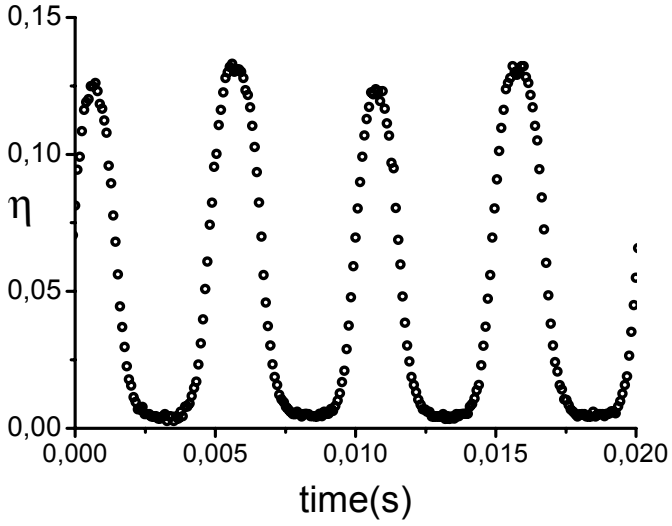


**Fig 2.8** Modulation of the intensity of the first order diffracted beam.

We can see that the response time of the grating is about $2ms$, which is comparable with the response times of H-PDLC obtained using equivalent writing intensity values.

In order to elucidate the mechanism of the grating optical recording and the liquid crystal orientation inside the droplets, the polarization diffraction properties of the holographic gratings have been investigated. The gratings are highly birefringent, which means that the diffraction is extremely polarization dependent. This dependence was tested for gratings recorded at several writing intensities. In particular, after the light polarization pattern exposition, the first order diffraction efficiency were measured as a function of the incident light polarization azimuthal angle $\alpha$. A half-wave plate was used to rotate the polarization direction of the probe beam. As can be seen in figure 2.9, in which the analysis of a grating recorded at $270mW/cm^2$ intensity and 5 minutes time exposure is reported, the diffraction efficiency is strongly dependent on the angle $\alpha$.

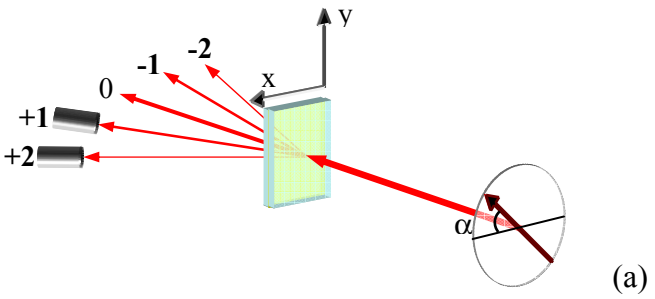


(a)

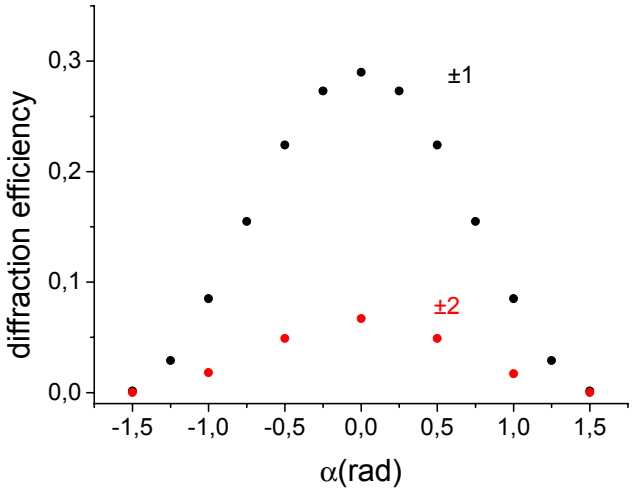


(b)

**Fig 2.9** Experimental geometry used for the measurement of the diffraction efficiency versus the angle α (a); experimental values of the first and second order diffraction efficiency versus the polarization azimuthal angle α for a grating recorded at 270mW/cm$^2$ intensity (b).

We experimentally observe that at higher recording intensities, the polarization dependence on the angle α becomes stronger, and that the second order diffraction intensities have the same polarization dependence of the first orders one, but smaller modulation amplitude.

Since the liquid crystal alignment occurs during the polymerization and its orientation inside the droplets is permanent after recording, we suppose that the alignment is imposed by the anchoring condition at the liquid crystals-polymer interfaces of the droplets. The permanence of the diffracted beam after the writing process and the possibility of totally modulating the diffraction efficiency by an applied voltage suggest that the photoinduced process induces a particular configuration of the liquid crystal-polymer droplets interface. This configuration, fixed by the polymerization, persists even after the optical polarization pattern is removed. The absence of intensity modulation and the presence of the polarization pattern suggest that the phase grating is due to an orientation effect induced by an optical field.

# 2.3 Theory

## 2.3.1 Surface relief grating

In order to understand the photoinduced processes involved in the gratings formation, and to explain the experimental behaviour of $\eta_{\pm i}(\alpha)$, we carried out a theoretical analysis of the diffraction properties of the holographic gratings in the PDLC recorded with this polarization technique.

When two coherent waves with equal intensity having orthogonal linear $+45°$ and $-45°$ polarization interfere, a light pattern with almost constant intensity and polarization state modulation as represented in figure 2.3 is obtained. In systems of liquid crystals and monomer mixture, this interference field is suppose to induce only linear anisotropy in the regions with linear polarization; no circular birefringence should take place. To build the transmission matrix of the structure we assume that the photo-induced change is mainly due to the refractive index; optical density anisotropy induced by the polarized light is neglected.

If we suppose photo-induced linear anisotropic changes, the Jones matrix describing the transmittance and the diffraction from the recorded grating [25] is

$$T_1 = \begin{bmatrix} \exp[(i\Delta\varphi)\cos\delta] & 0 \\ 0 & \exp[-(i\Delta\varphi)\cos\delta] \end{bmatrix} \tag{2.1}$$

where $\Delta\varphi = \dfrac{\pi \Delta n d}{\lambda}$ is the phase shift due to the birefringence grating, $\Delta n$ is the photo-induced change of the refractive index, $d$ is the thickness of the sample and $\lambda$ is the readout laser wavelength. To analyze the diffraction from the grating, we multiply a Jones vector representing the incident beam by the matrix (2.1). The expression obtained brought some information about the different orders of the diffracted waves, regarding their intensity and polarization state. Unfortunately, the experimental result does not agree with the theory. According to the SEM results, we considered a transmission matrix that account for photoinduced linear birefringence in presence of surface reliefs grating, as reported in [26].

It is well established that, upon any holographic grating inscription, at least two distinct

processes take place, namely the formation of a birefringence linear and/or circular grating, and the formation of a surface relief amplitude grating[27-30]. In fact, in several photosensitive materials, like azobenzene and azo-dye guest-host polymer systems, the topographic relief formation has been demonstrated. In systems without azo compounds, like PDLC[31] and photocrosslinkable polymer liquid crystals, SRGs have been only observed when exposed to an intensity light pattern[32]. Even if this phenomenon has been already investigated by several groups, the mechanisms responsible of surface relief formation are not yet clearly understood. Several models, in particular in the case of systems exposed to polarization pattern have been proposed in order to explain the driving forces responsible for its formation[33]. Kumar and coworkers have attributed the driving force of mass transport to the radiation force arising from a light intensity gradient[34-36]. Lefin and coworkers have proposed that the surface modulation could be partially due to a translational "wormlike" diffusion of the azo benzene chromophores from regions of higher isomerization rate to those of a lower rate, creating a concentration gradient[37,38]. Pederson and coworkers have also proposed that the chromophores are subject to strong anisotropic intermolecular interactions leading to mass transport[39-40]. Barret and coworkers have proposed that the reliefs were mainly due to a bulk deformation of the polymer in a viscoelastic state and to a volume change during the photoisomerization process, because the cis form requires a larger volume[41]. As we have seen, in this fundamental problem of surface relief formation it is evident that photoinduced and mass transport effects must play a key role.

The presence of surface reliefs in our gratings induced by polarization pattern is a relevant result: it is worth to stress that, in our case, the intensity across the plane film is constant, and then, mass transport arising from a light intensity gradient is not justifiable. Moreover, also if the polarization states of the field is changing along the wave vector of the grating, our polymeric acrylate mixture does not contain azo-compounds, and then all the models based on the trans-cis-trans isomerization cannot be effective.

The relevance of this result stimulates questions toward the controversial topic of the surface reliefs formation mechanism, and the demonstration that the surface reliefs are not just related to azobenzene based systems indicates that a more general explanation for the surface relief formation have to be found. The herein results suggest that both the anisotropic liquid crystalline medium and its coupling with the electric field of the writing beams are essential. Nevertheless, the lack of reliefs in polymer liquid crystals for polarization holography experiments[42], points out that the material anisotropy cannot bring on the relief formation by itself. Consequently, we

deduce that the phase separation process originating the material nonhomogeneity plays a significant role in the reliefs formation. In our case, the initial process could be anisotropic due to polarization selective crosslinking reactions of the polymer, which in principle can also be accompanied by mass transfer. Since in photocrosslinkable liquid crystal polymers the migration of polymer chains results only from intensity-based holography and no relief are induced during polarization holographic recording[42], we suppose that a significant role should be played by the phase separation kinetics that occurs during the PDLC formation. This statement is supported by some studies[43,44] showing that in several polymer mixtures selective crosslinking reactions driven by irradiation with linearly polarized light can give rise to an orientation dependent phase separation. This phase separation produces an anisotropic morphology of the polymer blend in the direction perpendicular to the linear polarization, implying that phase separation induced by linearly polarized light is a process that does not dependent exclusively on the light intensity through the reaction rate. The authors in reference 43 compare the morphological results obtained for photoinduced crosslinking reactions with those obtained inducing phase separation by means of photoisomerization, finding a stronger anisotropy in the first case. This difference is explained considering that polymer diffusion is directly frozen due to crosslinking reactions.
The above observations in binary polymer mixtures suggest that also in our case where the phase separation process is at the basis of PDLC formation, we can suppose polarization selective crosslinking reactions and directional phase separation. The latter, coupling with the polarization light pattern, could result in a surface morphology modulation with the same spatial periodicity of the polarization pattern. In our experimental geometry, in fact, the linear polarization of the light pattern is parallel or perpendicular to the grating wave vector, thus only for one polarization the propagation direction of the effect matches with the grating stripes direction, while for the other is perpendicular. Even if the above hypotheses are in our opinion fascinating, this point needs more and deeper investigations.

## 2.3.2 Theoretical determination of $\eta(\alpha)$

To taking into account also the presence of surface reliefs, we modify the theoretical model taking into account both linear photo-induced birefringence and surface relief gratings. The

transmission matrix of the surface reliefs grating can be written in the following way[26]:

$$T_2 = \begin{bmatrix} \exp[(i\Delta\psi)\cos(\delta+\delta_0)] & 0 \\ 0 & \exp[(i\Delta\psi)\cos(\delta+\delta_0)] \end{bmatrix}$$

where $\Delta\psi = \frac{2\pi}{\lambda} d_1 \frac{(n_p - n_a)}{2}$ is the phase shift due to the surface relief, $d_1$ is the surface modulation depth, $n_p$ is the PDLC refractive index, $n_a$ is the index of the vapours produced during the irradiation, and $\delta_0$ is a phase constant that accounts for the spatial phase shift between the two contribution. The diffracted fields can be evaluated by multiplying the Jones vector of the incident wave by the total transmission matrix $T_{TOT} = T_2 T_1$ as

$$E_{OUT} = T_2 T_1 \, E_{IN}$$

In this way it is possible to obtain the diffracted beam intensities and polarization states. As we will see, the experimental behaviour of $\eta(\alpha)$ is well reproduced by a model that take into account the PH-PDLC topography modulation besides the photo-induced linear birefringence due to nematic director orientation inside the droplets.

The total transmission matrix of the grating $T_{TOT} = T_2 T_1$ can be evaluated in this way:

$$T_{TOT} = T_2 T_1 = \begin{bmatrix} \exp[(i\Delta\psi)\cos(\delta+\delta_0)] & 0 \\ 0 & \exp[(i\Delta\psi)\cos(\delta+\delta_0)] \end{bmatrix} \begin{bmatrix} \exp[i\Delta\varphi\cos\delta] & 0 \\ 0 & \exp[-i\Delta\varphi\cos\delta] \end{bmatrix} =$$

$$\begin{bmatrix} \exp[(i\Delta\psi)\cos(\delta+\delta_0)]\exp[i\Delta\varphi\cos\delta] & 0 \\ 0 & \exp[(i\Delta\psi)\cos(\delta+\delta_0)]\exp[-i\Delta\varphi\cos\delta] \end{bmatrix} = \begin{bmatrix} A & 0 \\ 0 & B \end{bmatrix}$$

Using the following expansion in the Bessel functions

$$e^{ix\cos\alpha} = J_0(x) + \sum_{n=1}^{\infty} i^n J_n(x)\left[e^{in\alpha} + e^{-in\alpha}\right]$$

we obtain the subsequent expression for the coefficients $A$ and $B$, developing the series to the second order:

$$\begin{aligned} A = \; & \left[J_0(\Delta\varphi)J_0(\Delta\psi) + 2J_1(\Delta\varphi)J_1(\Delta\psi)\cos\delta_0 + 2J_2(\Delta\varphi)J_2(\Delta\psi)\cos 2\delta_0\right] + \\ & + i\left[J_1(\Delta\varphi)\left(J_0(\Delta\psi) - J_2(\Delta\psi)\,e^{2i\delta_0}\right) + J_1(\Delta\psi)\left(J_0(\Delta\varphi)e^{i\delta_0} - J_2(\Delta\varphi)\,e^{-i\delta_0}\right)\right] \quad e^{i\delta} + \\ & + i\left[J_1(\Delta\varphi)\left(J_0(\Delta\psi) - J_2(\Delta\psi)\,e^{-2i\delta_0}\right) + J_1(\Delta\psi)\left(J_0(\Delta\varphi)e^{-i\delta_0} - J_2(\Delta\varphi)\,e^{i\delta_0}\right)\right] \quad e^{-i\delta} + \\ & - \left[J_0(\Delta\varphi)J_2(\Delta\psi)e^{2i\delta_0} + J_1(\Delta\varphi)J_1(\Delta\psi)e^{i\delta_0} - J_2(\Delta\varphi)J_0(\Delta\psi)\right] \quad e^{2i\delta} + \\ & - \left[J_0(\Delta\varphi)J_2(\Delta\psi)e^{-2i\delta_0} + J_1(\Delta\varphi)J_1(\Delta\psi)e^{-i\delta_0} - J_2(\Delta\varphi)J_0(\Delta\psi)\right] \quad e^{-2i\delta} \end{aligned}$$

$$\begin{aligned} B = \; & \left[J_0(\Delta\varphi)J_0(\Delta\psi) + 2J_1(\Delta\varphi)J_1(\Delta\psi)\cos\delta_0 + 2J_2(\Delta\varphi)J_2(\Delta\psi)\cos 2\delta_0\right] + \\ & + i\left[J_1(\Delta\varphi)\left(-J_0(\Delta\psi) + J_2(\Delta\psi)\,e^{2i\delta_0}\right) + J_1(\Delta\psi)\left(J_0(\Delta\varphi)e^{i\delta_0} - J_2(\Delta\varphi)\,e^{-i\delta_0}\right)\right] \quad e^{i\delta} + \\ & + i\left[J_1(\Delta\varphi)\left(-J_0(\Delta\psi) + J_2(\Delta\psi)\,e^{-2i\delta_0}\right) + J_1(\Delta\psi)\left(J_0(\Delta\varphi)e^{-i\delta_0} - J_2(\Delta\varphi)\,e^{i\delta_0}\right)\right] \quad e^{-i\delta} + \\ & + \left[-J_0(\Delta\varphi)J_2(\Delta\psi)e^{2i\delta_0} + J_1(\Delta\varphi)J_1(\Delta\psi)e^{i\delta_0} - J_2(\Delta\varphi)J_0(\Delta\psi)\right] \quad e^{2i\delta} + \\ & + \left[-J_0(\Delta\varphi)J_2(\Delta\psi)e^{-2i\delta_0} + J_1(\Delta\varphi)J_1(\Delta\psi)e^{-i\delta_0} - J_2(\Delta\varphi)J_0(\Delta\psi)\right] \quad e^{-2i\delta} \end{aligned}$$

where $J_0$, $J_1$ and $J_2$ are the normal Bessel functions of the first kind. The total transmission matrix $T_{TOT}$ is the sum of $2n+1$ terms that represent the transmitted and the $2n$ diffracted beams:

$$T_{TOT} = T_0 + T_{+1}\ e^{i\delta} + T_{-1}\ e^{-i\delta} + T_{+2}\ e^{2i\delta} + T_{-2}\ e^{-2i\delta} + \ldots$$

with

$$T_0 = \begin{bmatrix} A_0 & 0 \\ 0 & B_0 \end{bmatrix},\ T_{+1} = \begin{bmatrix} A_{+1} & 0 \\ 0 & B_{+1} \end{bmatrix},\ T_{-1} = \begin{bmatrix} A_{-1} & 0 \\ 0 & B_{-1} \end{bmatrix},\ T_{+2} = \begin{bmatrix} A_{+2} & 0 \\ 0 & B_{+2} \end{bmatrix},\ T_{-2} = \begin{bmatrix} A_{-2} & 0 \\ 0 & B_{-2} \end{bmatrix},$$

...

in which the coefficients are equal to:

$$\begin{aligned} A_0 &= \left[J_0(\Delta\varphi)J_0(\Delta\psi) - 2J_1(\Delta\varphi)J_1(\Delta\psi)\cos\delta_0 + 2J_2(\Delta\varphi)J_2(\Delta\psi)\cos 2\delta_0\right] \\ B_0 &= \left[J_0(\Delta\varphi)J_0(\Delta\psi) + 2J_1(\Delta\varphi)J_1(\Delta\psi)\cos\delta_0 + 2J_2(\Delta\varphi)J_2(\Delta\psi)\cos 2\delta_0\right] \end{aligned}$$

$$\begin{aligned} A_{+1} &= i\left[J_1(\Delta\varphi)\left(J_0(\Delta\psi) - J_2(\Delta\psi)\,e^{2i\delta_0}\right) + J_1(\Delta\psi)\left(J_0(\Delta\varphi)e^{i\delta_0} - J_2(\Delta\varphi)\,e^{-i\delta_0}\right)\right] \\ B_{+1} &= i\left[J_1(\Delta\varphi)\left(-J_0(\Delta\psi) + J_2(\Delta\psi)\,e^{2i\delta_0}\right) + J_1(\Delta\psi)\left(J_0(\Delta\varphi)e^{i\delta_0} - J_2(\Delta\varphi)\,e^{-i\delta_0}\right)\right] \end{aligned}$$

$$\begin{aligned} A_{-1} &= i\left[J_1(\Delta\varphi)\left(J_0(\Delta\psi) - J_2(\Delta\psi)\,e^{-2i\delta_0}\right) + J_1(\Delta\psi)\left(J_0(\Delta\varphi)e^{-i\delta_0} - J_2(\Delta\varphi)\,e^{i\delta_0}\right)\right] \\ B_{-1} &= i\left[J_1(\Delta\varphi)\left(-J_0(\Delta\psi) - J_2(\Delta\psi)\,e^{-2i\delta_0}\right) + J_1(\Delta\psi)\left(J_0(\Delta\varphi)e^{-i\delta_0} - J_2(\Delta\varphi)\,e^{-i\delta_0}\right)\right] \end{aligned}$$

$$\begin{aligned} A_{+2} &= -\left[J_0(\Delta\varphi)J_2(\Delta\psi)e^{2i\delta_0} + J_1(\Delta\varphi)J_1(\Delta\psi)e^{i\delta_0} - J_2(\Delta\varphi)J_0(\Delta\psi)\right] \\ B_{+2} &= \left[-J_0(\Delta\varphi)J_2(\Delta\psi)e^{2i\delta_0} + J_1(\Delta\varphi)J_1(\Delta\psi)e^{i\delta_0} - J_2(\Delta\varphi)J_0(\Delta\psi)\right] \end{aligned}$$

$$\begin{aligned} A_{-2} &= -\left[J_0(\Delta\varphi)J_2(\Delta\psi)e^{-2i\delta_0} + J_1(\Delta\varphi)J_1(\Delta\psi)e^{-i\delta_0} - J_2(\Delta\varphi)J_0(\Delta\psi)\right] \\ B_{-2} &= \left[-J_0(\Delta\varphi)J_2(\Delta\psi)e^{-2i\delta_0} + J_1(\Delta\varphi)J_1(\Delta\psi)e^{-i\delta_0} - J_2(\Delta\varphi)J_0(\Delta\psi)\right] \end{aligned}$$

Using these expression, given a incident beam in the form $\begin{bmatrix} E_{INC\ x} \\ \\ E_{INC\ y} \end{bmatrix}$, we can calculate for example the +1 order diffracted beam $\begin{bmatrix} E^{+1}_{TOT\ x} \\ \\ E^{+1}_{TOT\ y} \end{bmatrix}$ as:

$$\begin{bmatrix} E^{+1}_{TOT\ x} \\ \\ E^{+1}_{TOT\ y} \end{bmatrix} = \begin{bmatrix} A_{+1} & 0 \\ \\ 0 & B_{+1} \end{bmatrix} \begin{bmatrix} E_{INC\ x} \\ \\ E_{INC\ y} \end{bmatrix}$$

In this way it is possible to obtain +1 st order diffracted beam intensity and polarization state.
We can now consider two situations: horizontal or vertical linearly polarized readout beam. For horizontally (H) polarized light $\begin{bmatrix} 1 \\ 0 \end{bmatrix}$ we get:

$$\begin{bmatrix} E^{+1}_{H\ x} \\ \\ E^{+1}_{H\ y} \end{bmatrix} = \begin{bmatrix} A_{+1} & 0 \\ \\ 0 & B_{+1} \end{bmatrix} \begin{bmatrix} 1 \\ \\ 0 \end{bmatrix} =$$

$$\begin{bmatrix} i\left[J_1(\Delta\varphi)\left(J_0(\Delta\psi) - J_2(\Delta\psi)\,e^{2i\delta_0}\right) + J_1(\Delta\psi)\left(J_0(\Delta\varphi)e^{i\delta_0} - J_2(\Delta\varphi)\,e^{-i\delta_0}\right)\right] \\ \\ 0 \end{bmatrix}$$

For vertically (V) polarized light $\begin{bmatrix} 0 \\ 1 \end{bmatrix}$ we get:

$$\begin{bmatrix} E^{+1}_{V\ x} \\ \\ E^{+1}_{V\ y} \end{bmatrix} = \begin{bmatrix} A_{+1} & 0 \\ \\ 0 & B_{+1} \end{bmatrix} \begin{bmatrix} 0 \\ \\ 1 \end{bmatrix} =$$

$$\begin{bmatrix} 0 \\ \\ i\left[J_1(\Delta\varphi)\left(-J_0(\Delta\psi) + J_2(\Delta\psi)\,e^{2i\delta_0}\right) + J_1(\Delta\psi)\left(J_0(\Delta\varphi)e^{i\delta_0} - J_2(\Delta\varphi)\,e^{-i\delta_0}\right)\right] \end{bmatrix}$$

where $E_{H\,x}^{+1}$ is the horizontal component of the diffracted light with horizontal input polarization, $E_{H\,y}^{+1}$ is the vertical component of the diffracted light with horizontal input polarization. $E_{V\,x}^{+1}$ and $E_{V\,y}^{+1}$ are the same for vertical input polarization.

Theoretic expression for $\eta(\alpha)$, defined as the ratio of the first diffracted beam intensity to the total incident intensity, can be written in terms of the above obtained relations as

$$\eta_{\pm 1}(\alpha) = \cos^2\alpha\,[J_1(\Delta\varphi)J_0(\Delta\psi) - J_1(\Delta\varphi)J_2(\Delta\psi) + J_1(\Delta\psi)J_0(\Delta\varphi) - J_1(\Delta\psi)J_2(\Delta\varphi)]^2 + \\ + \sin^2\alpha\,[-J_1(\Delta\varphi)J_0(\Delta\psi) + J_1(\Delta\varphi)J_2(\Delta\psi) + J_1(\Delta\psi)J_0(\Delta\varphi) - J_1(\Delta\psi)J_2(\Delta\varphi)]^2$$

$$\eta_{\pm 2}(\alpha) = \cos^2\alpha\,[-J_0(\Delta\varphi)J_2(\Delta\psi) - J_2(\Delta\varphi)J_0(\Delta\psi) - J_1(\Delta\varphi)J_1(\Delta\psi)]^2 + \\ + \sin^2\alpha\,[-J_0(\Delta\varphi)J_2(\Delta\psi) - J_2(\Delta\varphi)J_0(\Delta\psi) + J_1(\Delta\varphi)J_1(\Delta\psi)]^2$$

The plots of these equations are shown in figure 2.10

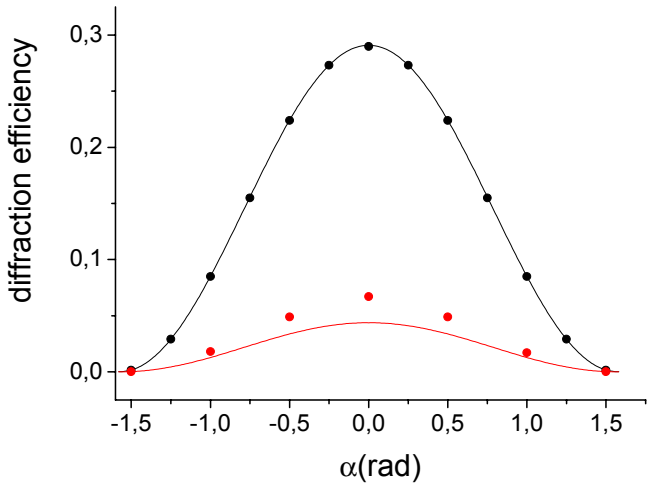


**Fig 2.10** Theoretical curves and experimental data of the diffraction efficiency versus the polarization azimuthal angle α for a grating recorded at 270mW/cm$^2$ intensity.

We can see that the theory that takes into account both the contributions, the linear birefringence and the topographical modulation, reproduces with good approximation the polarization

dependence observed in the experimental curves. From the measurements of the diffraction efficiency versus the angle α for gratings written at different light intensities we have calculated the values of $\Delta\varphi$ and $\Delta\psi$, reported in figure 2.11 and in table 2.1. These values, obtained by the fits, refer to the polarization characterization of gratings recorded at different writing intensities.

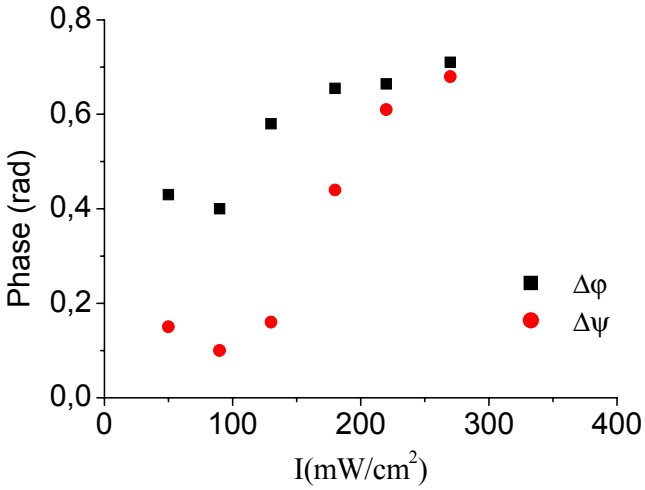


**Fig 2.11** $\Delta\varphi$ and $\Delta\psi$ values versus the recording intensity.

## Table 2.1

| $I(mW/cm^2)$ | $\Delta\varphi$ | $\Delta\psi$ |
|---|---|---|
| 50 | 0.43±0.02 | 0.13±0.01 |
| 90 | 0.40±0.02 | 0.10±0.01 |
| 130 | 0.58±0.03 | 0.16±0.01 |
| 180 | 0.65±0.03 | 0.44±0.02 |
| 220 | 0.66±0.03 | 0.61±0.03 |
| 270 | 0.71±0.03 | 0.68±0.03 |

These results indicate that, increasing the recording intensity, the relief depth probably grows, amplifying the anisotropy of the first orders diffracted intensities. In fact, the value of $\Delta\varphi$

remains almost constant, which means that the photoinduced linear birefringence does not change noticeably increasing the intensity.

For $\alpha = 0°$ and $\alpha = 90°$ the polarization state of the diffracted beams is equal to the incident beam one, which means that the diffracted beams have only a horizontal component for horizontal input polarization and a vertical component for the vertical input polarization of the readout beam. This behavior is in agreement with the experimental observations.

In figure 2.12 we report the Atomic Force Microscope image of the grating recorded at $270 mW/cm^2$ that shows the presence of the SRG. AFM measurements are performed on the surface opposite to the irradiated side of the sample after removing the glass substrate. In fact, after recording, the film adheres to the front plate, but easily separates from the rear glass where no polymer is left, so that on opening the cell the grating always sticks to the front plate. The relief grating profile shows a spatial periodicity of about $7\mu m$, corresponding to the polarization pattern one, and a depth of about $200nm$ (figure 2.12b). Moreover, the sinusoidal shape of the reliefs supports the negligible contribution of thermal effects on the SRG, as expected for uniform illumination.

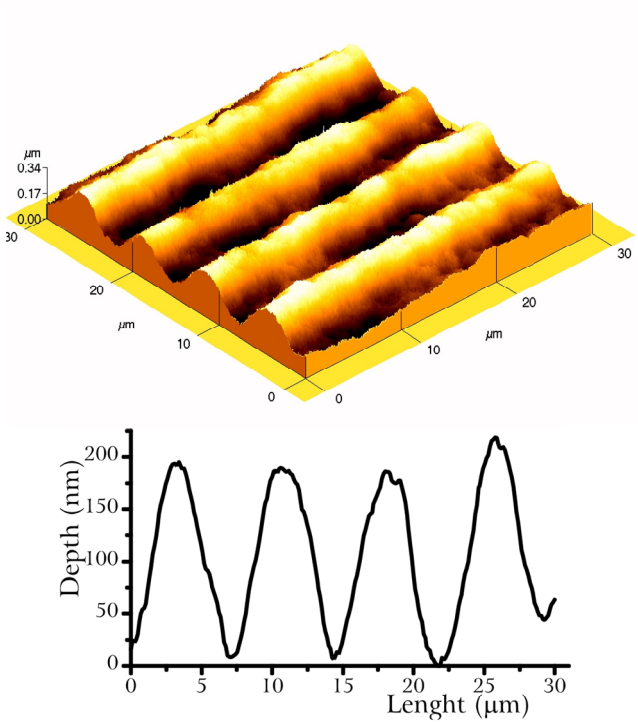


(a)

(b)

**Fig 2.12** Topography of the grating recorded at 270mW/cm$^2$. AFM image (a), and profile (b).

We estimated the phase shift $\delta_0$ between the SRG and the orientational grating. The intensity diffracted into the +1 st order by a linearly (vertically V and horizontally H) polarized beam is thus

$$I_{Vy} = \left|E_{Vy}^{+1}\right|^2 = \left|-J_0(\Delta\psi)J_1(\Delta\varphi) + J_0(\Delta\varphi)J_1(\Delta\psi)e^{i\delta_0}\right|^2 I_0$$

$$I_{Hx} = \left|E_{Hx}^{+1}\right|^2 = \left|J_0(\Delta\psi)J_1(\Delta\varphi) + J_0(\Delta\varphi)J_1(\Delta\psi)e^{i\delta_0}\right|^2 I_0$$

where $I_0$ is the incident light. From symmetry considerations we will expect that $\delta_0 \in \left\{0, \frac{\pi}{2}, \pi, \frac{3\pi}{2}\right\}$. In all our measurements we have found that $I_{Hx} \neq I_{Vy}$, then we can conclude that $\delta_0 \in \{0, \pi\}$. The two cases correspond to the following situations:

1. $\delta_0$=0, $I_{Hx} > I_{Vy}$
2. $\delta_0 = \pi$ $I_{Hx} < I_{Vy}$

Because $\Delta\varphi$>0 ($\Delta\psi \neq 0$ by definition), and for all our measurements $I_{Hx} > I_{Vy}$, we can therefore conclude that $\delta_0$=0. This means that peaks of the SRG coincide with the horizontal polarization of the total field, i.e. where the polarization is parallel to the grating vector.
To elucidate this point, in figure 2.13 the polarization light pattern scheme (a) is shown together with the sketch of the two grating components: the surface reliefs (b) and the linear birefringence modulation (c).

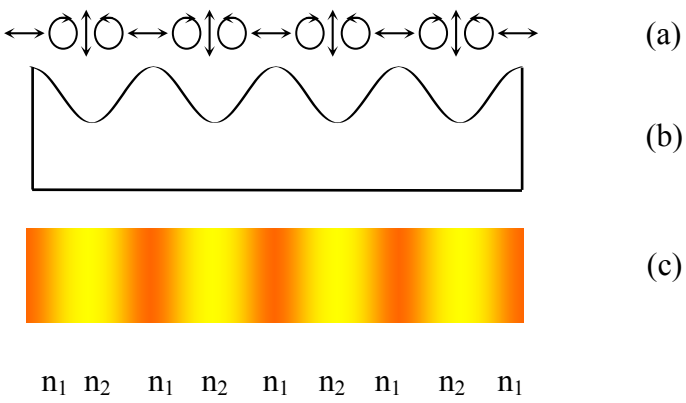


**Fig 2.13** Scheme of the composite grating and of the polarization pattern (a). Both contributions are represented: surface relief (b) and photoinduced birefringence modulation (c).

The birefringence modulations and the relief grating are in phase with the polarization pattern, and the reliefs correspond to the region irradiated by the linear polarization parallel to the grating vector.

## 2.3.3 Simple model of birefringence modulation

In order to achieve information on both internal morphology and topography of the composite gratings from the obtained data, we propose a simple model of birefringence modulation. Some assumption have been made: the amplitude of the phase modulations related to linear birefringence and relief modulation can be written as follows:

$$\Delta\varphi = \frac{\pi \Delta n d}{\lambda} \qquad \Delta\psi = \frac{2\pi}{\lambda} d_1 \frac{\left(n_p - n_a\right)}{2} \tag{2.2}$$

where $d$ is the sample thickness, $\Delta n$ is the photoinduced linear birefringence, $d_1$ the surface modulation depth, $n_p$ the average PDLC refractive index and $n_a$ the refractive index of the vapours produced during the irradiation. The refractive index modulation ($\Delta n$) is due only to the periodic change of the liquid crystal orientation inside the droplets, which are uniformly

distributed in the solid polymeric matrix. Afterward, a simple sketch of the internal optical modulation is done considering the two extreme regions having the largest and the smallest refractive indices indicated by $n_1$ and $n_2$ respectively, as reported in the figure 2.14:

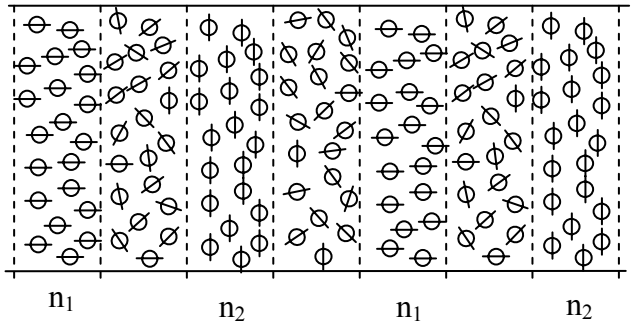


**Fig 2.14** Scheme of the distribution model of the liquid crystal droplets orientation

In one region, the optical axis of the liquid crystal droplets is oriented along the grating wave vector while in the other is oriented orthogonal. These conjectures are well supported by optical microscope observations reported in figure 2.6, where uniform orientation of the liquid crystal droplets in the grating stripes is shown. In addition, the scanning electron microscope images reported in figure 2.4 reveal a uniform internal morphology. As a consequence, $\Delta n$ can be written in terms of effective extraordinary $n_{ed}$ and ordinary $n_{od}$ refractive indices of the liquid crystal droplets, introducing some modification in the procedure reported in reference 47. The refractive index of the region where the optical axes of the liquid crystal droplets are mainly oriented along the grating wave vector can be written as:

$$n_1 = fn_{ed} + (1-f)n_p(LC)$$

while the refractive index of the region with liquid crystal droplets oriented orthogonally can be written as:

$$n_2 = fn_{od} + (1-f)n_p(LC)$$

where $f$ is the volume fraction of the liquid crystal inside the droplets, $n_p(LC)$ the refractive index of the polymeric matrix, $n_{ed}$ and $n_{od}$ the extraordinary and ordinary effective refractive indices of the droplets, that can be written as[47]

$$n_{ed}(S_d) = \frac{n_e n_o}{\left[ n_e^2 + \frac{1}{3}(n_o^2 - n_e^2)(2S_d + 1) \right]^{1/2}} \tag{2.3}$$

and

$$n_{od}(S_d) = \frac{2}{\pi} n_o F\left[ \frac{\pi}{2}, \frac{1}{n_e}\left[ \frac{2}{3}(n_e^2 - n_o^2)(1 - S_d) \right]^{1/2} \right] \tag{2.4}$$

Here $F(\theta, m)$ is the complete Legendre elliptic integral of the first kind, $S_d$ the order parameter of the liquid crystal droplets, $n_o$ and $n_e$ the ordinary and extraordinary refractive indices of the liquid crystal respectively[46]. From the equations (2.3) and (2.4), the photoinduced birefringence $\Delta n$ can be easily written as

$$\Delta n = n_1 - n_2 = f(n_{ed} - n_{od}).$$

From the values of $\Delta\varphi$ obtained by the fits, $\Delta n$ values are calculated, as reported in table 2.2. Interesting information regarding the internal morphology can be deduced. In the evaluation the droplets order parameter is supposed to be $0{,}7$, this value is justified by the optical microscope observation showing a good alignment of the liquid crystalline domain. Subsequently, the ordinary and extraordinary refractive indices of the droplets are calculated from the equation (2.3) and (2.4). Using $\Delta n$ obtained by the fits, the filling fraction of liquid crystal inside the droplets is thus evaluated. The obtained results are consistent with the hypothesis that a considerable fraction of liquid crystal still remains in the polymeric matrix, while the filling fraction of liquid crystal inside the droplets is only 15-25%. This outcome suggests a small size of the liquid crystal droplets, less than $100nm$, as also supported by the low scattering and the high diffraction efficiency of the recorded gratings. From equation of $\Delta\psi$ (2.2), taking an average refractive index of the PDLC $n_p = 1.5$, a weighted average of the polymer and the liquid

crystal refractive indices, $n_a = 1$, $d = 8\mu m$ and $\lambda = 632.8nm$, we obtain for the reliefs depth $d_1$ the values reported in the table 2.2.

**Table 2.2**

| $I(mW/cm^2)$ | $\Delta\varphi$ | $\Delta\psi$ | $\Delta n$ | $d_1(nm)$ |
|---|---|---|---|---|
| 50 | 0.43±0.02 | 0.13±0.01 | 0.011±0.001 | 50±3 |
| 90 | 0.40±0.02 | 0.10±0.01 | 0.010±0.001 | 37±2 |
| 130 | 0.58±0.03 | 0.16±0.01 | 0.015±0.001 | 58±3 |
| 180 | 0.65±0.03 | 0.44±0.02 | 0.016±0.001 | 140±7 |
| 220 | 0.66±0.03 | 0.61±0.03 | 0.016±0.001 | 200±10 |
| 270 | 0.71±0.03 | 0.68±0.03 | 0.018±0.001 | 220±10 |

We can see that a surface modulation depth of about $220nm$ has been evaluated in the case of grating written with intensity of $270mW/cm^2$, as obtained in the AFM experiment.

The best fit of experimental data, as reported in figure 2.16 curve (1), is obtained for $\Delta n = 0.018$ and $d_1 = 210nm$, with $d_1$ very close to the value measured by AFM. In the absence of reliefs, i.e. $d_1 = 0nm$, the diffraction efficiency versus $\alpha$ is uniform, as represented by curve (2) in the graph:

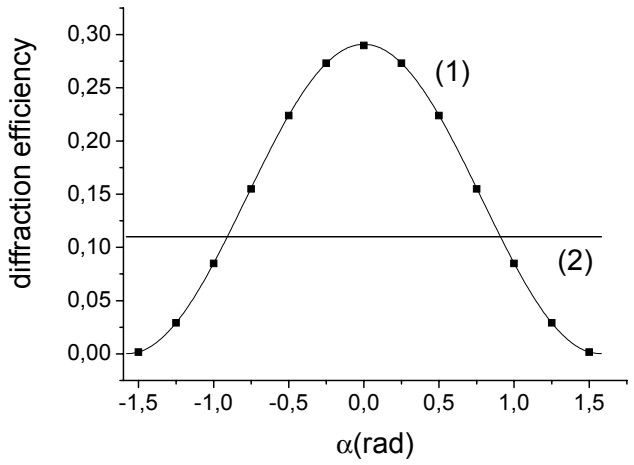


**Fig 2.15** Experimental values (dots) of the first order diffraction efficiency versus the polarization azimuthal angle a for grating recorded at 270mW/cm$^2$ intensity and theoretical curves of the efficiency calculated for $d_1$=210nm (curve1) and for $d_1$=0 (curve 2).

## 2.4 Conclusion

In conclusion, we have reported an experimental and theoretical study of holographic gratings recorded exposing a homogeneous mixture of prepolymer and liquid crystals to a polarization light pattern. The obtained PH-PDLC grating exhibits peculiar features, which differs from the ones produced by the standard intensity technique (H-PDLC): in the conventional method, in fact, the recorded gratings originate from the modulation of the internal morphology of the materials. On the contrary, the internal morphology of the PH-PDLC is fairly uniform, and the gratings originate from the liquid crystal orientation inside the droplets, that are produced after the phase separation. Then, in contrast to H-PDLC, where the optical axes of the droplets are randomly oriented, PH-PDLC has the optical axes direction of the droplets spatially modulated. A large anisotropy of the diffraction efficiency characterizes the recorded gratings, that reaches values ranging from 1% to 30%. Results from optical characterization of the diffracted and transmitted beam suggest that, beside linear birefringence due to the orientation of the liquid crystal director, also surface reliefs on the film topography should be considered. In fact, permanent reliefs with depth of few hundreds of nanometres are recorded on the surface of a polymeric material containing nanosized oriented liquid crystal droplets, as demonstrated by the AFM measurements.

The theoretical model, properly modified to take into account both the linear birefringence and surface reliefs, is in good agreement with the measured reliefs depth values. Some hypotheses are made on the role of the anisotropic phase separation related to the polarization sensitive crosslinking of the polymer, which can induce mass transport, such as in photoisomerizable systems.

Two main aspects have to be stressed. The building of composite materials by means of irradiation with a polarization pattern makes evidence of novel potentialities of polymer-dispersed liquid crystals, mainly for diffractive devices. The formation of surface reliefs grating under uniform intensity irradiation is a more general phenomenon, no strictly related to photoisomerization, which could involve photoinduced chemical reactions sensitive to the polarization. These photochemical effects influence the organization of anisotropic structures during the recording process.

# References:

**1** T.J. Bunning, L.V. Natarajan, V.P. Tondiglia, R.L. Sutherland,et al, *Polymer* **36**, 2699

**2** L.V. Natarajan, R.L. Sutherland, V.P. Tondiglia, T.J. Bunning, et al, *J. Nonlinear Opt. Phys. Mater.* **5**, 89

**3** D. Duca, A.V. Sukhov, C. Umeton, *Liq. Cryst.* **26**, 931

**4** A.Y.G. Fuh, T.C Ko.,et al, *J. Appl. Phys.,* **83**, 679

**5** A.Y.G Fuh., T.C Ko.,et al, *Appl. Phys. Lett.,* **74**, 2572

**6** G. Cipparrone, A. Mazzulla, F. Simoni, *Opt. Lett.,* **23**, 1505

**7** F. Simoni, G. Cipparrone, A. Mazzulla, P. Pagliusi, *Chem. Phys.,* **245**, 429

**8** P. S. Drzaic, Liquid Crystal Dispersion, *World Scientific,* 1995

**9** R.L. Sutherland, *J. Opt. Soc. Am. B*, **19**, No 12, 2995

**10** K. Tanaka, K. Kato, M. Date, *Jpn. J. Appl. Phys*.,**38**, 277

**11** C.C. Bowley, G.P. Crawford, *J. Opt. Techonol*. **67**, 717

**12** R. Smith, M. Popovich, *J. Soc: Inf. Disp.* **9**, 203

**13** R.L. Sutherland, L.V. Natarajan, V.P. Tondiglia, T.J. Bunning, *Chem. Mater.* **5**, 1533

**14** T.J. Bunning, L.V. Natarajan, V.P. Tondiglia, R.L. Sutherland, et al *Appl. Phys. Lett.* **64**, 1074

**15** J.J. Butler, M.S. Malcuit, *Opt. Lett.,* **25**, 420

**16** R.L. Sutherland, V.P. Tondiglia, L.V. Natarajan, T.J. Bunning, *Appl. Phys. Lett.* **79**, 1420

**17** J.J. Butler, M.S. Malcuit and M.A. Rodriguez, *J. Opt. Soc. Am. B*, **19**, 183

**18** N.V. Tabirian, A.V. Sukhov, B. Y. Zeldovich, *Mol. Cryst. Liq. Cryst.* **136,** 1-139

**19** I. C. Khoo, Liquid crystals: Phyical properties and nonlinear optical phenomena, *Wiley, New York*, 1995.

**20** N.C.R. Holme, P.S. Ramanujam, S. Hvilsted, *Appl. Opt*. **35**, 4622

**21** C. Decker, *Prog. Polym. Sci.*, **21**, 593

**22** A. Mazzulla, A. Dastoli, G. Russo, L. Lucchetti, G. Cipparrone, *Liq. Cryst.*, **30**, 87

**23** G. Cipparrone, A. Mazzulla, G. Russo, *J. Opt. Soc. Am. B*, **18**, 1821

**24** G. Cipparrone, A. Mazzulla, G. Russo, *Appl. Phys. Lett.,* **78**, 1186

**25** L. Nikolova and T. Torodov, *Opt. Acta* **31**, 579

**26** I. Naydenova, L. Nikolova, T. Torodov, et al, *J. Opt. Soc. Am. B* **15**, 1257

**27** N.C.R. Holme, L. Nikolova, S. Hvilsted, et al, *Appl. Phys. Lett.,* **70**, 1518

**28** F. Lagugnè Labarthet, T. Buffetteau, C. Sourriseau, *J. Phys. Chem. B,* **102**, 5754

**29** F. Lagugnè Labarthet, T. Buffetteau, C. Sourriseau, *J. Phys. Chem. B,* **102**, 2654

**30** F. Lagugnè Labarthet, T. Buffetteau, C. Sourriseau, *J. Phys. Chem. B,* **103**, 6690

**31** M. De Sarkar, N. L. Gill, J. B. Whitehead, G. P. Crawford, *Macromolecules* **36**, 630

**32** N. Kawatsuki, T. Hasegawa, H. Ono, T. Tamoto, *Adv. Mater* **15**, 991

**33** F. Lagugnè Labarthet, J. L. Bruneel, T. Buffetteau, et al, *Phys, Chem. Chem. Phys.*, **2**, 5154

**34** S. Bian, L. Li, J. Kumar, et al, *Appl. Phys. Lett.,* **73**, 1817

**35** J. Kumar, L. Li et al, *Appl. Phys. Lett.,* **72**, 2096

**36** S. Bian, J. M. Williams, D. Y. Kim, et al, *J. Appl. Phys.,* **86**, 4498

**37** P. Lefin, C. Fiorini, M. Nunzi, *Pure Appl. Opt., 7*, 71

**38** C. Fiorini, N. Prudhomme, P. Lefin, *Macromol. Symp.*, **137**, 105

**39** M. Pedersen, P. M. Johansen, et al, *J. Opt. Soc. Am. B* **15**, 1120

**40** M. Pedersen, P. M. Johansen, et al, *Phys. Rev. Lett.,* **80**, 89

**41** C. J. Barret, A. L. Natanshon, et al, *J. Phys. Chem. B,* **100**, 8836

**42** N. Kawatsuki, T. Hasegawa, H. Ono, *Adv. Mater.* **15**, 991

**43** Tran Cong Miyata O., *Macromol. Symp.,* **160**, 91

**44** Q. Trang Cong, K. Kataoka, O. Urakawa, *Phys. Rev. E,***57**, R1243

**45** A. Mazzulla, P. Pagliusi, C. Provenzano, et al, *Appl. Phys. Lett.,* **85**, 2505

**46** F. Simoni, Nonlinear Optical Properties of Liquid crystals, *World Scientific,* Teaneck NJ, 1997

**47** M.E.Holmes, M.S. Malcuit, *Phys Rev E* **65**, 066603, and reference therein

# Chapter 3

## 3.1 Introduction

In this chapter we discuss the possibility to obtain highly efficient and electrically switchable liquid crystal based diffraction grating, exploiting polarization holography, in order to modulate the anchoring axis at the surface of a liquid crystal cell. Taking advantage of the interactions at the interface between a holographic patterned substrate and a thin film of liquid crystal, we obtain diffractive devices characterized by high diffraction efficiency, low scattering and whose diffracted and transmitted beams can be modulated in intensity by means of a low external voltage[1]. The idea of our work is based on the fact that holographic gratings on some photosensitive material provide a periodic alignment of the nematic liquid crystals. This effect originates from the anisotropic van der Waals interactions between elongated partially conjugated liquid crystal molecules and strongly conjugated dye molecules[2-4]. Therefore, recording the holographic grating on a photosensitive material insoluble in a nematic liquid crystal, and putting the grating in contact with the liquid crystal, we expect that the diffraction properties of the grating will be transferred to the liquid crystal. Exploiting the electro-optical manipulation of liquid crystal based devices, it would be possible completely control the diffracted energy distribution by means of an external voltage[1-3].

The alignment of liquid crystals has received a considerable attention by scientists and engineers. For this reason a number of materials and techniques have been proposed in order to create multidomain configurations for liquid crystal materials, with particular electro-optic behaviour compared to the well described single domain liquid crystal alignment typically imposed by a polyimide layer.

Control over the surface anchoring is an important issue in the preparation of liquid crystal based electro-optical devices, and several approaches, which means several alignment techniques, have been proposed with the aim to obtain homogenous liquid crystal film with periodic orientation of the nematic director. In the last ten years, the field of patterning surface alignment layers for liquid crystals has become larger. Chen and co-workers have shown a hybrid liquid crystal configuration using photolithography to create a double rubbed polyimide layer for a high

efficiency polarization grating[5]. Wen and co-workers have shown a dual-domain polarization grating configuration created from scribing a polyimide layer with an atomic force microscope that produces right and left handed twisted regions[6]. Versteeg and co-workers have applied direct laser writing methods to melt polyimide regions, creating multidomain configurations of planar and twisted alignments[7]. Varghese and co-workers have demonstrated a four domain liquid crystal alignment using a microrubbing technique on homeotropic polyimide[8,9].

All these methods (photolithography, laser scanning, atomic force microscope patterning etc.) are multi-steps processes and in some cases require very complicated procedures and give a discrete alignment for the liquid crystal. Another method of surfaces patterning for liquid crystal alignment is obtained using a holographic recording on a photosensitive layer[10-14]. Compared with the previous methods of spatial patterning, polarization holography exposure is a flexible technique, that presents several advantages, as for example, it is a single step process, it is possible to obtain different configuration changing the polarization states of the writing beams, it is possible for same configurations to obtain diffraction gratings with 100% of diffraction efficiency, even in thin film. Moreover, the polarization recording provides a continuously varying polarization imprint on the alignment layer. Exploiting several possible polarization patterns, polarization holographic recording of photo-polymeric or azo-dye doped polymeric aligning layers has demonstrated spatial modulation of the optical axis direction in the liquid crystal. For example, recently Crawford and co-workers[15,16], and Sarkissian and co-workers[17] confirmed the possibility to obtain liquid crystal based diffraction grating using this method. Nevertheless, the reported results do not show very exciting performances of the devices, because of diffraction efficiency lower than 10%, and high scattering.

Our work is based on the creation of periodic boundary conditions in liquid crystal cell, using an azo-dye doped polymeric layer exposed to a polarization interference pattern. In particular, the uniform rotation imposed to the liquid crystal optical axis is obtained in an indirect way: in fact, the periodic alignment previously stored by holographic technique at the aligning surfaces, is transferred to the molecular director of the liquid crystal in the bulk. Our experiments have been made with different cell configurations, depending on the aligning behaviour of the two confining substrates. Planar-periodic – planar-periodic liquid crystal cell has been obtained using both patterned polymeric layers. Planar – planar-periodic and homeotropic – planar-periodic hybrid cells have been obtained using only one patterned polymeric layer together with a

homogenous planar and a homeotropic substrate, respectively. Crossed cells have been obtained using two patterned polymeric layers, but assembled with orthogonal pattern orientation. Here we discuss in more details the systems in which both the substrates are patterned.

The planar-periodic – planar-periodic liquid crystal grating is obtained by writing on both the surfaces the same polarization hologram. In this case, we produce one dimensional (1D) diffractive optical elements with a periodic modulation of the refractive index. The results show devices with very high performances, because of their diffraction efficiency that reaches about 100%, and the possibility to switch the intensity between the diffracted and the transmitted beams by means of an external electric field. Because of their properties these gratings may have numerous applications in photonic systems and displays, including highly efficient projection displays, polarized beam splitting devices, multiplexing and polarization dispersion applications.

Hybrid planar – planar-periodic and homeotropic – planar-periodic cells have been assembled using a rubbed polyimide layer and a DMOAP layer, respectively. Also in this case we obtain electrically switchable diffractive devices, with low scattering and good diffraction efficiency.

Finally, we report on the features of crossed cells which show two dimensional (2D) structures: as in the case of 1D gratings, both the substrates are photosensitive polymeric aligning layers, which were independently exposed to the polarization pattern. After recording of the holograms, the crossed cell is assembled sandwiching these two substrates together with the alignment layers facing each other, but rotating them by 90° with respect to each other. The experiment has yielded excellent results: we have obtained 2D gratings that diffract the incident beam in several diffracted beams with various polarization states at the same time. They are characterized by low scattering and high diffraction efficiency. The energy distribution can be controlled by means of the polarization state of the incident beam. Additionally, exploiting the high sensitivity of the liquid crystal based devices to the external fields, the distribution of the intensity on the diffracted beams can be completely controlled by means of a low external voltage.

# 3.2 Material and experiment

## 3.2.1 Material

A polarization sensitive photoaligning material, which exhibits photoinduced optical anisotropy and is insoluble in liquid crystals, is needed for polarization holographic recording and for replicating the surface polarization holograms in the liquid crystal bulk. A polymeric mixture of an azo-dye, the P4G whose chemical formula is depicted in figure 3.1, and a polyimide has been selected as photosensitive material, because it possess the required features.

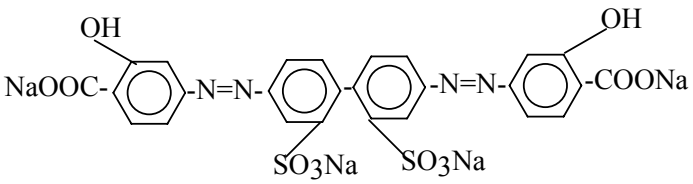


**Fig 3.1** Chemical formula of the dye P4G.

The dye P4G and the polyimide mixture (1:1 by weight) were dissolved in dimethilformamide. In the figure 3.2 is reported the absorption spectrum of the 2% solution, in which the writing wavelength $\lambda = 457nm$ and the probe beam wavelength $\lambda = 632.8nm$ are highlighted.

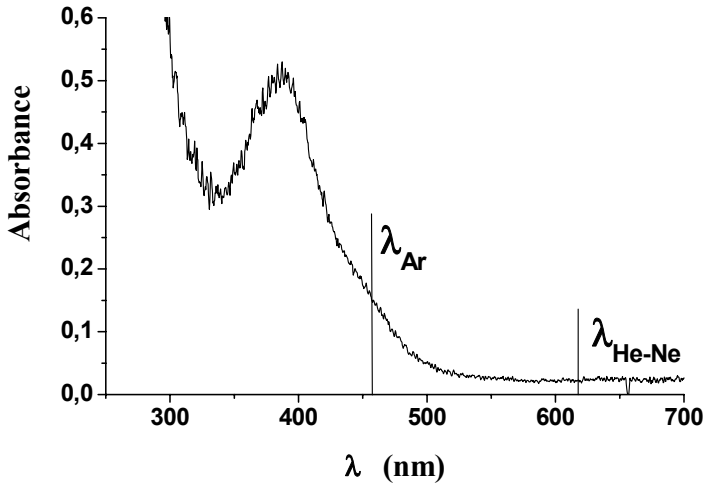


**Fig 3.2** Absorption spectrum of the 2% solution, in which are highlighted the writing wavelength λ=457nm and the probe beam wavelength λ=632.8nm.

The photoinduced alignment of a liquid crystal on azo-dye films and new photoaligning materials has been subject of extensive researches for the liquid crystal display applications[18], because photo alignment is a non contact method which enables the creation of high quality orientation of the liquid crystal layer without mechanical damage of the substrate, electrostatic charge or dust contamination. The quality of the photoaligned cells based on photochemical reactions proves to be very high[19], and the substances developed can be classified by the physical origin of the photoaligning phenomenon. In fact, there are several photo chemical reactions involved in the photoalignment phenomena: reversible cis-trans isomerization, photodimerization or crosslinking and photodegradation. The photosensitive azo compounds are known to produce alignment of the liquid crystal director as a result of the reversible cis-trans isomerization chemical reaction. But, in case of P4G[19] both photochemical reactions and cis-trans-isomerization should not significantly contribute to the photo-induced reorientation in azo dye. One of the possible photoaligning mechanisms in films of P4G is a pure reorientation of the azo dye molecules[19]. When the azo dye molecules are optically pumped by a linearly polarized light beam, the probability of reorientation is proportional to the square of cosine of the angle between the absorption oscillator of the azo dye molecules and the polarization direction of the light. Therefore, the azo dye molecules which have their absorption oscillators, the chromophores, parallel to the light polarization will most probably acquire the increase in energy which results in their reorientation from the initial position. These results in an excess of chromophores aligned in a direction such that the absorption oscillator is perpendicular to the polarization of the light. For P4G, the chromophores are parallel to the long molecular axis of the azo dye, that is the azo dye molecules tend to align with their long axes perpendicular to the light polarization. Hence, a thermodynamic equilibrium in the new oriented state will be established. Consequently, anisotropic dichroism or birefringence is photoinduced permanently. The azimuthal anchoring energy of the photoaligned substrate is $E>10^{-4}$ J $m^{-2}$, which is comparable with the anchoring of rubbed polyimide layer[19]. Then, the photo aligning phenomenon in case of the P4G can be explained by a model of rotational diffusion of the azo dye molecules in the field of the polarized light, whereby, in the final state, the azo dye chromophores or molecular long axes are perpendicular to the polarization direction of the light.

## 3.2.2 Experiment

Photosensitive aligning layers of $20nm$ thickness have been obtained by spin coating of the 2% polyimide and azo-dye solution on indium tin oxide (ITO) coated glass substrate. After the spin coating, the substrates were heated to remove the solvent from the alignment layers.

The experimental set-up used for the polarization hologram writing process is shown in the following figure:

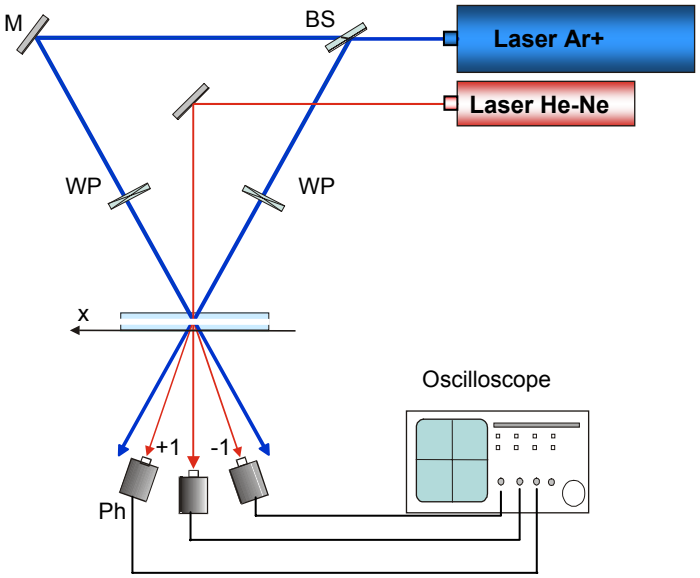


**Fig 3.3** Experimental set-up used for the holographic writing. BS: beam splitter, M: mirror; WP: λ/4 wave plate; Ph: photodiode.

The empty cells were prepared by sandwiching these two substrates with the alignment layers facing each other. In 1D configurations, the empty cells were exposed to the polarization pattern obtained by interference of two $Ar^+$ laser wave with orthogonal polarization states. In the case of crossed cells, the dye-doped polyimide films were separately exposed to the same interference pattern and then assembled in order to obtain the 2D structures.

In all the empty cells diffraction was below the detection limit, because of small thickness and low photoinduced birefringence of the polymer layer. When the liquid crystalline material was infiltrated into the empty cells by capillary action in isotropic phase, and slowly cooled down in the nematic phase at room temperature, the diffracted beams appeared.

## 3.3 One dimensional grating

### 3.3.1 Planar periodic-planar periodic configuration: theory

Starting from the 1D gratings, we want to create a cell with a periodically planar alignment of the nematic film, in which the liquid crystal director $\vec{n}$ is confined in the ($x$, $y$)-plane and monotonously rotate in transverse direction $x$, so that a periodic structure[20]

$$\vec{n} = \vec{n}_0(x) = [\cos(qx), \sin(qx), 0] \qquad q = 2\pi/\Lambda, \tag{3.1}$$

is realized. Here $\Lambda$ is the director's modulation period. Since liquid crystal's vector of director $\vec{n}$ and its negative, $-\vec{n}$, are physically equivalent, physical properties of such nematic liquid crystal are modulated with the period $\Lambda/2$. Such liquid crystal film is locally birefringent, with the optical axis lying in ($x$, $y$)-plane and rotating along the $x$ direction continuously, see Figure 3.4a and 3.4b. We now consider the effect of this birefringence on normally incident light using the Jones matrix analysis[21] , as described in chapter 2:

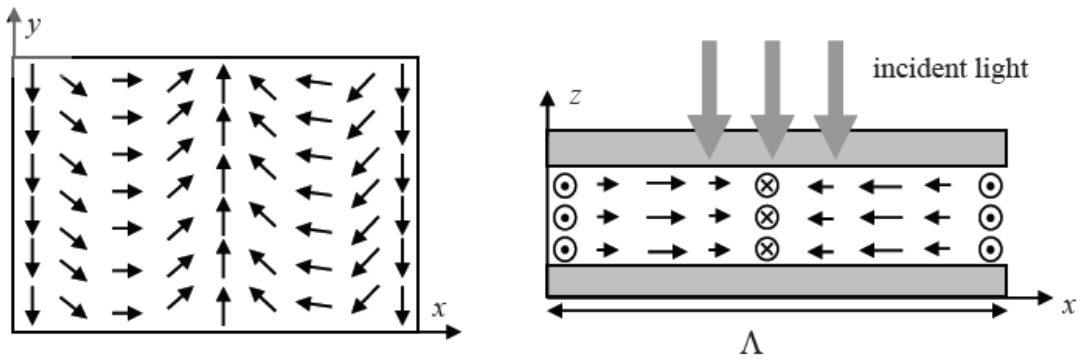


(a) (b)

**Fig 3.4** Orientation of liquid crystal in a planar cell 0≤z≤d, in which the liquid crystal director $\vec{n}$ is confined in the ($x$, $y$)-plane and monotonously rotate in transverse direction $x$. Figure a: top view. Figure b: side view.

The transmission matrix describing this kind of device can be written in the following form:

$$T_{TOT} = \begin{bmatrix} \cos(\Delta\varphi) + i\sin(\Delta\varphi)\cos qx & i\sin(\Delta\varphi)\sin qx \\ i\sin(\Delta\varphi)\sin qx & \cos(\Delta\varphi) - i\sin(\Delta\varphi)\cos qx \end{bmatrix}$$

with $\Delta\varphi = \frac{\pi(n_e - n_o)\,d}{\lambda}$ in which $\Delta n = (n_e - n_o)$ is the photoinduced birefringence, $d$ is the thickness of the film, and $\lambda$ is the wavelength of the light.

Using a probe beam, with arbitrary polarization state,

$$E_{IN} = \begin{pmatrix} E_x \\ E_y \exp i\vartheta \end{pmatrix}$$

we get the following result for the field just after it has passed through the nematic film:

$$E_{OUT} = \begin{bmatrix} \cos(\Delta\varphi) + i\sin(\Delta\varphi)\cos qx & i\sin(\Delta\varphi)\sin qx \\ i\sin(\Delta\varphi)\sin qx & \cos(\Delta\varphi) - i\sin(\Delta\varphi)\cos qx \end{bmatrix} \begin{pmatrix} E_x \\ E_y \exp(i\vartheta) \end{pmatrix}$$

The diffracted beams, written in terms of Jones matrix are:

$$E_0 = \cos(\Delta\varphi) \begin{pmatrix} E_x \\ E_y \exp(i\vartheta) \end{pmatrix},$$

$$E_{+1} = i\frac{\sin(\Delta\varphi)}{2}\left(E_x - iE_y \exp(i\vartheta)\right) \begin{pmatrix} 1 \\ -i \end{pmatrix}$$

$$E_{-1} = i\frac{\sin(\Delta\varphi)}{2}\left(E_x + iE_y \exp(i\vartheta)\right) \begin{pmatrix} 1 \\ i \end{pmatrix}$$

This grating shows the same feature of a pure polarization grating, as described in chapter 2, and in particular, the zero order preserves the polarization state of the incident wave, and the first orders $\pm 1$ are always opposite circularly polarized, independently from the polarization state of the incident wave.

The diffraction efficiency of the diffracted beams is equal to

$$\eta_{+1} + \eta_{-1} = \sin^2(\Delta\varphi)$$

$$\eta_0 = \cos^2(\Delta\varphi)$$

As it is well know, the diffraction efficiency $\eta_{\pm 1}$ in the first order spots and the zero order diffraction $\eta_0$, can be controlled by the photo induced optical anisotropy $\Delta n = n_e - n_o$ of the photosensitive material and by the thickness of the film $d$ through the value of its phase retardation $\Delta\varphi$[1-3].

Another important characteristic can be obtained for proper architecture of the liquid crystal cell, and for which it is possible to obtain 100% of diffraction efficiency: in fact, if the thickness of the cell $d$ satisfies the condition of half-wave plate[1,20],

$$d(n_e - n_o) = \left(m - \frac{1}{2}\right)\lambda, \qquad \text{with } m \text{ integer}$$

then all power of incident wave is transferred in the diffracted beams, and in particular the right circular polarization is transferred into the +1 diffraction order, which is left circularly polarized. Similarly, incident wave with left circular polarization is 100% transferred into the −1 diffraction order, which is right circularly polarized.

Liquid crystal devices with the described features can be useful for many practical applications.

The easiest way to obtain the described nematic liquid crystal structure is through the modulation of the planar alignment at the top and the bottom interfaces. The anchoring of the liquid crystal at the boundary is usually achieved by mechanical rubbing of the surface coated with a very thin polymer layer. Orientation of equation (3.1) evidently cannot be realized with rubbing. However, there is another method to create the prescribed anchoring: monotonously rotating azimuth can be obtained by means of holographic recording. In particular with the interference pattern produced by overlapping of a pair of two mutually coherent circularly polarized waves, right and left circular respectively. In fact, as described in the chapter 2 the periodic spatially rotating linear polarization pattern, represented in figure 3.5, is obtained by interference of two waves with opposite circular polarization.

**Fig 3.5** Polarization modulation of the interference light field recording the grating in the opposite circular polarization configuration

The rest of this section deals with the problem of stability of the ideal structure of the director, equation (3.1), in the bulk of the nematic liquid crystal cell. In fact, in our case, the uniform rotation of optical axis is not obtained writing directly the polarization grating in the material; the periodic alignment is transferred from the aligning layers to the liquid crystal bulk. For this reason, the achievement of highly efficient diffraction gratings implies additional condition to the cell geometry. Our goal is to preserve for the liquid crystal in the bulk the same rotation imposed at the surfaces. When thickness $d$ is small, the director distribution in the bulk should follow the configuration imposed by the surfaces. For thicker cells, such distribution becomes unstable. Indeed, the increasing contribution of the elastic energy in the bulk over the aligning energy at the surfaces promotes the relaxation of the modulation imposed by the surfaces towards a homogeneous director configuration in the bulk. The onset of this instability is characterized by the value of a critical thickness, above which the structure of equation (3.1) can not be achieved over the liquid crystal film.

In order to analyze the stability of the director distribution in the bulk, we have to solve the equilibrium equations with appropriate boundary conditions, taking into account the elasticity of the liquid crystal. This solution is convenient to achieve via consideration of time-dependent process of build-up of the steady-state distribution of the director. Dynamics of the director of the nematic liquid crystal can be described with the evolution equation[22,23],

$$\frac{\delta F}{\delta n_i} - \partial_k \frac{\delta F}{\delta(\partial_k n_i)} = \frac{\delta R}{\delta n_i}$$

where $R$ is the dissipative function, and $F$ is the nematic free energy, respectively:

$$R = \gamma \left\{ (\partial \vec{n} / \partial t) \cdot (\partial \vec{n} / \partial t) \right\} / 2 \tag{3.2}$$

$$F = (1/2) \cdot \left[ K_1 (div\ \vec{n})^2 + K_2 (\vec{n} \cdot curl\ \vec{n})^2 + K_3 (\vec{n} \times curl\ \vec{n})^2 \right] \tag{3.3}$$

After substituting (3.3) into (3.2) one can write the evolution equation in terms of director $\vec{n}$

$$\partial \vec{n} / \partial t = \vec{h} / \gamma, \qquad \vec{h} = \vec{H} - \vec{n} (\vec{n} \cdot \vec{H}) \tag{3.4}$$

Vector $\vec{H}$ is known as the "molecular field" before the procedure of its orthogonalization to local director $\vec{n}$, while vector $\vec{h}$ is the "molecular field' after that procedure. Cartesian components of $\vec{H}$ are:

$$H_i = (K_1 - K_2)\partial_i(\partial_\alpha n_\alpha) + K_2(\partial_\alpha\partial_\alpha)n_i + (K_3 - K_2)(n_\alpha n_\beta(\partial_\alpha\partial_\beta n_i) + n_\alpha(\partial_\beta n_\beta)(\partial_\alpha n_i) + \\ + n_\alpha(\partial_\alpha n_\beta)(\partial_\beta n_i) - n_\alpha(\partial_\alpha n_\beta)(\partial_i n_\beta)) \tag{3.5}$$

The solution we are looking for should satisfy the boundary conditions at the surfaces $z = 0$ and $z = d$,

$$\vec{n}(x, z{=}0) = \vec{n}(x, z{=}d) = \vec{n}_0(x) \equiv \{\cos(qx), \sin(qx), 0\} \tag{3.6}$$

In the general case this equation, as written through the director and its spatial derivatives, cannot be solved analytically. However, an analytical solution exists in monoconstant case, that is relatively simple and illustrative, but it represents real nematic liquid crystal only to some approximation. To examine real nematic orientation, we have solved the dynamic equations (3.4) and (3.5) numerically. We assume arbitrary initial distribution with fixed periodic boundary conditions (3.6) at the surfaces. We then use equation (3.4) to allow the liquid crystal to relax into the steady-state equilibrium distribution. When the ideal periodically aligned structure $\vec{n}_0(x)$ from equation. (3.1) is stable, the volume average

$$\langle n_z \rangle = \frac{1}{V}\iiint_V n_z dV \tag{3.7}$$

is zero. It usually becomes non-zero in the presence of the considerable distortions in comparison with the ideal structure. Since the initial distribution and boundary conditions do not depend on the *y*-coordinate, we have omitted *y*-derivatives in our computation.

Figures 3.6a and 3.6b demonstrate the plots of $\langle n_z \rangle$ as a function of thickness for monoconstant liquid crystal and for 5CB respectively. It has a pronounced critical point, which separates stable and unstable regions.

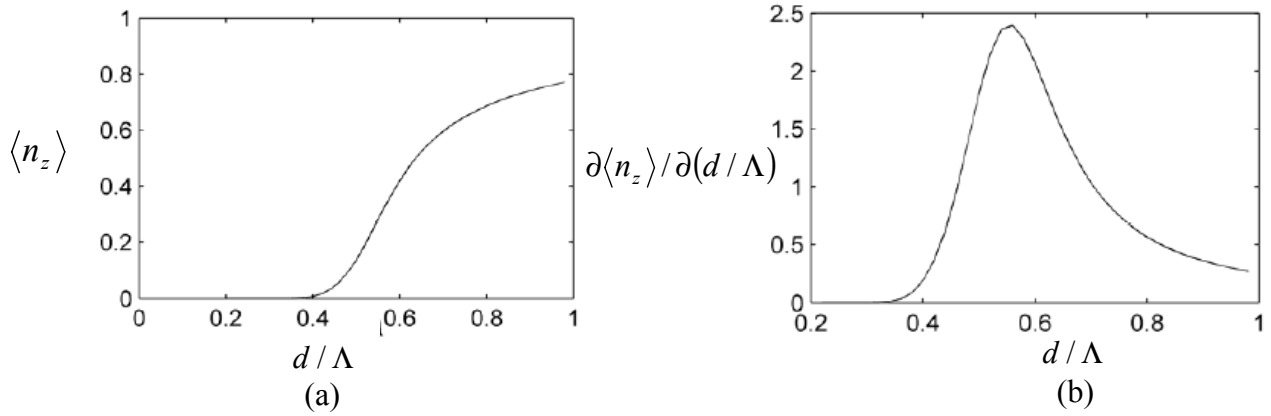


**Fig 3.6** Instability of the ideal periodically aligned structure of the nematic liquid crystal arises at the thickness $d<\alpha\Lambda$, where the dimensionless parameter $\alpha$ characterizes the threshold. Figure 3.6a: monocostant case, for wich both analytic and numeric calculations yield $\alpha$=0.5. Figure 3.6b: derivate of previous function better illustarte the sharp onset of instability [20]

The derivative of $\langle n_z \rangle$ with respect to parameter ($d/\Lambda$) is presented in Figures 3.7a and 3.7b; this derivative has a sharp peak at the critical thickness. As expected, critical thickness is $d = 0.5\Lambda$ for monoconstant case.

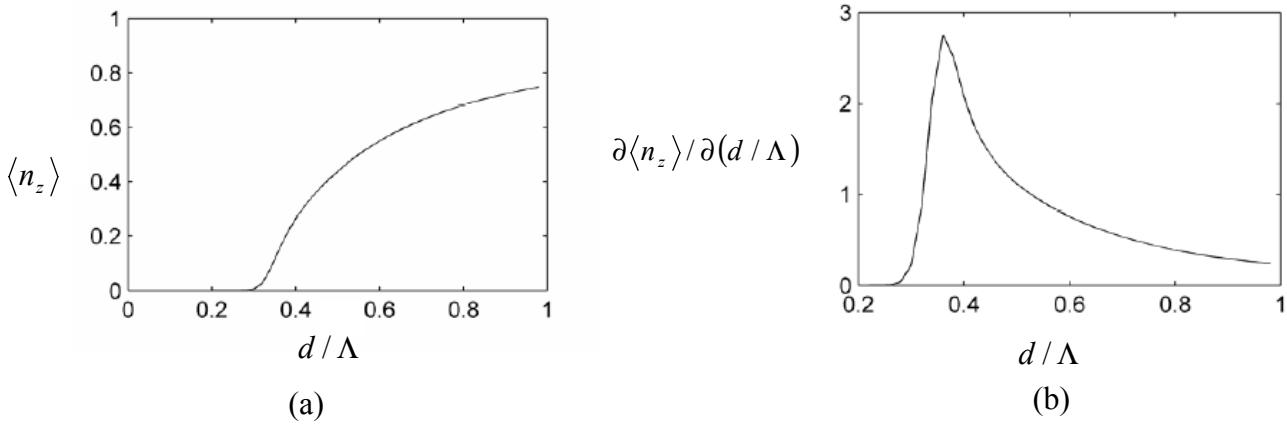


**Fig 3.7** Instability of the periodically aligned structure of the nematic liquid crystal for the non monocostant nematic liquid crystal; particular values were taken as for 5CB. Figure 3.7a: symmetry breaking perturbation onset at $d>0.33\Lambda$. Figure 3.7b: derivate of previous function better illustrate the sharp onset of instability [20].

This solution shows that a perfect bulk replica of the orientation imposed by the surfaces is stable if the ratio of the thickness of the cell and the periodicity of the modulation ($d/\Lambda$) is small enough, typically less of 0.4. A table in which critical thickness is calculated for a number of nematic liquid crystals is reported[20]:

## Table 3.1

| LC type | $\Delta n$ | $K_1$ | $K_2$ | $K_3$ | Critical value $d/\Lambda$ |
|---|---|---|---|---|---|
| MBBA | 0.22 | $6.2 \times 10^{-12}$N | $3.8 \times 10^{-12}$N | $8.6 \times 10^{-12}$N | 0.39 |
| K15(5CB) | 0.19 | $6.4 \times 10^{-12}$ N | $3 \times 10^{-12}$N | $10 \times 10^{-12}$N | 0.33 |
| K21(7CB) | 0.16 | $5.95 \times 10^{-12}$ N | $4 \times 10^{-12}$N | $6.6 \times 10^{-12}$N | 0.43 |
| M15(50CB) | 0.19 | $6.1 \times 10^{-12}$ N | $3.74 \times 10^{-12}$N | $8.4 \times 10^{-12}$N | 0.39 |
| E7 | 0.23 | $12 \times 10^{-12}$N | $9 \times 10^{-12}$N | $19.5 \times 10^{-12}$N | 0.37 |

Because we use the nematic liquid crystal E7 in our experiment, the threshold value is $d/\Lambda \leq 0.37$.

To conclude, in this section we theoretically described a new design of a liquid crystal cell based on transverse periodicity of azimuthal alignment of nematic liquid crystal. This ideal structure is possible but there are two different conditions that must be fulfilled: the first is related to the rotation of the liquid crystal in the bulk and the second one is associated with the value of diffraction efficiency. We have calculated the conditions of stability of such liquid crystal structure as well as the conditions to get 100% diffraction efficiency. This important property of the sinusoidally aligned liquid crystal constitutes the basis of the use of the nematic liquid crystal structure (3.1) as element of a projection display [20]. In fact, when no voltage is applied and the nematic liquid crystal structure is periodically aligned, the waves diffract and can be blocked with an aperture. In this case the cell works in the "off" regime. The cell can be switched to the "on" regime by application of voltage sufficiently high to destroy the periodic structure. Then, the liquid crystal cell becomes homogeneous, light is not diffracted, and passes through the aperture. In addition, this diffractive element can be used as an electrically controllable polarization beam splitter since the only diffracted orders are the two first orders, which are right and left-circularly, polarized. However, if the cell is illuminated by two right and left-circularly polarized waves, corresponding to plus and minus-first diffracted orders, they combine into a single beam. In this way, this cell may be used as an electrically controllable incoherent beam combiner[14].

## 3.3.2 Planar-periodic – planar-periodic configuration: experiment

In the 1D gratings, by sandwiching the substrate together prior to the holographic recording, using the experimental set-up described in figure 3.3, a liquid crystal grating structure was created with periodic boundary conditions registered on both surfaces. Because the top and the bottom surfaces are simultaneously registered during the exposure, the planar periodic alignment propagates unperturbed through the depth of the cell to create a uniform alignment through the bulk of the cell. The empty cell was exposed to the polarization pattern obtained by interference of two $Ar^+$ laser wave with $\lambda = 457nm$ and with opposite circular polarization states. The intensity of the two writing beams was $200mW/cm^2$ and the time exposure $t = 60s$. These writing parameters were fixed for all the configurations experimented.

In order to verify the good quality of the liquid crystal cell and to prove that all the wanted features are really obtained, we prepare two different kinds of sample: a wedge cell and a uniform $3\mu m$ thick cell. Since we use the nematic liquid crystal E7 in our experiments, using $\Delta n = 0.23$, we estimate that the smallest thickness required to achieve 100% diffraction efficiency, according to the half wave plate condition, is $1.4\mu m$ [1,20]. In order to achieve a liquid crystal cell with the specific thickness that fulfils the wave plate condition, we assemble a wedge cell with thickness varying from $1.2\mu m$ to $2.2\mu m$. In this sample, several gratings are recorded and characterized at different thickness. Both for the wedge cell and for the uniform cell, the periodicity of the grating are calculated in order to satisfy the stability condition[1,20]. In particular, in our experiment, gratings with periodicity varying from $5\mu m$ to $8\mu m$ are recorded.

The diffraction efficiencies were investigated varying the polarization direction of the probe beams and are reported in polar plots. Moreover, a two gratings photopolarimeter (TGP)[24] was used to completely investigate left or right elicity of the circular polarization state.

### 3.3.2.1 Wedge cell

In figure is reported the cell geometry:

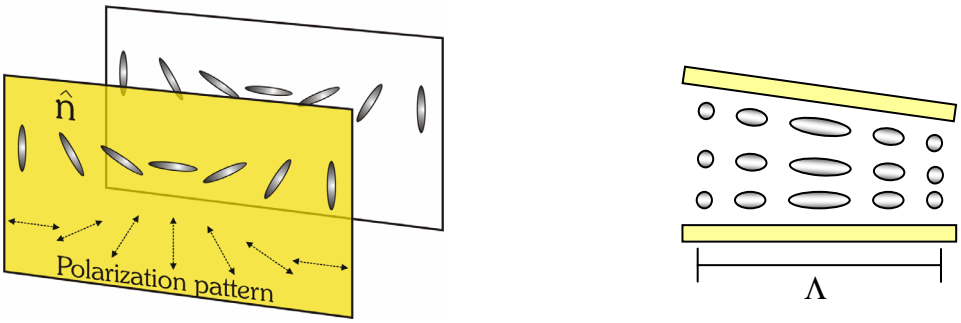


**Fig 3.8** Pictures of the cell geometry

In correspondence of $d = 1.4\mu m$, we observe a diffraction grating with 100% of diffraction efficiency. In figure 3.9 we report the diffraction patterns produced by the grating, depending on the polarization of the probe beam:

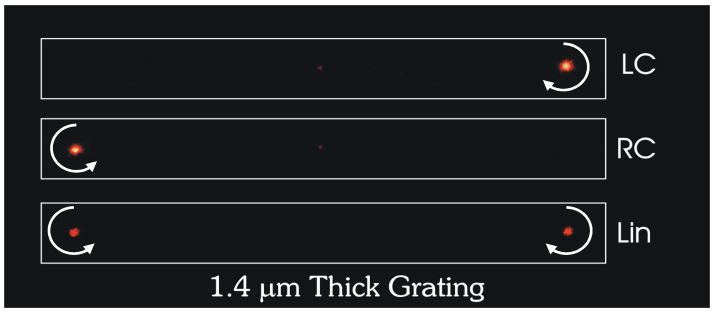


**Fig 3.9** Diffraction patterns produced by the grating for 1.4μm cell thick in the wedge cell. LC: left circular polarization state of the impinging beam; RC: right circular polarization state of the impinging beam; Lin linear polarization state of the impinging beam.

It is possible to see that for linear polarized impinging beam, both the first +1 and -1 order are present, with equal intensities and opposite circularly polarization states; for right (left) circular

polarized impinging beam, only one order is present with intensity doubled with respect to the previous case and with left (right) circular polarization state. In all the cases, zero order is almost absent: we are in 100% diffraction efficiency condition.

The optical microscope image of the grating, between crossed polarizers, shows a very neat optical modulation, without defects. Even if the pitch of the recorded grating is $5\mu m$, the expected spatial periodicity is $2.5\mu m$, since orthogonal director orientation (0° and 90°, or -45° and 45°) are optically equivalent between crossed polarizers.

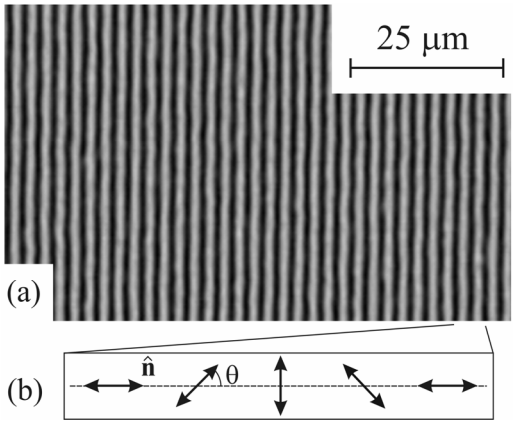


**Fig 3.10** Optical microscope image of the grating between crossed polarizers. (a) Director configuration along the grating wave vector in the liquid crystal film. (b)

In figure 3.11 we report the values of diffraction efficiency for circularly polarized probe bema, versus the cell thickness and retardance, together with the theoretical curve:

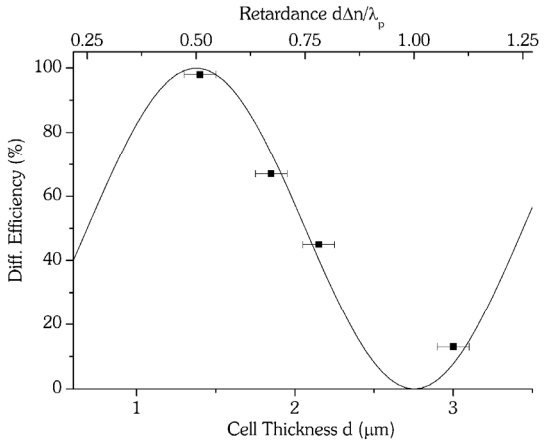


**Fig 3.11** First order diffraction efficiency versus the cell thickness and retardance. Black square are experimental data and solid line is the theoretical curve.

We can observe that the four experimental points agree with the theoretical curve of the diffraction efficiency. In particular, in correspondence of $d = 1.4\mu m$, half wave plate condition and near 100% diffraction efficiency are verified. These results supporting that almost ideal liquid crystal director configuration, monotonously varying along the grating wave vector, is achieved.

### 3.3.2.2 Uniform cell

For an arbitrary cell thickness, low external voltage uniformly applied to the liquid crystal polarization grating replica, yields control of the effective birefringence $\Delta n$, and therefore allows properly adjusting the diffraction efficiency in the 0-100% range.

In this figure we report the efficiency value of the $3\mu m$ thick grating versus the ac voltage ($f = 5kHz$), for a circularly polarized probe beam:

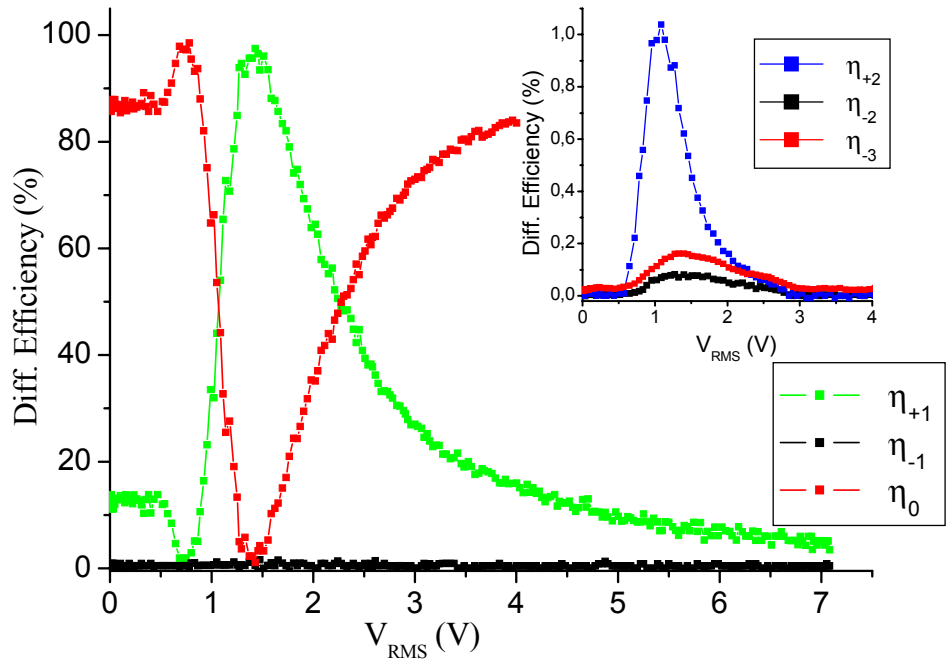


**Fig 3.12** Zero order (red squares), +1 order (green squares) and -1 order (black squares) diffracted beams versus applied voltage $V_{rms.}$ Inset: +2 order (blue squares), -2 order (black squares) and -3 (red squares) diffracted beams versus applied voltage $V_{rms.}$

Starting from the value of 13% of the diffraction efficiency in the +1 order, when $V_{rms}$ = 0V, first the diffraction efficiency decrease to zero, at $V_{rms}$=0.77V and then increases up to 98% for $V_{rms}$=1.4V, whereas the minus one is constantly about equal to zero. The external voltage easily allows to switch on and off the diffraction grating. The inset in the figure report the diffraction efficiency of few higher diffracted orders, namely +/-2 and +3. The growth of the higher diffracted orders, not present in case of ideal structure, suggests that the field induced polar distortion of director is coupled with a slight transverse deviation of the bulk director configuration from ideal structure imposed by the surfaces.

Here is an image of the diffraction patterns showing the polarization of the transmitted beams when circular or linear polarizations are used:

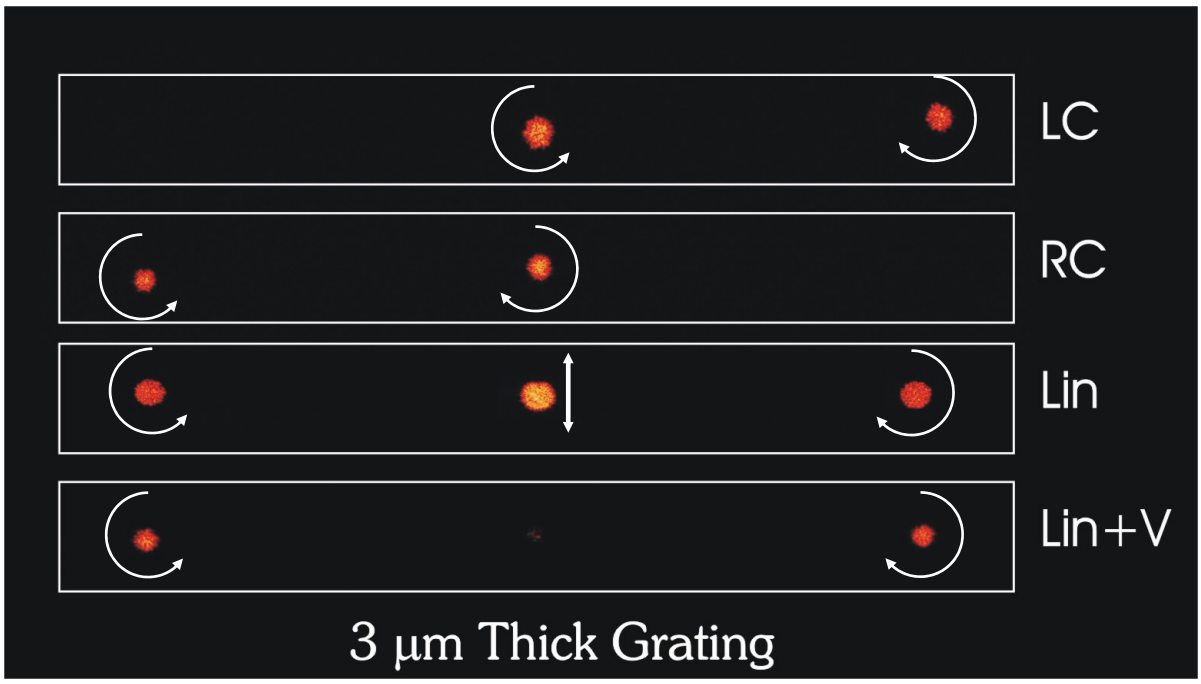


**Fig 3.13** Diffraction patterns of the grating in the uniform cell 3µm thick. LC: left circular polarization state of the impinging beam; RC: right circular polarization state of the impinging beam; Lin linear polarization state of the impinging beam; Lin+V linear polarization state of the impinging beam with a voltage applied to the cell.

In case of circular polarization, only one diffracted order appears with circular opposite polarization respect to the incident one; in case of linearly polarized impinging beam, both first orders appear with equal intensity and opposite circular polarizations, as expected from the

theory. The application of an external voltage allows almost 100% diffraction efficiency, and the zero order disappears.

In figure 3.14 we report the diffraction pattern and the optical microscope image of a grating characterized by a stability parameter value $d/\Lambda = 1.10$ which is higher than the threshold (0.37) imposed by the stability condition.

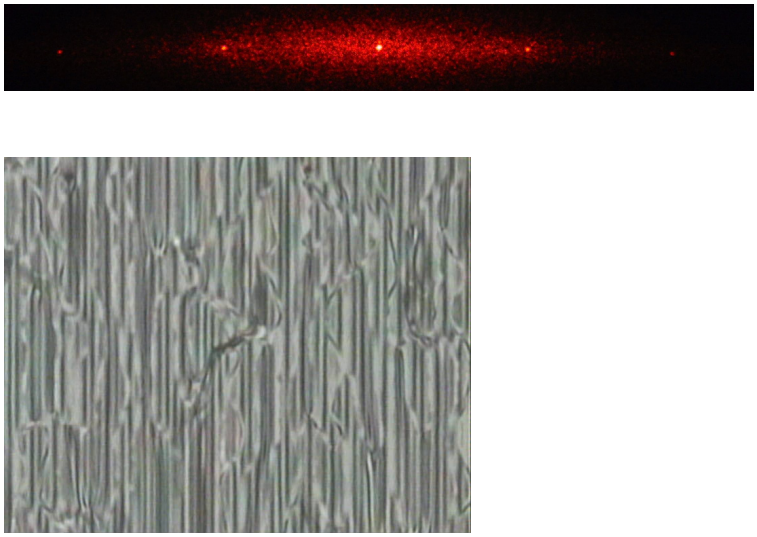

**Fig 3.14** Diffraction pattern and optical microscope image between crossed polarizers of a grating in a cell where the stability condition is not fulfilled: $d/L = 1.10$

In the case of $d/L$ higher than 0.37, it is evident, from the microscope image, that the ideal structure is not well reproduced in the bulk. The optical modulation is not neat and there are several defects. High scattering is observed, and a diffraction efficiency lower than 1% is measured.

In conclusion, taking advantage of polarization holography, we obtained a low scattering and highly efficient grating, modulating the in-plane anchoring axis at both surfaces of a planar nematic cell. We have seen that, for proper values of cell thickness and spatial periodicity of the grating, the director configuration in the nematic bulk is a perfect replica of the polarization gratings recorded on the aligning layer. Diffraction efficiency up to 98% is obtained even in thin grating regime, and changing the thickness of the samples or applying an external low voltage it is possible not only to modulate the diffraction efficiency in the 0-100% range, but also to have energy transfer between the diffracted and the transmitted beams[1].

## 3.3.3. Hybrid configurations

This section deals with diffraction grating obtained in hybrid configurations, this means that only one aligning substrate has planar periodic boundary condition, while the second one is uniformly planar or homeotropic[2,3,15]. These cells were prepared using polyimide coated ITO glass substrate in the case of planar-planar periodic cell, and DMOAP coated ITO glass in the homeotropic-planar periodic configuration. The planar polyimide material was spin coated and then cured at 250°C to achieve a film thickness of about $20nm$. After curing, the polyimide coated glass was mechanically rubbed with a velvet wheel to achieve a uniform planar alignment in the rubbing direction. The DMOAP is deposited by dip-coating technique and cured at 120°. Also in hybrid configurations we sandwiched both substrates together prior to the holographic recording, and after the exposure we filled the cells with the nematic liquid crystal in isotropic phase. The pitch of the gratings recorded and the thickness of the samples was fixed to $20\mu m$ and $5\mu m$ in planar–planar-periodic and homeotropic–planar-periodic configurations, respectively.

The planar–planar-periodic configuration results in a hybrid structure of alternating regions of planar and twisted geometry. The scheme of the cell and the optical polarizing microscope image taken between crossed polarizers of this structure is shown in figure 3.15.

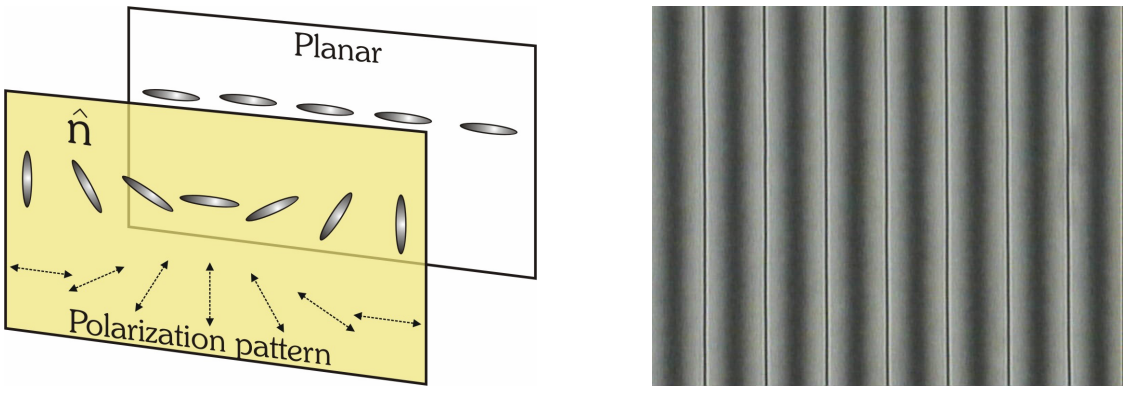


**Fig 3.15** Pictures of the planar-planar periodic cell geometry and optical microscope image between crossed polarizers of the grating recorded.

The regions where the optical axis at the patterned substrate is aligned parallel to the rubbing direction of the planar substrate result in a planar alignment of the nematic in the bulk and can be seen as dark regions in the image. The regions where the optical axis at the patterned substrate is aligned at some angle (<90°) with respect to the rubbing direction of the polyimide coated substrate, result in a continuous twisted alignment of the liquid crystal through the depth of the cell. This can be seen as light grey areas in the optical polarizing microscope image. Due to the continuous rotating polarization pattern, the amount of twist spatially varies across the grating pitch between 0° and 90°, as observed by the grey levels in the optical microscope image. Defects line are present in this configuration, because the competition between opposite twisting directions in the cell. The defect line appears as a dark line within a thin white line. The planar periodic alignment imposed by the polarization pattern and the planar polyimide alignment create twisted regions, which exhibit both right-handed and left-handed directions. These right-handed and left-handed directions collide in the region where the liquid crystal alignment imposed by the planar polyimide is orthogonal to the liquid crystal alignment imposed by the polarization pattern: defect lines appear due to the competition between right-handed and left-handed twisted domains.

The described grating structure present a very good diffraction efficiency $\eta_{\pm 1} = I_{\pm 1} / I_0 \approx 20\%$, where $I_0$ is the intensity of the impinging beam, low scattering and several diffracted orders, as reported in the following figure.

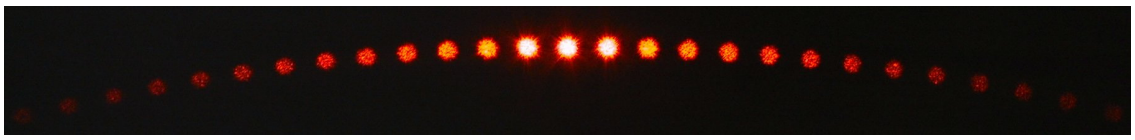

**Fig 3.16** Photo of the diffraction pattern produced by the grating in the planar-planar periodic configuration.

The homeotropic–planar-periodic hybrid configuration results in a structure that combines periodic regions of different bent geometries. This is a defect-free configuration, because the periodic regions do not generate a frustrated liquid crystal alignment within the cell. The scheme of the cell geometry and the optical polarizing microscopy image between crossed polarizers of

this structure is shown in figure 3.17.

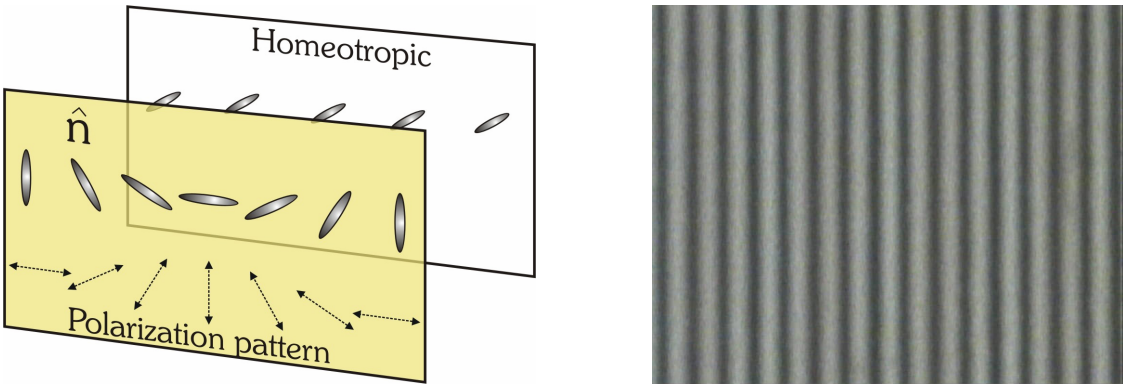


**Fig 3.17** Pictures of the homeotropic-planar periodic cell geometry and optical microscope image between crossed polarizers of the actual grating.

The darker grating lines represent bent regions where the planar aligned liquid crystal is at 0° or 90° with respect to the polarizer or analyzer. Lighter grey grating lines represent bent regions where the planar aligned liquid crystal is at a certain angle with respect to the polarizer and analyzer. We report the diffraction pattern of the planar periodic-homeotropic grating, when the impinging beam is linearly polarized:

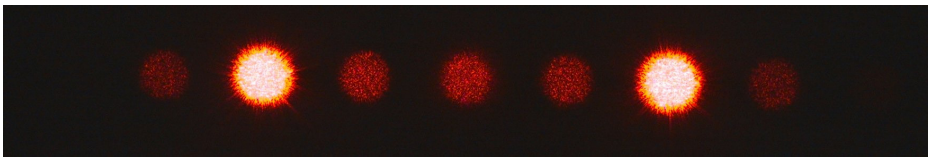

**Fig 3.18** Photo of the diffraction pattern produced by the grating in the homeotropic-planar periodic configuration.

Together with the diffracted orders expected for the imposed spatial periodicity, other diffracted beams appear, indicating the presence of a structure with a doubled spatial periodicity (2Λ). This double pitch grating can be seen with the optical microscope, focusing on a different plane, as represented in the figure 3.19.

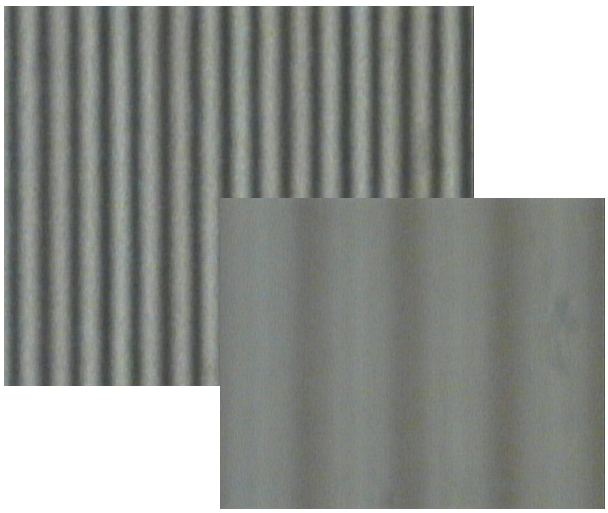

**Fig 3.19** Optical microscope image of the grating in the homeotropic–planar-periodic configuration. Focusing in another plane, it is possible to see another grating with double periodicity.

Also in this case, we obtain very good diffraction efficiency, $\eta_{\pm 1} = I_{\pm 1} / I_0 \approx 35\%$, where $I_0$ is the intensity of the impinging beam, and low scattering. Moreover, the liquid crystal grating shows the characteristic asymmetric diffraction for the reconstructing beams of opposite circular polarizations[2].

## 3.4 Two dimensional structures

There is a wide interest in optical devices that can perform beam steering, beam shaping and other modifications of light intensity or phase. The increasing need to manipulate the optical signal has stimulated interest in the development of highly functionalised and multibeam optical devices. Liquid crystal devices have been proposed for such needs[25]. Several concepts of liquid crystal gratings have been proposed. One possibility is to use surface structures to form liquid crystal micro-prism[26] or filled grating structure[27]. Multi-electrode cells to create a phase profile with an array of parallel electrodes[28] allow many configurations, but they are complicated to drive. Here we want to focus on 2D diffraction gratings with periodic alignment of the liquid crystal, consisting in a 2D array of different twisted structures of the nematic liquid crystal,

obtained by a crossed assembling of polarization holograms recorded at the surfaces of the aligning substrates. The resulting gratings not only influence the spatial energy distribution of the incident beam, but also convert the polarization state of the transmitted beams. In fact, they diffract in different directions with different polarization states at the same time: opposite circularly polarized light beams and $\pi/2$ rotated linearly polarized beams can be simultaneously obtained irradiating the grating with light beam. The energy distribution can be easily controlled by means of the polarization state of the incident beam. Additionally, exploiting the electro-optical manipulation of liquid crystal based devices, an external ac voltage can be used to completely control the diffracted energy distribution.

For this experiment, we used the same dye-doped polyimide substrates of 1D gratings, which were exposed to the spatially rotating linear polarization pattern obtained by interference of two opposite circular polarized beams of an $Ar^+$ laser at $\lambda = 457nm$, with intensity of $200mW/cm^2$ and fixed exposure time of $60s$. Spatial periodicity of the polarization pattern $\Lambda$ is about $20\mu m$. Differently from 1D gratings, the photosensitive substrates were independently exposed to the polarization pattern. After the recording of the holograms, the empty cells were assembled sandwiching these two substrates together with the alignment layers facing each other, but rotating them by 90° with respect to each other. A schematic illustration shows the 2D assembling:

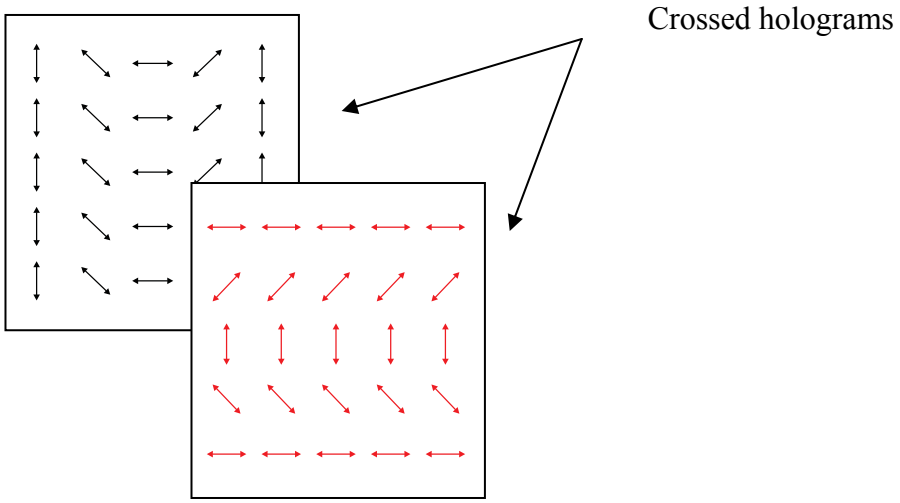


**Fig 3.20** Schematic illustration of the assembling of 2D configuration, obtained rotating one substrate by 90° respect with the other.

The black and red arrows represent the easy axes for liquid crystal alignment at the bottom and top substrates, respectively. In the assembled empty cell, the diffracted beams were invisible and appeared only after filling the cell with liquid crystal. The resulting configuration following the nematic filling procedure is a 2D array of different twists of the liquid crystal alignment, varying from 0° (planar alignment) to 90° (complete twist), created by the overlapping planar periodic patterned surfaces, as represented in this picture:

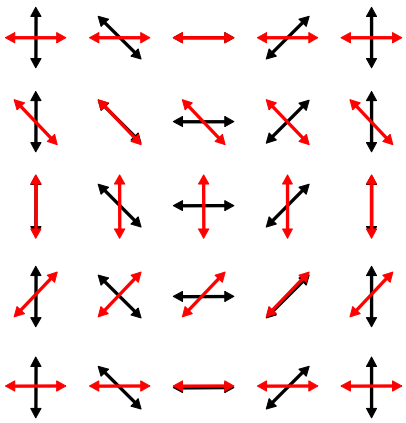

**Fig 3.21** Schematic illustration of the expected alignment of the liquid crystal inside the cell created by the overlapping planar periodic patterned surfaces.

Regions with parallel arrows indicate planar alignment propagating through the depth of the cell. Regions with orthogonal arrows represent 90° twisted configurations. Finally, regions with arrows directions between 0° and 90° represent twisted configurations coinciding with the angle between the two arrows.

Polarization gratings were recorded with the same pitch length $\Lambda = 20\mu m$, but with different cell thickness, 3, 5, 7 and $10\mu m$, in order to study the behaviour of this devices. The cells were filled by capillary action with the nematic liquid crystal mixture E7 above the clearing temperature and slowly cooled down in the nematic phase at room temperature. A He-Ne laser at $\lambda = 632.8nm$ was used as probe beams to investigate the diffraction properties of the gratings. The polarization state of the incident beam was varied using a combination of polarizer and quarter wave-plate, and the diffraction efficiencies were investigated varying the polarization direction of the probe beams and sketched in polar plots. Furthermore, the TGP[18] was used to

completely investigate the left or right elicity of the circular polarization state.
In the figure is shown an example of typical 2D visible diffraction pattern created by these gratings in a $3\mu m$ thick liquid crystal cell. Low scattering and good efficiency is observed. The gratings wave vectors are slanted with 0°, 90° and 135° respect to the horizon, while grating with wave vector at 45° do not appears. Moreover the grating at 135° have a spatial periodicity $\Lambda\sqrt{2}$. Efficiency of 15-20% can be reached for each grating at 0° and 90°, while the grating at 135° reaches values of about 5%.

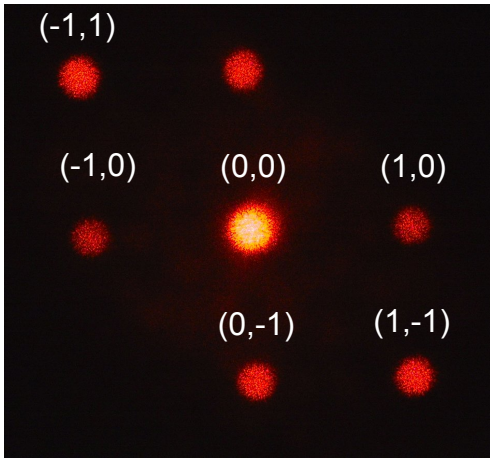


**Fig 3.22** Photo of the diffraction pattern produced by two dimensional grating.

The 0° and 90° gratings behave as the 1D planar-periodic–planar-periodic grating, and in particular[1]: only the first order diffracted beams (-1,0) and (1,0), for the 0° grating, and (0,-1) and (0,1), for the 90° grating, are present. Both diffracted beams (-1,0), (1,0) and (0,-1), (0,1) have circular polarization state and opposite elicity. The zero order (0,0) presents the same polarization state of the incident beam. These features are independent of the cell thickness.
In the case of the grating at 135° we observed that for linear polarization of the probe beam, the plus (1,-1) and minus one (-1,1) orders have linear polarization but the direction is perpendicular with respect to the zero order and consequently with respect to the incident beam. These properties are evident from the pattern observed adding an analyzer parallel or crossed with respect to the incident polarization. In figure 3.23, we report the diffraction pattern and the

polarization states of the diffracted beams obtained for linearly polarized impinging beam.

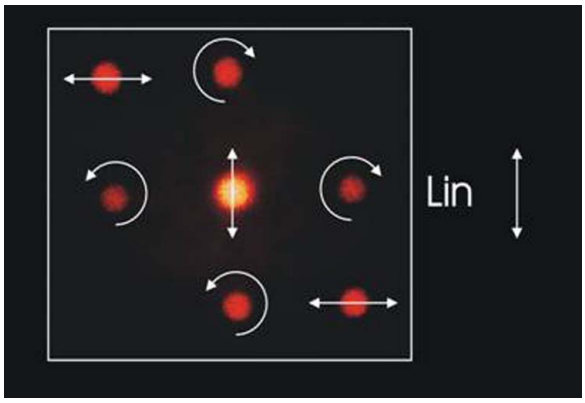


**Fig 3.23** Photo of the diffraction pattern produced by two dimensional grating 3µm thick for a linear impinging beam: the polarization states of the transmitted and diffracted beams are represented by the arrows.

For circular polarization of the probe beam, the gratings at 0° and 90° show only one diffracted beam for each grating, that can be switched on or off changing the elicity of the incident beam, while the grating at 135° degree has both first order beams. All transmitted and diffracted beams are circularly polarized (see figure 3.23) with different elicity (left or right) depending on the incident beam polarization.

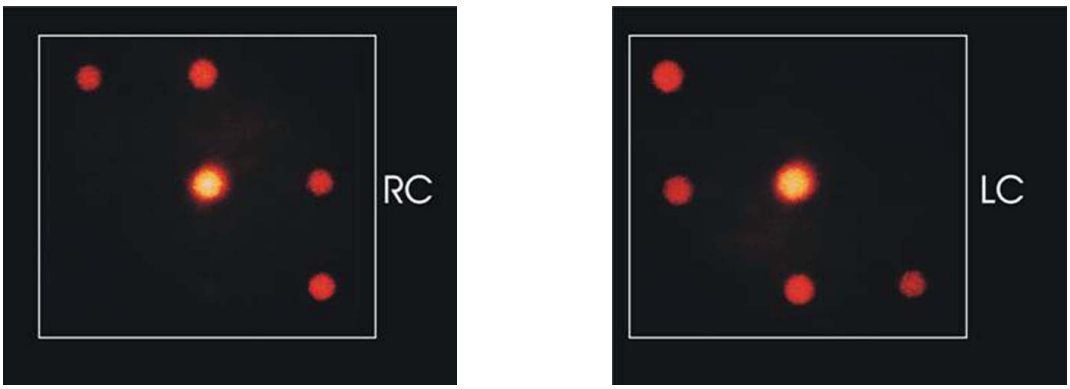


**Fig 3.24** Photo of the diffraction pattern produced by two dimensional grating 3µm thick for right circular and left circular impinging beams.

The good quality of the polarization states of the diffracted beams is demonstrated by the following polar graph, obtained by rotating an analyzer:

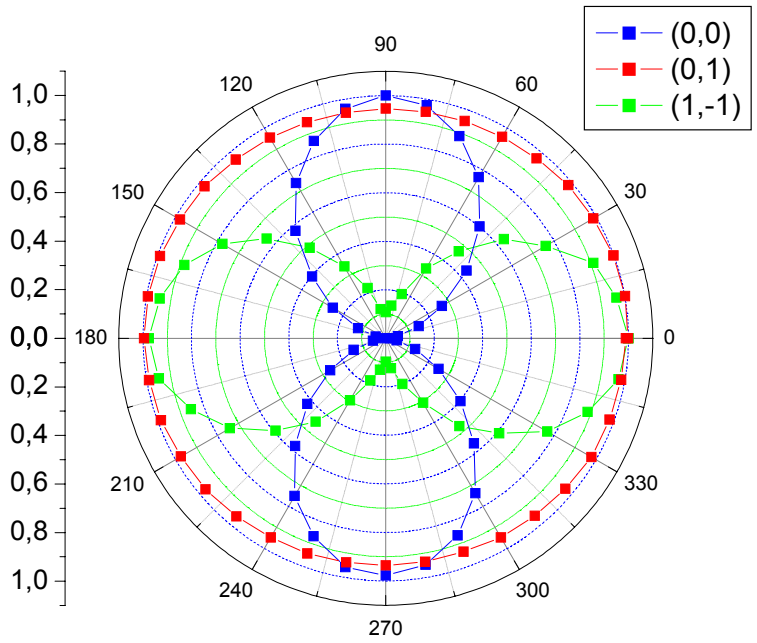


**Fig 3.25** Polarization states of the linear s transmitted beam (0,0) (red squares), of the linear p (1,-1) diffracted beam from the 135° grating (black squares), and of the circular (0,1) diffracted beam from the 90° grating (blue squares), for the 3µm thick cell.

We can observe that, for a linear s impinging beam, the polarization states of the diffracted beams of the diagonal grating are linear but orthogonal with respect to the incident beam, and the polarization states of the 0° and 90° diffracted beams are circular.

Even if the above described features can be also obtained exploiting several methods and material, as for example overwriting differently oriented polarization gratings in thin film of photosensitive material[29], the peculiarity of this multibeam device allows to add further functions to the 2D gratings. In particular, the diffracted beam distribution can be modulated by means of the application of an external voltage.

The application of an electric field allows to find a situation in which the zero order reduces dramatically and the main incident power is transferred in the diffracted beams. In figure 3.25 we report the diffraction efficiency values of the (0,0), (-1,0), (0,1) and (1,-1) orders of the $3\mu m$ thick cell versus the ac voltage ( $f = 5kHz$ ), for a circularly polarized probe beam.

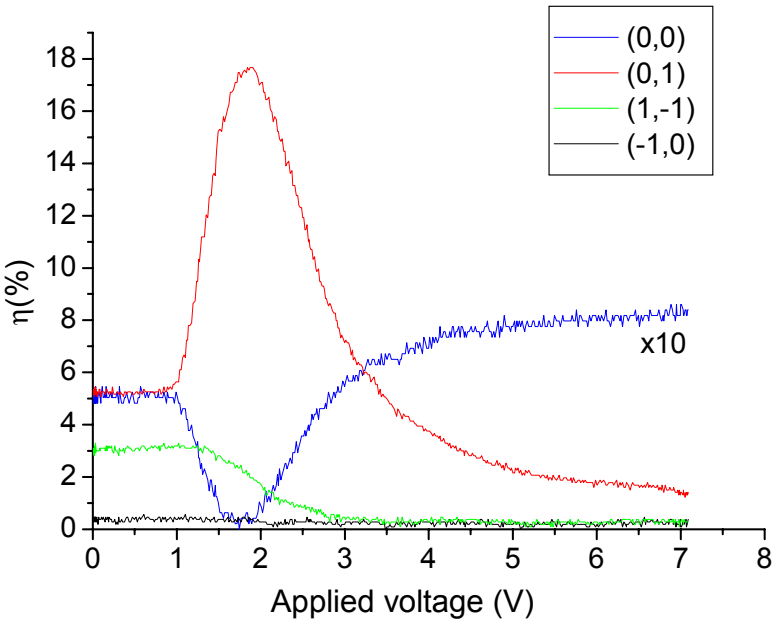


**Fig 3.26** Diffraction efficiency values of the orders (0,0) blue curve, (0,1) red curve, (1,-1) green curve, (-1, 0) back curve of the 3µm thick cell versus the ac voltage (*f*=5kHz), for a circularly polarized probe beam.

Starting from a value of about 5% for the (0,1) and about 3% for (1,-1) when $V_{rms}$=0V, the (0,1) first increases up to ~18% for $V_{rms}$~2V, then decreases towards zero, whereas (1,-1) decreases from ~3% at $V_{rms}$=0 at zero when $V_{rms}$~3V. The transmitted beam (0,0) becomes zero when (0,1) reach the maximum value: the external voltage easily allows to switch on or off the diffracted beams.

The polarization properties of the diagonal grating of the 2D structure changes varying the thickness of the cell. In figure 3.27 the 2D diffraction pattern produced by a $5\mu m$ thick crossed cell is reported.

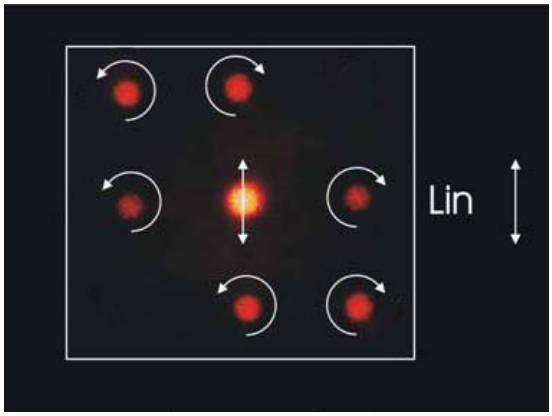


**Fig 3.27** Photo of the diffraction pattern produced by two dimensional grating 5µm thick for a linear impinging beam: the polarization states of the transmitted and diffracted beams are represented by the arrows.

In this case, all grating behave as the 1D planar-periodic–planar-periodic grating, and in particular for a linear impinging beam, all the diffracted beams are circularly polarized. For circular polarized impinging beam, only one diffracted beam for each grating is present, as reported in the following figure:

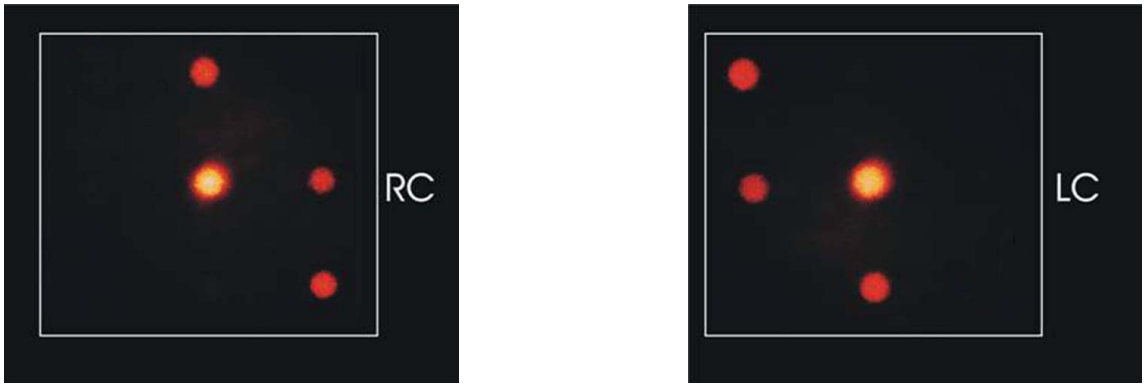


**Fig 3.28** Photo of the diffraction pattern produced by two dimensional grating 5µm thick for right circular and left circular impinging beams.

Also in this case, the polarization analysis on the transmitted and the diffracted beams shows a good quality of the polarization states of the light. Figure 3.29, shows that for a s polarized impinging beam, the polarization states of the 135° diagonal grating diffracted beams and the polarization states of the 0° and 90° diffracted beams are circular.

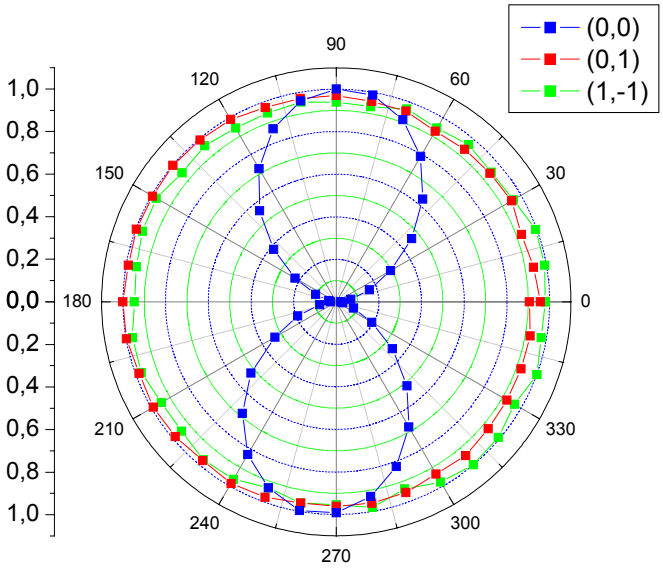


**Fig 3.29** Polarization states of the linear s transmitted beam (0,0) (red squares), of the circular (1,-1) diffracted beam from the 135° grating (black squares), and of the circular (0,1) diffracted beam from the 90° grating (blue squares), in the 5µm thick cell.

In figure 3.30 we report the diffraction efficiency values of the (0,0), (-1,0), (0,1) and (1,-1) orders for the $5\mu m$ thick cell versus the ac voltage (*f*=5kHz), for a circularly polarized probe beam:

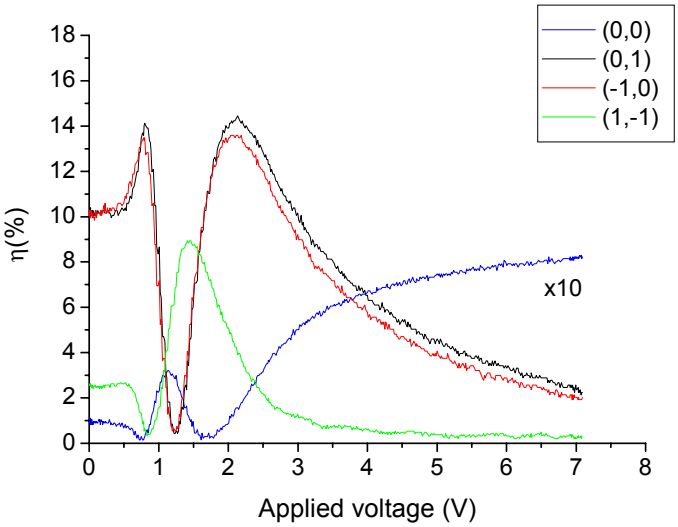


**Fig 3.30** Diffraction efficiency values of the orders (0,0) blue curve, (0,1) red curve, (1,-1) green curve, (-1, 0) back curve of the 5µm thick cell versus the ac voltage (*f*=5kHz), for a circularly polarized probe beam.

Also for thicker cells, low external voltage applied to the liquid crystal device, yields control of the effective birefringence $\Delta n$ and therefore allows properly adjusting the diffraction efficiency of the different orders. In fact, we can see that starting from a value of ~10% for the (0,1) and ~2% for (1,-1) when $V_{rms}$=0V, the the (0,1) first increases up to ~14% for $V_{rms}$~1V, then decreases towards zero, whereas (1,-1) increases from ~2% at $V_{rms}$=0 to ~9% when $V_{rms}$~1.5V, and then goes to zero.

Figures 3.31a, 3.31b, 3.31c are the optical microscope images obtained for different positions of the polarizer and analyzer: we can observe a very complex structure, with a large number of defects. The dark regions coincide with planar alignments that are parallel or perpendicular to the polarizer or analyzer. Regions characterized by a twist angle <90° can be seen as grey regions. Likewise, 90° twisted regions appear like white areas. For parallel polarizer and analyzer, contrast inversion occurs. The planar aligned regions that were dark regions, between crossed polarizers, appear as bright regions; the 90° twisted regions that were bright, now appear as dark regions.

If the analyzer is oriented at 45° with respect to the polarizer, the diagonal grating, that produce the diffraction at 135° with respect to the horizon, becomes evident.

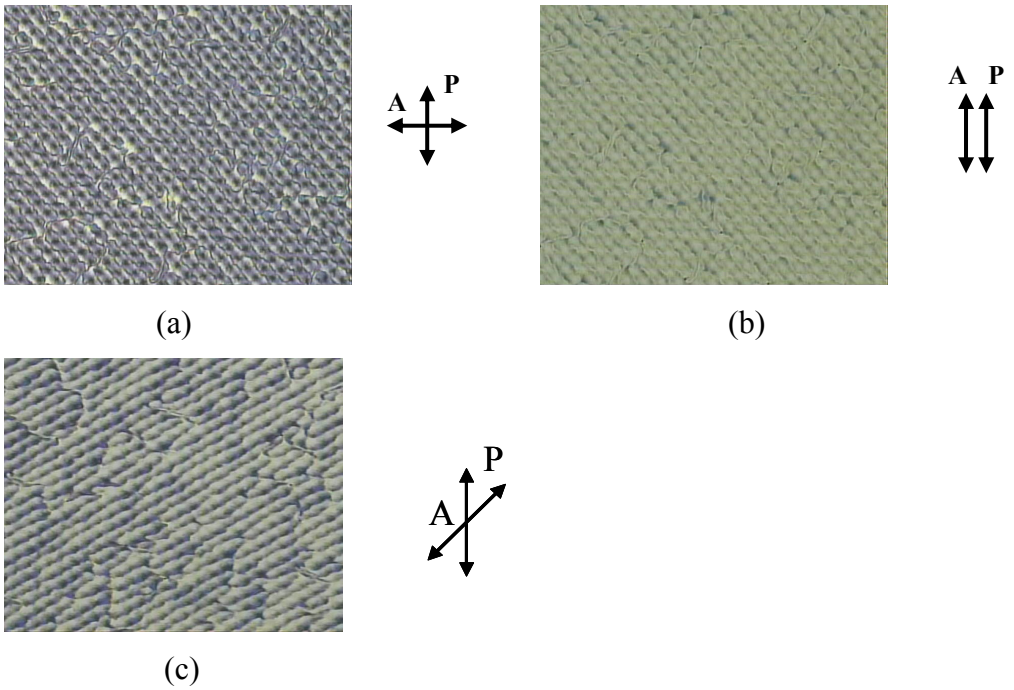


**Fig 3.31** Optical microscopy images of the two dimensional structure; in 3.31a polarizer and analyzer are orthogonal, in 3.31b polarizer and analyzer are parallel and in 3.31c analyzer is at 45° with respect to the polarizer.

In the 2D devices we observe a different behaviour in the diffraction properties of the 135° diagonal grating, depending on the thickness of the sample. In particular, for liquid crystal cell with thickness equal or lower than $3\mu m$, we have seen that the polarization states of the diffracted beams (-1,1) and (1,-1), for a linear impinging beam, are linear but orthogonal with respect to the incident beam. For liquid crystal cell with thickness higher than $3\mu m$, the polarization states of the diffracted beams (-1,1) and (1,-1), for a linear impinging beam, are circular with opposite elicity. On the contrary, gratings along 0° and 90° direction do not change their diffraction properties varying the thickness.

In order to explain this different behaviour, we can suppose that, as in the case of 1D gratings[1], in which the stability condition related to the thickness of the sample and the periodicity of the stored holograms is essential in order to obtain a perfect bulk replica in the liquid crystal cell, also in the 2D structures exists a threshold that controls the proper replica of the twisted regions in the volume. We can roughly think of the nematic film in thicker cells like a three layers system: the two outer layers, near the aligning substrates, in which the liquid crystal follows the direction imposed by the surfaces, and the inner homogeneous layer in which the nematic distortion relaxes due to the competition between the anchoring and elastic energies. Then, in the ticker cells, the twisted configurations do not propagate correctly in the bulk, and, because all alignment directions are present in the patterned substrates, the liquid crystal behaves as an isotropic fluid in the inner layer.

This hypothesis is supported by a simple model obtained multiplying the transmission matrix describing a grating with wave vector along the horizontal direction $T_X$ by the transmission matrix describing a grating with wave vector along the vertical direction $T_Y$. Here we theoretically calculate the transmission matrix of the following systems, composed by two consecutive and orthogonal polarization gratings:

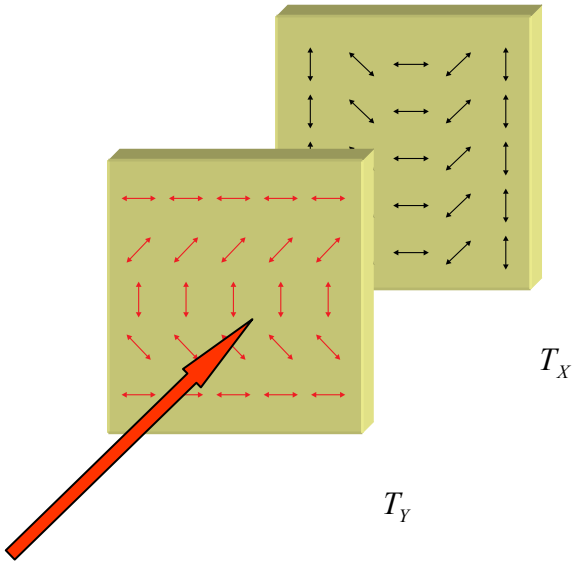


**Fig 3.32** Systems of two polarization grating in succession rotated of 90°, with an optically isotropic layer between them.

$$T_{TOT} = T_X \times T_Y = \begin{bmatrix} \cos(\Delta\varphi) + i\sin(\Delta\varphi)\cos qx & i\sin(\Delta\varphi)\sin qx \\ i\sin(\Delta\varphi)\sin qx & \cos(\Delta\varphi) - i\sin(\Delta\varphi)\cos qx \end{bmatrix} \times$$

$$\begin{bmatrix} \cos(\Delta\varphi) + i\sin(\Delta\varphi)\cos qy & i\sin(\Delta\varphi)\sin qy \\ i\sin(\Delta\varphi)\sin qy & \cos(\Delta\varphi) - i\sin(\Delta\varphi)\cos qy \end{bmatrix}$$

For a linear polarized impinging beam $E_{IN} = \begin{bmatrix} E_x \\ 0 \end{bmatrix}$, the diffracted beams can be calculated as:

$$E_{OUT} = T_{TOT} \times E_{IN}$$

and we get the following interesting results for the field just after it has passed through the two gratings:

**-0° grating:**

$$E_0 = \cos^2(\Delta\phi)\begin{bmatrix} E_x \\ 0 \end{bmatrix}$$

$$E_{+1} = iE_x \frac{\sin(2\Delta\phi)}{4}\begin{pmatrix} 1 \\ -i \end{pmatrix} e^{i\vartheta(x)}$$

$$E_{-1} = iE_x \frac{\sin(2\Delta\phi)}{4}\begin{pmatrix} 1 \\ i \end{pmatrix} e^{-i\vartheta(x)}$$

**-90° grating:**

$$E_0 = \cos^2(\Delta\phi)\begin{bmatrix} E_x \\ 0 \end{bmatrix}$$

$$E_{+1} = iE_x \frac{\sin(2\Delta\phi)}{4}\begin{pmatrix} 1 \\ -i \end{pmatrix} e^{i\vartheta(y)}$$

$$E_{-1} = iE_x \frac{\sin(2\Delta\phi)}{4}\begin{pmatrix} 1 \\ i \end{pmatrix} e^{-i\vartheta(y)}$$

**-135° grating:**

$$E_0 = \cos^2(\Delta\phi)\begin{bmatrix} E_x \\ 0 \end{bmatrix}$$

$$E_{+1} = -iE_x \frac{\sin^2(\Delta\phi)}{2}\begin{pmatrix} 1 \\ -i \end{pmatrix} e^{i\vartheta(x-y)}$$

$$E_{-1} = -iE_x \frac{\sin^2(\Delta\phi)}{2}\begin{pmatrix} 1 \\ i \end{pmatrix} e^{-i\vartheta(x-y)}$$

This simple model of crossed polarization gratings, in which an optically isotropic layer between the two grating is assumed, predicts the experimentally reported behaviour of the 2D $5\mu m$ thick structure, and in particular: diffraction along the $(x-y)$ direction, that corresponds to the 135°

direction, but not along the 45° direction. The polarization state of the transmitted beam is the same of the incident beam. For each grating, the order +1 is a left circularly polarized wave. For each grating, the order -1 is a right circularly polarized wave.
However, in order to gain better understanding of this particular behaviour, further experimental and theoretical investigations are needed.

## 3.5 Conclusions

In conclusion, taking advantage of polarization holography and of the interactions at the interface between a patterned substrate and a thin film of liquid crystal, we obtained highly efficient gratings, modulating the in-plane anchoring axis at both surfaces of a planar nematic cell. The diffractive devices present low scattering and diffraction efficiency up to 98%, even in thin grating regime. We have seen that, for proper values of cell thickness and spatial periodicity of the grating, the director configuration in the nematic bulk is a perfect replica of the polarization gratings recorded on the aligning layer. In this way, the gratings present all the diffraction peculiarities of pure polarization holograms, and, exploiting the electro-optical manipulation of liquid crystal based devices, can be completely controlled in the diffracted energy distribution by means of an external voltage. Accurate control of the cell thickness make it possible to tune the diffraction efficiency in the 0-100% range and to have energy transfer between the diffracted and the transmitted beams. This important property of the sinusoidally aligned liquid crystal constitutes the basis of the use of the nematic liquid crystal structure in various practical applications; for example, as an element of a projection display, as an electrically controllable polarization beam splitter, as an electrically controllable incoherent beam combiner.
Additionally, our results demonstrate the possibility to obtain a highly functionalised multibeam optical devices exploiting large sensitivity and flexibility of liquid crystal device. Two dimensional diffraction gratings are obtained combining polarization holograms recorded on photosensitive substrates and the assembling procedure of a nematic liquid crystal cell. A 2D array of chiral supramolecular structures is obtained.
The resulting 2D devices diffract the incident beam in several diffracted beams having various polarization states, orthogonal linearly and circularly polarised, that can be optically controlled.

Low scattering and high efficiency have been reported. An external ac voltage can be used to completely control the diffracted and transmitted energy distribution. Our results demonstrate the possibility to obtain a highly functionalised multibeam optical device attractive for beam steering and beam shaping processes, and other modifications of light intensity or phase[30].

# References:

**1** C. Provenzano, P. Pagliusi. and G. Cipparrone, *Appl. Phys. Lett.* **89,** 121105

**2** L.M. Blinov, G. Cipparrone, A. Mazzulla, C. Provenzano, et al, *Appl. Phys. Lett.* **87,** 061105

**3** L.M. Blinov, G. Cipparrone, A. Mazzulla, C. Provenzano, et al, *Molecular Crystal and Liquid Crystal* **449,** 147-160

**4** M. L.Blinov, R.Barberi, G.Cipparrone, et al *Liquid Crystals* **26,** 427-436

**5** J. Chen, P. J. Bos, H. Vathana, L. Johnson, *Appl. Phys. Lett.* **67**, 2588

**6** B. R. Wen, Petschek G., Rosenblatt C., et al, *Appl Opt*. **41**, 1246

**7** D.J. Versteeg, et al, *J. Appl. Phys.* **91,** 4191

**8** S. Varghese, et al *Appl. Phys. Lett.* **85,** 230

**9** S.Varghese, et al *Adv. Mat.* **16,** 1600

**10** L. Nikolova and T. Torodov, *Opt. Acta* **31**, 579

**11** T. Torodov and L. Nikolova *Opt.Lett,***17**, 358

**12** G. Cipparrone, A. Mazzulla and L.M. Blinov, *J. Opt. Soc. Am. B* **19**, 1157

**13** N.C.R. Holme, L. Nikolova, S. Hvilsted, and P.S. Ramanujam, *Appl. Phys. Lett.* **70**, 1518

**14** F. Lagugnè Labarthet, P. Rochon and A. Natanshon, *Appl. Phys. Lett.* **75**, 1377

**15** G.P. Crawford, J. N. Eakin, M.D. Radcliffe, A. Callan-Jones, A. Pelcovits, *J. Appl. Phys.* **98***,* 123102

**16** Suraj P. Gorkhali, Sylvain G. Cloutier, Gregory P. Crawford, Robert A. Pelcovits, *Appl. Phys. Lett.* **88,** 251113

**17** Sarkissian H, Serak S. V., Tabiryan N. et al, *Optics Letters*, **31**, 2248

**18** V. Chigrinov, A. Muravski, H. S. Kwok, et al *Phys. Rev. E*, **68**, 061702 and references

**19** V. Chigrinov, E. Prudnikova, V. Kozenkov, et al *Liquid Crystals*, **29**,1321–1327

**20** Sarkissian H., Tabirian N., Park B., Zeldovich B., *Molecular Crystal and Liquid Crystal* **451,** 1-19

**21** R. M. A. Azzam and N. M. Bashara. *Ellipsometry and polarized light*. Elsevier

**22** L.M. Blinov, V.G. Chigrinov, *Electrooptic Effects in Liquid Crystal Materials*, Springer-Verlag, 1994.

**23** B.Ya. Zeldovich, A.V. Mamaev, V.V. Shkunov, *Speckle-Wave Interactions in Application to Holography and Nonlinear Optics*, CRC Press, 1995, Boca Raton.

**24** C. Provenzano, G. Cipparrone, A. Mazzulla, *Applied Optics*, **45**, No 17, 3929

**25** M. Bouvier, T. Scharf, *Opt. Eng.*, **39** (8), 2131

**26** K. Hirabayashi, T. Yamamoto, and M. Yamaguchi, *Appl. Opt.* **34** (14), 2571

**27** M. Jepsen and H. J. Gerritsen, *Opt. Lett.* **21**(14), 1081

**28** Z. He, T. Nose, and S. Sato, *Opt. Eng.* **37**(11) 2885

**29** H. Ono, A. Emoto, N. Kawatsuki, T. Hasegawa, *Opt. Expr.***11**, 2379

**30** C. Provenzano, P. Pagliusi and G. Cipparrone, Electrically tunable 2D gratings of twisted nematic liquid crystal induced by polarization holograms, submitted to *Opt. Expr.*

# Summary

This dissertation reported the results obtained from optical studies related to polarization holographic recording in photosensitive materials. We have investigated the effects of polarization holography on photosensitive azo-dye Langmuir-Blodgett films, on PDLC, and on liquid crystal layers confined by dye-doped polymers aligning substrates.
During our investigation, we have found a number of interesting results that can be summarized as follows:

- we have carried out an investigation of the polarization properties of light diffracted by a thin permanent phase polarization grating recorded in Langmuir-Blodgett (LB) films composed of amphiphilic azo-dye molecules, using two orthogonal circularly polarized laser beams. The layered structure, obtained by means of LB deposition technique, obstructs the topographic relief formation, under the experimented writing conditions.
- The diffractive element is characterized by very long time stability and very high induced birefringence: the gratings become permanent and not rewritable because, after a certain time, the film becomes crystalline.
- The experimental results show that a pure polarization grating has been obtained whose diffraction properties make it a very interesting device for various applications. In particular, the polarization grating obtained has been selected as basic element for a photopolarimeter able to measure simultaneously and in real time the Stokes parameters of an electromagnetic wave, in order to determine its polarization state.
- We have reported the design and implementation of a photopolarimeter based on two diffraction gratings recorded by means holographic techniques on thin films of organic materials. The proper holographic recording geometries, the material composition, and film preparation allowed us to obtain diffraction properties of the gratings suitable to be combined for a spectropolarimeter extension.
- The photopolarimeter proposed in this work has an extreme simplicity of tuning, is free of modulating or moving parts, and is easy to calibrate. It has been satisfactorily tested for a single wavelength, but it can operate over the whole visible spectral range. Proper

research of materials is required to enlarge the working spectral range of the device, mainly in the UV range where the device could have interesting applications.

- We have reported an experimental and theoretical study of holographic gratings recorded exposing a homogeneous mixture of prepolymer and liquid crystals to a polarization light pattern. The obtained PH-PDLC grating possesses different features from the ones produced by the standard intensity technique: the internal morphology of the PH-PDLC is fairly uniform, and the gratings originate from the liquid crystal orientation inside the droplets, that are produced after the phase separation.
- A large anisotropy of the diffraction efficiency characterizes the recorded gratings, that reaches values ranging from 1% to 30%. Results from optical characterization of the diffracted and transmitted beam suggest that, beside the linear birefringence due to the orientation of the liquid crystal director, also SRG on the film topography should be considered. In fact, permanent reliefs with depth of few hundreds of nanometres are recorded on the surface of a polymeric material containing nanosized oriented liquid crystal droplets, as demonstrated by the AFM measurements.
- A theoretical model, opportunely modified to take into account both the linear birefringence and surface reliefs has been proposed, which is in good agreement with the measured reliefs depths. Some hypotheses are made on the role of the anisotropic phase separation related to the polarization sensitive crosslinking of the polymer, which can induce mass transport, such as in photoisomerizable systems.
- Two main aspects have to be stressed: the building of composite materials by means of irradiation with a polarization pattern makes evidence of novel potentialities of polymer-dispersed liquid crystals, mainly for diffractive devices; the formation of surface reliefs grating under uniform intensity irradiation is a more general phenomenon, no strictly related to photoisomerization, which could involve photoinduced chemical reactions sensitive to the polarization.
- We obtained highly efficient gratings, taking advantage of polarization holography and of the interactions at the interface between a patterned substrate and a thin film of liquid crystal, modulating the in-plane anchoring axis at both surfaces of a planar nematic cell. The diffractive devices present low scattering and diffraction efficiency up to 98%, even in thin grating regime.

- We have seen that, for proper values of cell thickness and spatial periodicity of the grating, the director configuration in the nematic bulk is a perfect replica of the polarization gratings recorded on the aligning layer. In this way, the resultant gratings present all the diffraction peculiarities of pure polarization grating, and, exploiting the electro-optical manipulation of liquid crystal based devices, the diffracted energy distribution can be completely controlled by means of an external voltage. Also changing the thickness of the samples it is possible to modulate the diffraction efficiency in the 0-100% range and to have energy transfer between the diffracted and the transmitted beams.
- This important property of the sinusoidally aligned liquid crystal constitutes the basis of the use of the nematic liquid crystal structure in various applications; for example, as an element of a projection display, as an electrically controllable polarization beam splitter, as an electrically controllable incoherent beam combiner.
- Our results demonstrate the possibility to obtain a highly functionalised multi-beam optical device exploiting large sensitivity and flexibility of liquid crystal device. Two dimensional diffraction gratings are obtained combining polarization holograms recorded on photosensitive substrates and the assembling procedure of a nematic liquid crystal cell. A two dimensional array of chiral supramolecular structures is obtained.
- The resulting two dimensional devices diffract the incident beam in several diffracted beams with various polarization states at the same time. Low scattering and high efficiency has been obtained. An external ac voltage can be used to completely control the diffracted and transmitted energy distribution.
- Our results demonstrate the possibility to obtain a highly functionalised multi-beam optical device attractive for beam steering and beam shaping processes, and other modifications of light intensity or phase.

# List of publications:

1. C. Provenzano, P. Pagliusi and G. Cipparrone, "Electrically tunable 2D gratings of twisted nematic liquid crystal induced by polarization holograms", submitted to *Optics Express*.

2. C. Provenzano, P. Pagliusi. and G. Cipparrone, "Higly efficient liquid crystal based diffraction grating induced by polarization holograms at the aligning surfaces", *Applied Physics Letters* **89** (12)**:**121105, 2006.

3. C. Provenzano, G. Cipparrone, A. Mazzulla, "Photopolarimeter based on two gratings recorded in thin organic films", *Applied Optics* **45** (17): 3929-3934, 2006

4. M.L. Blinov, G. Cipparrone, A. Mazzulla, C. Provenzano et al, "A nematic liquid crystal as an amplifying replica of a holographic polarization grating", *Molecular crystal and Liquid Crystals* **449**: 147-160, 2006.

5. M.L. Blinov, G. Cipparrone, A. Mazzulla, C. Provenzano et al, "Electric field controlled polarization grating based on a hibryd structure "photosensitive polymer-liquid crystal" ", *Applied Physics Letters* **87** (6)**:** 061105, 2005.

6. J.A. Reyes, C. Provenzano, G. Cipparrone, et al, "Optical properties of a nematic sample in the low-frequency regime of an external electric field", *Journal of Applied Phisics* **97** (12): 123108, 2005.

7. A. Mazzulla, P. Pagliusi, C. Provenzano, et al, "Surface relief gratings on polymer dispersed liquid crystals by polarization holography", *Applied Physics Letters* **85** (13)**:** 2505-2507, 2004.